METALLURGICAL ASPECTS OF FATIGUE AND FRACTURE TOUGHNESS

ADVISORY GROUP FOR AEROSPACE RESEARCH AND DEVELOPMENT

DECEMBER 1973

AGARD-R-610

AGARD

ADVISORY GROUP FOR AEROSPACE RESEARCH & DEVELOPMENT

7 RUE ANCELLE 92200 NEUILLY SUR SEINE FRANCE

AGARD REPORT No. 610

on

Metallurgical Aspects of Fatigue and Fracture Toughness

NORTH ATLANTIC TREATY ORGANIZATION

NORTH ATLANTIC TREATY ORGANIZATION

ADVISORY GROUP FOR AEROSPACE RESEARCH AND DEVELOPMENT

(ORGANISATION DU TRAITE DE L'ATLANTIQUE NORD)

AGARD Report No.610

METALLURGICAL ASPECTS OF FATIGUE AND FRACTURE TOUGHNESS

This Report was prepared at the request of the Structures and Materials Panel of AGARD.

THE MISSION OF AGARD

The mission of AGARD is to bring together the leading personalities of the NATO nations in the fields of science and technology relating to aerospace for the following purposes:

- Exchanging of scientific and technical information;
- Continuously stimulating advances in the aerospace sciences relevant to strengthening the common defence posture;
- Improving the co-operation among member nations in aerospace research and development;
- Providing scientific and technical advice and assistance to the North Atlantic Military Committee in the field of aerospace research and development;
- Rendering scientific and technical assistance, as requested, to other NATO bodies and to member nations in connection with research and development problems in the aerospace field;
- Providing assistance to member nations for the purpose of increasing their scientific and technical potential;
- Recommending effective ways for the member nations to use their research and development capabilities for the common benefit of the NATO community.

The highest authority within AGARD is the National Delegates Board consisting of officially appointed senior representatives from each member nation. The mission of AGARD is carried out through the Panels which are composed of experts appointed by the National Delegates, the Consultant and Exchange Program and the Aerospace Applications Studies Program. The results of AGARD work are reported to the member nations and the NATO Authorities through the AGARD series of publications of which this is one.

Participation in AGARD activities is by invitation only and is normally limited to citizens of the NATO nations.

Published December 1973

669.01:539.422:539.431:629.7.023

Set and printed by Technical Editing and Reproduction Ltd
Harford House, 7–9 Charlotte St, London, W1P 1HD

PREFACE

The development of aircraft that fly faster, higher, farther and carry more load has been made possible by the introduction of alloys that are increasingly stronger for the same specific weight. This development has in some ways been detrimental to the durability of the product because the resistance to fatigue and stress corrosion was in many cases not raised with static strength, and sometimes even adversely affected.

Stress corrosion has in a way been regarded largely as a disease of the alloy, while fatigue has become a design consideration. The latter applies also to fracture toughness, the capacity of the alloy to resist failure in the presence of a crack. Chemical compositions have been altered and heat treatments invented to raise the resistance to SCC, although special design measures – e.g. the avoidance of tensile stresses in the short transverse direction of the anisotropic microstructure – can also be very effective. Fatigue design is characterized by the avoidance of stress raisers, the provision of crack stopping elements, multiple load paths, etc., while relatively little has been done to combat fatigue by metallurgical means.

In AGARD the need was recognized to inspect whether the fatigue and fracture behaviour of the aerospace structural alloys was affected to an important extent by changes in their microstructure. If so this could be exploited to improve the alloys by special processes e.g. thermomechanical treatments.

Specialists were invited to inform the Structures and Materials Panel on this topic through pilot lectures. The information presented proved to be highly valuable, not only for the purpose of the Panel but for everybody interested in aerospace structural materials. Therefore the four papers are herewith presented to a much wider audience.

On behalf of the Structures and Materials Panel sincere gratitude is expressed to the authors for their efforts.

Discussions in an Ad Hoc Group devoted to the topic resulted in the recommendation to the Panel to pursue the matter further through the organization of a specialists meeting on Alloy Design for Fatigue and Fracture. A Conference Committee was formed for that purpose. The aim is to have this meeting in the Spring of 1975.

H.P. van Leeuwen, Chairman,
Conference Committee on
Alloy Design for Fatigue and Fracture
AGARD Structures and Materials Panel

CONTENTS

THE METALLURGICAL ASPECTS OF FATIGUE AND FRACTURE TOUGHNESS

by

P.J.E.Forsyth
Materials Department
Royal Aircraft Establishment
Farnborough, Hants
United Kingdom

1. INTRODUCTION

The integrity of a part subjected to repeated stress is, in the first instance, dependent on fatigue resistance, but at some stage, when a crack has grown, the fracture toughness of the alloy will play a part in curtailing life.

There is, perhaps, a suggestion in the title of this paper that fatigue resistance and fracture toughness are connected properties which are similarly dependent on microstructure. There are enough exceptions to this to make it seriously worthwhile examining in some detail why they arise.

We are immediately faced with the problem that fatigue resistance can be defined in various ways, e.g. fatigue strength in terms of an S/N curve or fatigue crack growth rates measured at various stress intensities. Similarly the toughness of an alloy cannot be attributed one unique number, but is dependent on the type of test. It is evident that fatigue strength as measured on a plain specimen where the initiation period is a large proportion of total life should be more sensitive to the near surface microstructure than fatigue crack growth resistance or fracture toughness. Similarly time dependent processes may contribute in the prolonged initiation period but not where cracks grow rapidly. The importance of environment has been widely demonstrated, and it is evident that this must be strongly associated with microstructure, but this aspect cannot be discussed in any detail in this paper.

2. FATIGUE CRACK INITIATION AND GROWTH

It would seem logical to consider first the reasons for the appearance of fatigue cracks after a period of repeated stressing. The results of a considerable number of researches suggest that the onset of plastic strain is an essential part of the fatigue process. There have been several demonstrations of complete resistance to cyclic stress where the conditions have been chosen to inhibit the movement of dislocation, e.g. germanium at room temperature[1] or zinc single crystals cycled at −196°C (Reference 2). Some ionic crystals have also been shown to exhibit no fatigue[3]. Single crystal work has shown the importance of slip direction with respect to the crystal surface. Except in the case where the slip direction is parallel to the surface, cyclic slip will serrate the surface and intrusions or Stage I cracks will be formed. This notching of the surface can be largely suppressed by the presence of a tenacious surface coating such as an anodic coating on aluminium or by the periodic dissolution of the crystal surfaces[4].

Slip band notching has been grasped as one of the few obvious ways in which plastic deformation can generate a crack, and while it will account for cracking in a number of cases, most engineering alloys do not fail in this manner. Probably the only important practical situation where classic Stage I cracking by surface notching can freely occur is in the aluminium cladding used on sheet aluminium alloy aircraft skins and members. Cladding is bright rolled, suffers complete recrystallization during the solutionizing of the core alloy, and contains very few particles. Thus Stage I cracking following slip band notching is the predominant mode of failure.

Surface notching is the direct result of localised slip, and this localisation is the peculiar characteristic of fatigue deformation. Fatigue deformation may be localised elsewhere than in slip bands such as at grain boundaries, particle interfaces or particle cracks, and at voids.

In some metals, notably magnesium and titanium, fatigue deformation may be by twinning[5], and remarkable twinning-untwinning damage results. Such damage includes the formation of dislocation dipoles with resulting slip band extrusion[6]. Nevertheless, the peculiarity of localisation of the deformation still occurs.

Apart from the localisation of deformation the reversibility of the slip is also important. It is clear that if slip was perfectly reversible no damage would result. Unless ratchetting of slip can occur no notch will develop. It is reported that materials of lower stacking fault energy have an increased resistance to notching which has been

explained by their decreased tendency to cross slip[7]. Although, in priciple, the surface notch resulting from cyclic slip could deepen into an appreciable Stage I crack and cause failure, the concentrated slip itself results in structural changes on slip planes[8] than can be defined as damage that will reduce the cohesive strength of the slip plane. This suggests that the normal tensile stress on the plane may at some stage cause rupture thus precluding the unslipping or notching[9].

The disturbing observation that throws a certain doubt on the generalisation that localised slipping leads to Stage I damage is illustrated in Figure 1a, b, c, d. In this case, which is very commonly observed, the operative slip planes do not develop into slip plane cracks, but another plane (in this case another (111) plane) fractures. If the most heavily slipped (111) plane is also oriented for cleavage then it will fail, but otherwise failure will occur on another slip plane even though there be no appreciable slip displacement on it. The conclusion from this is that fatigue slip on one set of (111) planes damages another set of (111) planes. This was an early conclusion of Gough[10] which must now be reiterated. *This more general embrittlement damage is the basic problem of fatigue* and Figure 2 shows, in schematic form, how this Stage I fracture may occur. More recently Wood[11] has demonstrated 'slipless' cracking in titanium. Thus while there are obvious signs of structural damage in a variety of metals and alloys, and under various stressing conditions, the most insidious cracking occurs on planes and in regions where no apparent change has occurred. This focusses on the importance of local tensile stress intensity.

Whatever this lattice damage is that reduces the fracture strength, we know that certain metallurgical effects such as strain ageing in steels or zone ageing in aluminium alloys have beneficial effects on fatigue. Feltner and Beardmore[12] suggest that for dynamic strain ageing to be a potentially useful fatigue strengthening mechanism two considerations are essential (1) a solute migration energy that is sufficient to permit the solute to keep up with the mobile dislocation (2) a high solute-dislocation binding energy. The beneficial effects resulting from the effective pinning of dislocations against cyclic stress seem to be mainly in resisting crack initiation, and, although the initial impedance to dislocation motion presented by the microstructure will play a part here, the dynamic effect is required to combat inherent instability that would otherwise lead to local strain accumulation. This dynamic pinning should homogenise the strain, at least up to a point at which dislocations break away from the influence of the pinning solute atoms. Thus high static yield strength may control low cycle fatigue strength— but long term dislocation stability is best achieved by a dislocation locking mechanism.

There are clearly potential ageing effects in unstable aluminium alloys where some supersaturation exists. Finney[13] has fatigued an aluminium copper-magnesium alloy in the underaged, peak aged and overaged condition and it is clear that the underaged state has superior fatigue strength to the peak and overaged material. The overaged is second in the list and the peak aged material has the lowest fatigue strength. The underaged alloy was at a point on the ageing curve at which S′ precipitation starts to nucleate on dislocations. It is likely that some dislocation pinning is occurring although evidence in other fields would suggest that the pinning in this alloy system is not likely to be strong.

The characteristic fatigue limit found in plain carbon steels is generally considered to be the result of the strain ageing phenomenon and Figure 3 illustrates how ageing is expected to raise the limit and move the knee of the S/N curve[12]. It is interesting to note that the fatigue limit is not the stress below which no cracks grow to failure[14]. Strain ageing is not entirely a question of pinning dislocations in the lattice because there is a strong grain size influence which is not evident in the simple explanation. Yield points are more marked in fine grain size materials and grain size can have a considerable influence on the fatigue limit of ferritic steels.

As with steels it has been found that State I slip plane cracks can form below the fatigue limit of α brass and the fatigue limit is a higher stress that just causes these cracks to cross the obstacle presented by the grain boundary[15].

It is generally true that if grain size affects the tensile strength of an alloy then it will also affect its fatigue strength so that the fatigue strength/ultimate tensile strength ratio remains the same. In duplex structures, where phase boundaries exist, the clear relationship between fatigue strength and grain size tends to break down and this is also true for aluminium alloys where so many other obstacles to slip exist.

At this point we should consider the possible sites and mechanisms for crack initiation. Having already stated that initiation is not exclusively by slip plane ratchetting it is necessary to identify the features in the microstructure that form sites for fatigue cracks, i.e. to look for features that amplify the strain locally.

Figure 4 shows some of these sites existing or developing on a specimen fatigued transversely to the rolling direction. The material is an Al-Cu-Mg alloy, RR 58, which contains additions of Fe and Ni that form the intermetallic compound Fe Ni Al_9.

Slip plane notching does occur in this alloy and may lead to incipient cracks, but strain is also concentrated at the grain boundaries and cracking may occur here also. It can be seen that particle interfaces also form sites for cracks. In a number of aluminium alloys slip plane cracking is preceded by precipitate dissolution[16] which suggests that slip plane softening will occur. The grain boundary crack may develop because of the presence of a precipitate free zone, but, certainly at slightly elevated temperatures there is again, as on the slip planes, evidence of precipitate dissolution and coalescence[16,17]. The other very effective site for fatigue crack initiation is the cracked intermetallic

particles[9]. These cracks are formed by the post solution treatment stretch that plates and sheet receive. Many cracks must be formed during rolling but with Fe Ni Al_9 healing occurs during solution treatment. This is not so with many other compounds and one could expect to retain cracks from the rolling stage. As would be expected these cracks that are introduced by stretching longitudinally with respect to rolling are only effective stress raisers when the material is fatigued in the longitudinal direction. Figure 5 shows fatigue cracks originating from these cracked particles apparently directly as Stage II cracks.

It is more difficult to classify the grain boundary origins but as slip prevails in these regions, then in terms of the micro mechanism of fracture they should be termed Stage I, particularly as extrusion and reverse glide evidence has been found.

If the classical Stage I cracks form they are commonly observed to change to Stage II at some depth, and it has been reported[18] that, for a titanium alloy processed to give various microstructures, and testing at various fatigue stress levels, the changeover occurred consistently at a stress intensity of 6.0 ksi$\sqrt{\text{in}}$.

It may be that such features as particle cracks can raise the local stress intensity to Stage II requirement. It has been demonstrated that by removing intermetallic particles from a microstructure, where the particle/matrix interface originated cracks, some small fatigue benefit was gained[19] see Figure 6. However, experiments with RR 58 have shown that reducing the population of cracked particles, although clearly reducing the numbers of particles exploited in the propagation phase, did not reduce the crack growth rate[20]. Unfortunately with all of these experiments, altering the particle content or distribution alters other microstructural features such as grain size and the effects of the particles themselves on the fatigue behaviour may be misjudged.

Inclusion size in a SAE 4340 high strength steel affected fatigue behaviour[21]. At high stresses large inclusions were found to be of little importance because fracture was caused by the joining of numerous small cracks that initiated and propagated practically simultaneously. At low stresses/long lives a simple large inclusion could initiate a crack that would itself grow to failure. Fatigue cracks have also been shown to initiate from non-metallic inclusions in a tempered martensitic high strength steel, although prior austenite boundaries and martensite sub boundaries were also sites for cracking[22]. It was also noticed that for harder steel matrices the frequency of fatigue crack initiation from non metallic inclusions increased, and with softer matrices sub boundaries or even slip bands became the predominant sites for cracks.

Attempts have been made to homogenise fatigue slip by alloying and by heat treatment[23] and by the introduction of dispersoids[24]. Figures 7 and 8 show how fatigue slip can change with composition and with ageing condition. Introducing dispersoids by addition to Ni and Mn increased fatigue resistance as shown in Figure 9 but there was an accompanying decrease in grain size. Figure 10 shows the two microstructures. This result is in conflict with Reference 19 and shows that one cannot generalise with regard to the effects of particles.

Considerable differences in fatigue properties may be experienced between lightly amd more heavily forged and worked alloys[18]. The fatigue strength of thick, forged Ti-6Al-4V bars was 60% lower than that for small diameter rolled and annealed bars as measured at 10^7 cycles. The values obtained were ±553 to ±621 MN/m^2 for 16 mm diameter rolled bars and ±345 to ±414 MN/m^2 for forged bars 360 mm x 57 mm section. The loading was 0 ± P. The large section bars contained extensive regions of similarly oriented α phase whereas the small bars had a fine $\alpha + \beta$ fibrous structure. These fine structures had higher fatigue strength because they limited the extent of Stage I crack growth. The tensile strength of the more heavily rolled bar was ~ 10% higher than the lightly forged bar. The structures of the two bars are shown in Figure 11.

The general theme of thermo-mechanical treatment is also receiving considerable attention. The purpose of these various heat treatment-deformation routes would be for fatigue applications, to homogenise fatigue slip. The field has been surveyed[25] and the importance of removing 'soft spots' from precipitated studies has been emphasised. It is suggested that this could be achieved TMT. The promotion of homogeneous slip might be obtained by sequential deformation and ageing or by warm working which should set up stable dislocation structures. It should be pointed out that, for various reasons, deformation prior to ageing has been used in commercial practice and there is no doubt beneficial effects have been obtained and used in the past. The scope for further improvement may, therefore, not be as great as is expected. It is also a fact that fatigue not only selects the weakest points in the microstructure but is able to provide soft spots. It is also to be expected that the Al-Zn-Mg-Cu alloys will not respond well to TMT where the prime aim is to provide dislocation nuclei. These alloys homogeneously precipitate at useful hardening temperatures. On the other hand Al-Cu and Al-Cu-Mg alloys also precipitate on dislocations as part of their normal ageing sequence and do in fact benefit in strength from these nucleation sites. Figure 12 shows the improvement in fatigue strength obtained by TMT on an Al 4% Cu alloy[26] but these are only the improvements that might be gained by conventional working and ageing techniques and this on an alloy that should show maximum response to TMT.

The effects of anisotropy of micro and macrostructure have been studied with regard to (a) total fatigue life and (b) crack propagation rates. It was found[27] that at low stresses/high number of cycles the fatigue strength depended very little on orientation with respect to extrusion direction in a large section (6" x 6") Al-Zn-Mg-Cu wing spar, but at higher fatigue stresses the fatigue strength reflected the tensile properties.

Fatigue crack growth rates have been measured in a hot rolled steel plate for the three orientations shown in Figure 13, and the growth rates deviated from a common value at low ΔK to greater differences at higher ΔK values. It was found that striation spacing (i.e. local growth rate) was independent of orientation and the conclusion was that the macroscopic differences in growth rate resulted from the fracture of inclusion stringers. Other work[28] agrees with this last conclusion.

The general indications are that particles, and anisotropy in terms of the particle stringers, have little effect on crack growth rate, when the plastic zone is small compared with the particle spacing. This is supported by fractography where it is commonly observed that the number of particles exposed on fatigue fractures increases appreciably with ΔK.

It is well known that fatigue crack growth in the Stage II mode may be closely confined to crystallographic planes, i.e. a cleavage crack extension with perhaps some microscopically visible arrest marking or, at higher stress intensities, a plastic crack extension with each successive cycle giving a non-crystallographic path lying normal to the maximum principal tensile stress. Thus, having said that, at least at low ΔK, the crack ignores the presence of the coarser intermetallic compounds, the question of why a cleavage plane is selected now arises. The degree to which the crack adheres to the cleavage plane differs for differing materials. If the normal mode of tensile crack extension for a material is by cleavage then it would not be surprising if the fatigue crack grew along cleavage planes. What is perhaps a little more surprising is that it can grow by cleavage or quasi cleavage in alloys that would fail by some ductile mode in a tensile test. Even so, the tendency for cleavage is greater in highly alloyed materials where a fine zone or precipitate structure exists.

In classical tensile cleavage situations the cleavage mechanism is encouraged by high strain rate but in fatigue the converse seems to apply. Not only does low frequency encourage cleavage[8] but it appears that time in the unloaded state can cause an abnormally large crack extension on the application of the next tensile load. This behaviour may suggest that corrosion, strain ageing or even creep may be in some way involved. It is clear that, for a cleavage mechanism to operate in an alloy where the normal tensile failure mode would be ductile, the crack tip must be maintained sharp or be periodically resharpened. A high tensile stress intensity will blunt the crack tip and destroy the continuity of the cleavage plane. Resharpening may occur depending on the degree of damage or disorientation that exists[9]. Corrosion could help to remove this damage and expose further undisturbed cleavage paths. Similarly strain ageing[29] or hydrogen[30] has been observed to encourage cleavage.

The problem that arises when cleavage behaviour is prevalent is that fatigue crack growth rate is less predictable in terms of plastic strain behaviour. This is not surprising as metallurgical effects such as corrosion and strain ageing are introducing other variables. Thus the predictability of fatigue crack growth should be greatest with intermediate levels of ΔK where the plastic zone size is such that ductile striations are formed. At very high ΔK values, where K_{max} has an influence, the coarse microstructure may begin to again introduce less predictable behaviour.

Fatigue crack growth curves have been normalised by the introduction of various tensile parameters and Figures 14 (Reference 31) and Figure 15 (Reference 32) show such plots for a variety of materials.

3. FRACTURE TOUGHNESS

The determination of the plane strain fracture toughness parameter K_{Ic} is subject to rigorous requirements in terms of specimen dimensions and the calculated plastic zone size. The testing conditions are also closely defined. Most of these rules of testing have been developed to enable the sensible testing of tough materials. Plane stress testing is more complicated still and it is very likely that the forms of test impose certain behaviour on various types of alloy. Thus an alloy that has a high K_{Ic} may not necessarily have a high K_c with respect to other alloys.

As with fatigue crack growth resistance, the considerable differences observed in the K_{Ic} for an embracing range of alloy systems (e.g. steels, titanium and aluminium alloys) can be normalised on the basis of tensile properties, as shown in Figure 16 (Reference 33). This suggests, as for fatigue crack growth, that the elastic strain is the predominant parameter. If K_{Ic} was completely defined by elastic strain there would clearly be no opportunity for the metallurgist to improve the toughness of alloys. This is not so, however. A closer look at the distribution of alloys in any one system shows considerable scatter with occasional values in the top right hand area of the K_{Ic}/σ_y curve, see Figure 17. Similarly it is disturbing to find that some widely used alloys lie well to the lower left hand side of the line. There is no metallurgical problem in shifting values along the line in either direction, but this is rarely of use in optimising design, although a reduction in yield strength might be acceptable as a trade off for safety, at least in some circumstances. One factor that can move the K_{Ic} across the line, as is well known, is the plane and direction of crack propagation with respect to the forged or rolled structure, i.e. the anisotropy of the material. This is particularly true for aluminium alloys where there are features in the microstructure that are particularly detrimental because they offer easy crack paths. This is not always so in steels where the non-metallic inclusions are usually too widely spaced to affect K_{Ic} and in these situations the more finely dispersed residual carbides control crack extension. This point brings one to the very important question of the relationship between microstructural feature size and distribution and the zone of influence at the extending crack tip. It seems reasonable

to discuss these effects in a general way, assuming that they are similarly involved in the toughness of ferrous, aluminium and titanium alloys. One thing that should be noted is that K_{Ic} and ductility as measured in the tensile test frequently do not correlate. This is clearly an effect of scale. The K_{Ic} test, almost by definition, exploits the properties of only a very small plastic zone. The tensile test samples the whole bulk of the gauge length of the specimen. Thus coarsely dispersed non-metallic inclusions in steels or the precipitate free grain boundary zones in aluminium alloys may have a considerably greater deleterious affect on ductility than on K_{Ic} where the plastic zone may be so small as not to embrace any of these features.

This leads the metallurgist to ask the designer – what emphasis do you put on ductility as a requirement in components that are neither deformed during manufacture nor in service? In view of the current interest in K_{Ic} and the desire to raise the value of this parameter for structural applications it should be stated that in some circumstances this can be done by microstructural modifications that cause an actual decrease in ductility. For this reason it is necessary to be clear what our priorities are.

Consider first the effects of forging or rolling direction on K_{Ic}. This is to separate the data as shown in Figure 18. The longitudinal values for aluminium alloys are rarely cause for concern, it is the short transverse values, particularly as this is also the stress corrosion sensitive direction in aluminium alloys, which can be so low as to seriously limit design. Although this would not appear to apply to plate applications it still cannot be disregarded, as integrally machined thick plates may be subject to local short transverse stressing at attachments etc.

The fact that aluminium alloys show a marked orientation sensitivity suggests that the intermetallic particle stringers, unlike those in the steels already quoted, are of such a spacing as to be damaging to the toughness.

Krafft has developed the expression shown below for fracture toughness in terms of the process zone size d_T, and the strain hardening index n. The process zone is the region at the crack tip where the metal has exceeded the necking strain ϵ_n. For a material obeying the Ludwik equation $\sigma = C\epsilon^n$, $n = \epsilon_n$

$$K_{Ic} = En\sqrt{2\pi d_T} \qquad (1)$$

The above equation applies only to fracture occurring by void formation and ductile dimples and in some cases[34] a good correlation has been obtained. The average spacing of sulphide inclusions has correlated well with the process zone predicted by the Krafft equation. Nevertheless in other cases it has been found that the dimple dimension bore no relationship to the measured particle spacing. This suggests that particles of various sizes may not be equally involved in the fracture process and the presence of a few large ones may override and suppress the contribution of the smaller ones.

Unfortunately forms of fracture other than ductile may occur. Cleavage in steels is a classic form that is encouraged by low temperature and high strain rates. The acuity of the stress concentration can affect the brittle/ductile transition temperature. Thus the sharper the initiator flaw the higher the transition temperature. This low ductility form of fracture may obscure the effects of particles and must upset the relationship based on void formation and ductile dimples, and on strain hardening index[35]. It is assumed that the higher the strain rate the less relaxation by plastic deformation that can occur at the crack tip, but if strain ageing effects occur, delay or reduced strain rate may increase the yield stress. The effect of this can be to encourage cleavage or quasi-cleavage in some materials, e.g. intermittent strain ageing in fatigue encourages a cleavage facetted fracture[29]. Similarly an aluminium-zinc-magnesium alloy tested in the supersaturated condition showed strain rate sensitivity on yield point, and at low frequencies fatigue cleavage striations were encouraged[36]. Intergranular tensile fracture is not uncommon in strong aluminium alloys and also in some steels under certain conditions of heat-treatment. In some microstructures mixed trans and intergranular fracture paths are observed suggesting that the two paths have similar fracture energies. It has been observed that large grain size, sometimes the result of local depletion in the number of intermetallic particles that are associated with grain refining and controlling elements, can result in local intergranular crack paths. Figures 19 and 20 show mixed fracture paths in RR 58 aluminium alloy and in a cast maraging steel.

The competition between grain boundaries and other fracture paths has been observed in other alloys and the effects of the two alternative modes of failure on K_{Ic} have been studied[37]. A ternary aluminium 6Zn-3Mg alloy was heat treated in various ways to independently alter precipitate free zone width and the area fraction of grain boundary precipitate. Above a certain area fraction, the crack path was intergranular and below this value it became transgranular. The K_{Ic} was lowest for complete intergranular fracture. The width of the PFZ had no affect on K_{Ic}. The results are summarized in Figure 21. This is, perhaps, what would be expected, as intergranular fracture is normally a low ductility mode of failure. However, commercial Al-Zn-Mg-Cu alloys have even lower energy paths than the grain boundaries viz the sheets of intermetallic compounds that are typically found in their microstructure. These alloys may commonly contain ~ 1% vol fraction of intermetallic particles resulting from the presence of Fe, Cr, Mn and Si. The Al-Cu-Mg-Si alloy RR 58 has ~ 1% Fe and 1% Ni which form, with aluminium, the bulky compound Fe Ni Al_9. Although the mean volume fraction of particles in these alloys may be considered high, the important fact is that the particles are segregated in such a way as to form sheets or stringers where locally there is a considerably higher volume fraction, up to ~ 25% as shown in Figure 22 (Reference 38). It is not surprising that these sheets of intermetallic compound, in themselves brittle and sometimes containing cracks and voids, form easy crack paths for tensile failure. As would be expected they are most effective in reducing the

K_{Ic} when the tensile stress is applied perpendicular to the sheet, i.e. in the short transverse direction[39]. Table I shows how orientation affected K_{Ic} for an alloy with the following composition:–
Al5.76 Zn2.48 Mg0.67 Cu0.28 Mn0.3 Fe Si < 0.02 Ti0.025.

The longitudinal K_{Ic} may be very high, even with a considerable volume fraction of intermetallic particles present. It is of some practical interest to note that the 'as cast' condition is comparable with the T/ST value which supports a more general conclusion from other work that the K_{Ic} values for castings are considerably higher than would be expected from considerations of their ductilities.

The effects of reducing the volume fraction of particles by reducing the iron content are shown in Figure 24 (Reference 40) where it can be seen that the short transverse K_{Ic} benefits more from removing the intermetallic particles than does the longitudinal K_{Ic}. It is interesting to note that by reducing the volume fraction of intermetallic particles the grain size increases and ductility decreases, and yet the K_{Ic} is improved. The fracture path for this higher K_{Ic} value is intergranular. This is not necessarily in conflict with the work described earlier where the tougher condition was associated with transgranular fracture, but indicates how effective the intermetallic particles are in reducing K_{Ic}.

The fracture feature on the K_{Ic} test piece that reflects the K_{Ic} value is the height of the cliff that connects the end of the fatigue fracture to the general plane of tensile fracture[41]. Figure 25 and Table II show the various dimensions of fracture and microstructural features, and zones that might interact to influence toughness. It can be seen that cliff height correlates well with half of the mean distance from fatigue crack tip to the nearest easy fracture path. The greater this distance the greater the K_{Ic} value.

True stress/true strain curves were determined using the transverse strain measuring technique[42], and Figure 26 shows plots of $G_{Ic}/C_{\epsilon f}$ for the Al-Zn-Mg-Cu alloys used in the previous investigation[43]. It can be seen that a linear relationship is obtained for each of the three alloys with different Fe content, but that varying the other elements and the direction of testing affects only their position on each of the parent lines. The plots are based on the following argument:

In the fracture toughness test an increasing load is applied until an increment of crack growth is detected. Since the local stresses are in excess of the yield strength a small plastically deformed zone is formed and pushed ahead of the advancing crack tip leaving a strip of deformed material on either side of the crack.

The plastic work done in this zone depends on (1) the size of the zone, (2) the extent to which plastic deformation occurs before void formation causes fracture, and (3) the fracture stress.

Assuming the material obeys Ludwik's law then the plastic work done in straining a unit volume to fracture

$$= \int_0^{\epsilon f} C\epsilon^n d\epsilon$$

$$= \frac{C\epsilon_f^{1+n}}{1+n} .$$

In the fracture toughness test the plastic deformation is concentrated in a strip of height $2r$ where r is the radius of the plastic zone at the advancing crack tip, so for a unit length of crack of unit thickness the total plastic strain would be

$$\frac{2r\, C\epsilon_f^{1+n}}{1+n} .$$

For the critical condition at the onset of fracture the elastic energy released as the crack grows equals the plastic work done to fracture.

Thus for the critical fracture conditions –

$$\frac{K_{Ic}(1-\nu^2)}{E} = \frac{2r\, C\epsilon_f^{1+n}}{1+n} .$$

Since for the alloys tested variations in C and n were small, ϵ_f and r were the main variables that controlled fracture toughness.

Thus the slopes of the plots in Figure 26 are equal to $2r$, the zone diameter involved in local fracture. The results suggest that the intermetallic particles can control plastic zone size by the quantity present, but that orientation does not affect zone size but affects ϵ_f. It is also interesting to note that magnesium does not affect the zone size, but again the amount of strain that occurs in the zone before fracture.

Similarly the effects of fine structure in general are not as clearly understood as the large particle/dimple contribution. Although it has been shown that there is a general yield strength – K_{Ic} relationship there are clearly anomalies present in the literature that suggest that the fine microstructural state, irrespective of its affect on tensile yield, can influence toughness, e.g. if one compares the underaged with the overaged state in some aluminium alloys (where the yield strengths are the same) it is commonly found that the material is considerably tougher and more resistant to fatigue crack propagation in the underaged state. Similarly this condition shows certain general characteristics in the true stress/true strain behaviour that appear to be significant. For equivalent yield strength the underaged state may have considerably higher n, ϵ_n and ϵ_f values than the overaged alloy. Thus the plastic work done to fracture is considerably greater in this state. Yield strength n, ϵ_f and C are inter-related properties, but the parameter $C\epsilon_f$ seems to control K_{Ic} for any given zone size. The reasons for the low n and ϵ_f exhibited by the overaged structure is not clear, and it should be added that extensive overageing may recover these values. There is some evidence for increased intergranular fracture in overaged alloys but it may be that total volume fraction of particles may be important. In a number of cases fracture has been observed to initiate at fine precipitate interfaces and the tendency for GP zones to form with attendant high precipitate density may be important.

4. CONCLUSION

The differences that may arise in both fatigue crack resistance and fracture toughness when comparing a variety of structural alloys must always be dependent on plastic or fracture zone size – microstructural relationships. Anomalies may appear where properties are critically dependent on these size relationships, thus the commonly measured tensile properties may not correlate with toughness or any of the fatigue parameters.

The literature highlights the common ground between the various metals and alloys. The metallurgist already has a considerable knowledge of the underlying fracture mechanisms and can now go some way towards outlining the principles of alloy optimization.

REFERENCES

1. Mason, W.P. — Symposium on Basic Mechanisms of Fatigue, ASTM STP 237, 1958 pp.36–50.
2. Fegredo, D.M. Greenough, G.B. — J. Inst. Metals. 87, 87 (1958–59).
3. McEvily, A.J. Machlin, E.S. — *Fracture* ed Averbach et al. Technology Press, Cambridge, Mass., 1959.
4. Thomson, N. et al. — Phil Mag 1, 113, 1956.
5. Partridge, P.G. — Phil Mag 12, 119 pp.1043-1054, 1965.
6. Partridge, P.G. — Acta Met 13, pp.517-525, May 1965.
7. McEvily, A.J. Boettner, R.C. — International Conference on Mechanisms of Fatigue, Orlando, Florida published in Acta Met 11, July 1963, pp.725-743.
8. Forsyth, P.J.E. — Cranfield Symposium on Fatigue crack propagation, October, 1961.
9. Forsyth, P.J.E. — Proceedings 15th Colloquium of Metallurgy – Fatigue (to be published), Saclay, June 1972.
10. Gough, H.J. — Edgar Marburg Lecture. Proc ASTM Vol.33, Part II, 1933.
11. Wood, W.A. — J. Inst. Met. Vol.100, p.73, 1972.
12. Feltner, C.E. Beardmore, P. — *Achievement of High Fatigue Resistance in Metals and Alloys.* ASTM STP 467, June 1969.
13. Finney, J. — Private Communication.
14. Hempel, M. — *Performance of Steel Under Repeated Loading.* Fatigue in aircraft structures, Academic Press, NY, 1956.
15. Forrest, P.G. Tate, A.E.L. — J. Inst. Metals, 1965, 93, 438.

16. Forsyth, P.J.E. Stubbington, C.A. — J. Inst. Metals, 85, pp.339-343, March 1957.

17. Stubbington, C.A. Forsyth, P.J.E. — Acta Met 14, pp.5-12, January 1966.

18. Stubbington, C.A. Bowen, A.W. — RAE Tech Report 72091, August 1972.

19. Grosskreutz, J.C. — USAF Conference on Fatigue and Fracture of Aircraft Structures – Miami, Florida, December 1969.

20. Forsyth, P.J.E. Smale, A. — Unpublished work.

21. Stulen, F.B. et al. — International Conference on Fatigue of Metals – Institution of Mechanical Engineers – London, 1956.

22. Yokobori, T. et al. — *Report of Research Inst. for Strength and Fracture of Materials* – Tohoku University, Vol.7, No.1, pp.1-23, November 1971.

23. Stubbington, C.A. Forsyth, P.J.E. — RAE Tech. Report 66201, June 1966.

24. George, R.W. Forsyth, P.J.E. — RAE Tech. Note Met/Phys. 352, January 1962.

25. Ostermann, F.G. Reimann, W.H. — *Achievement of High Fatigue Resistance in Metals and Alloys*, ASTM STP 467, June 1969.

26. Krause, A.R. Laird, C. — *Materials Science and Engineering*, MSCEA Vol.2, pp.331-347, 1967–68.

27. Williams, T.R.G. — RAE Tech. Note Met 274, October 1957.

28. Weber, J.H. — *Ph. D. Thesis – Effects of Crystallography and Thermomechanical Treatment on Fatigue Crack propagation*, Lehigh University, 1969.

29. Sandor, B.I. — *Achievement of High Fatigue Resistance in Metals and Alloys*, ASTM STP 467, June 1969.

30. Ryder, D.A. — *The Elements of Fractography*, AGARDograph No.155.

31. Pearson, S. — *Nature*, Vol.211, No.5053, pp.1077-1078, September 1966.

32. McEvily, A.J. Johnson, T.L. — International Conference on Fatigue, Sendai, Japan, September 1965.

33. Tiffany, C.F. Masters, J.N. — *Fracture Toughness Testing and Application*, STP 381.

34. Birkle, A.J. et al. — Trans. ASM Vol.59, pp.981-990, 1966.

35. Vishnevsky, C. Steigerwald, E.A. — Trans. ASM Quarterly, Vol.62, No.2, June 1969.

36. Archer, M.J. Martin, J.W. — J. Inst. Metals, Vol.96, pp.167-171, 1968.

37. Unwin, P.N.T. Smith, G.C. — J. Inst. Metals, Vol.97, pp.299-310, October 1969.

38. Forsyth, P.J.E. Smale, A. — Unpublished RAE work.

39. Peel, C.J. Forsyth, P.J.E. — RAE Tech. Report 69011, January 1969.

40. Peel, C.J. Forsyth, P.J.E. — RAE Tech. Report 70162, September 1970.

41. Peel, C.J. et al. — Metal Science Journal, Vol.6, pp.102-106, May 1972.

42. Forsyth, P.J.E. Smale, A. — *Engineering Fracture Mechanics*, Vol.3, pp.127-138, 1971.

43. Peel, C.J. Forsyth, P.J.E. — RAE Tech, Report 72173, November 1972.

TABLE I (See also Figure 23)

Condition	*Direction of test*	YS ksi	K_{Ic} ksi$\sqrt{in}$	*Elongation* % on $4\sqrt{A}$
As cast	Trans/long mean of four values	70	20.2	2.9
Fully forged	Long/trans mean of two values	71.7	35.9	12.5
	Trans/S trans mean of two values	68.3	19.3	8.0
	S trans/long mean of two values	70.3	14.8	2.0

TABLE II (Ref. 41)

Measured and Calculated Feature Size (μm)

	Alloy 1 0.05% Fe	*Alloy 2* 0.30% Fe	*Alloy 3* 0.74% Fe
Stretched zone	20 ± 4.1	6.5 ± 0.9	3.4 ± 0.8
Cliff height	28 ± 5.2	12 ± 2.1	12 ± 2.7
Grain-boundary spacing	111 ± 22	21 ± 2.2	44 ± 4.6
Intermetallic-stringer spacing	–	48 ± 7.8	50 ± 6.8
Dimple dia.	1.8	3.3	4.0
Plastic zone size $\frac{1}{6\pi}\left(\frac{K_{Ic}}{\sigma_y}\right)^2$	104	54	54
Plastic zone size $\frac{1}{6\pi}\left(\frac{K_f}{\sigma_y}\right)^2$	33	19	12
Crack-opening displacement $\frac{K_{Ic}^2}{E\sigma_{YS}}$	13	6.8	6.4
Crack-opening displacement $\frac{K_f^2}{E\sigma_{YS}}$	4.3	2.4	1.4

(a)

(b)

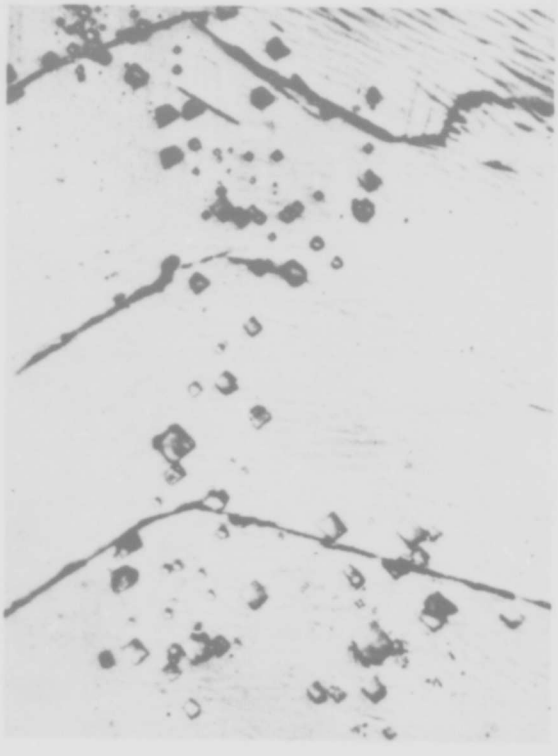

(c)

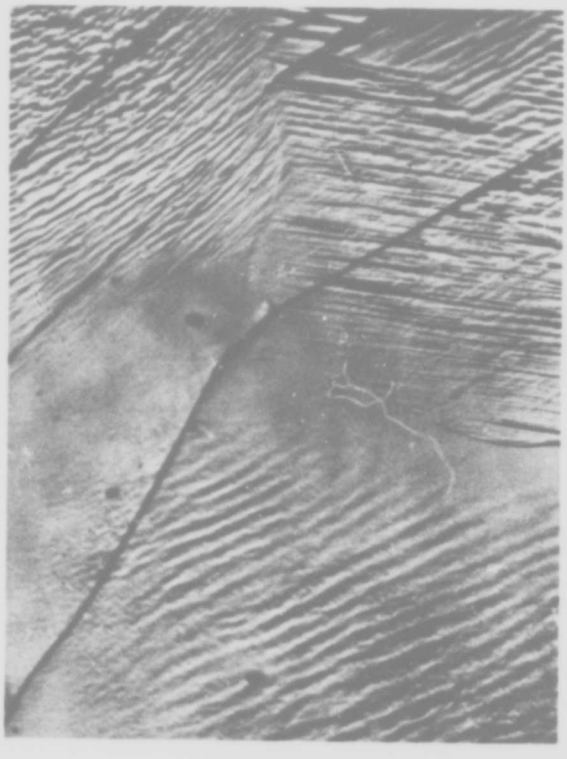

(d)

Fig.1 (a), (b), (c) and (d). Fatigue aluminium showing slip bands, cracks and etch pits. X500

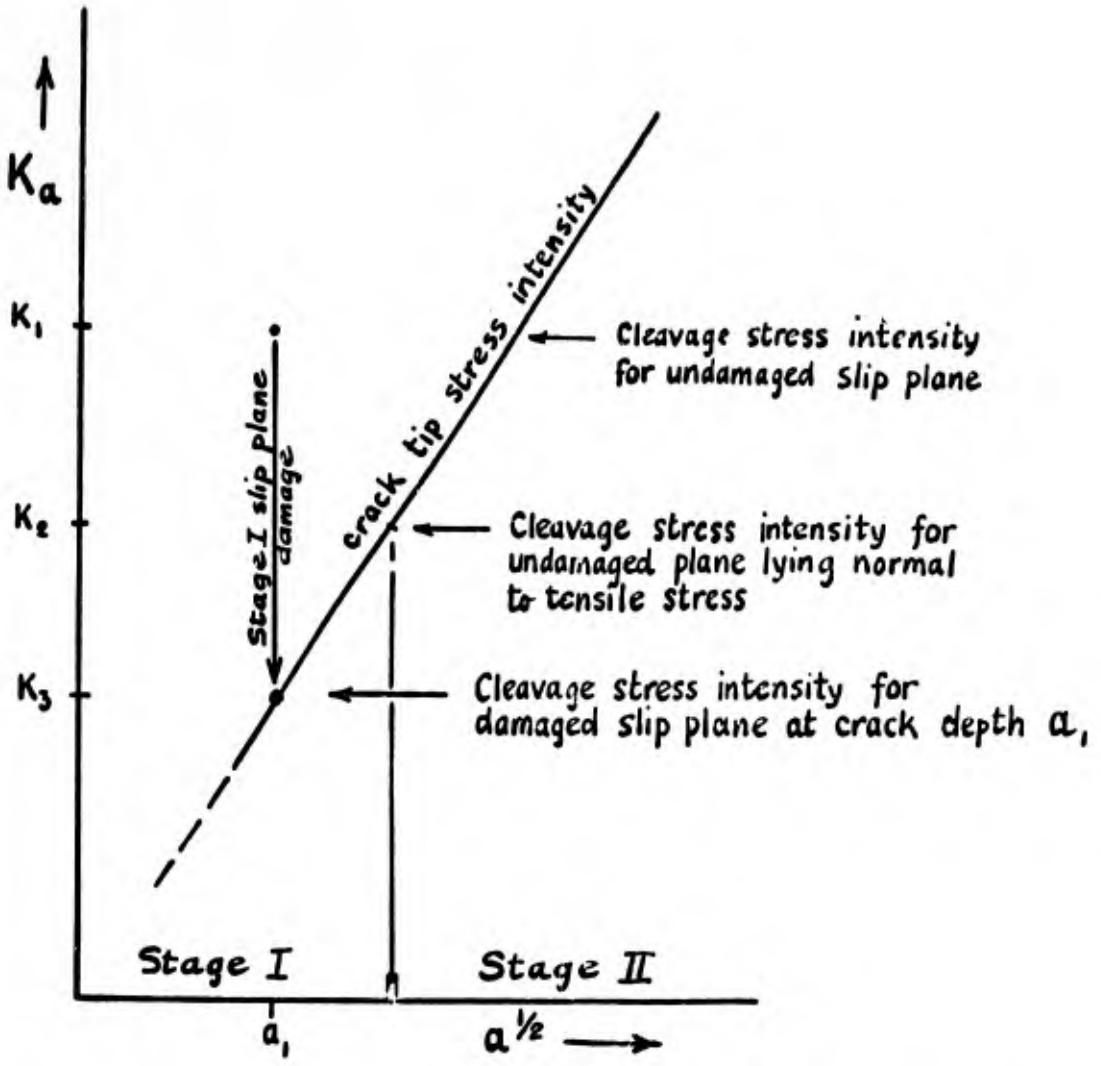

Fig.2 Stress intensity/crack depth relationship with Stage I/II changeover

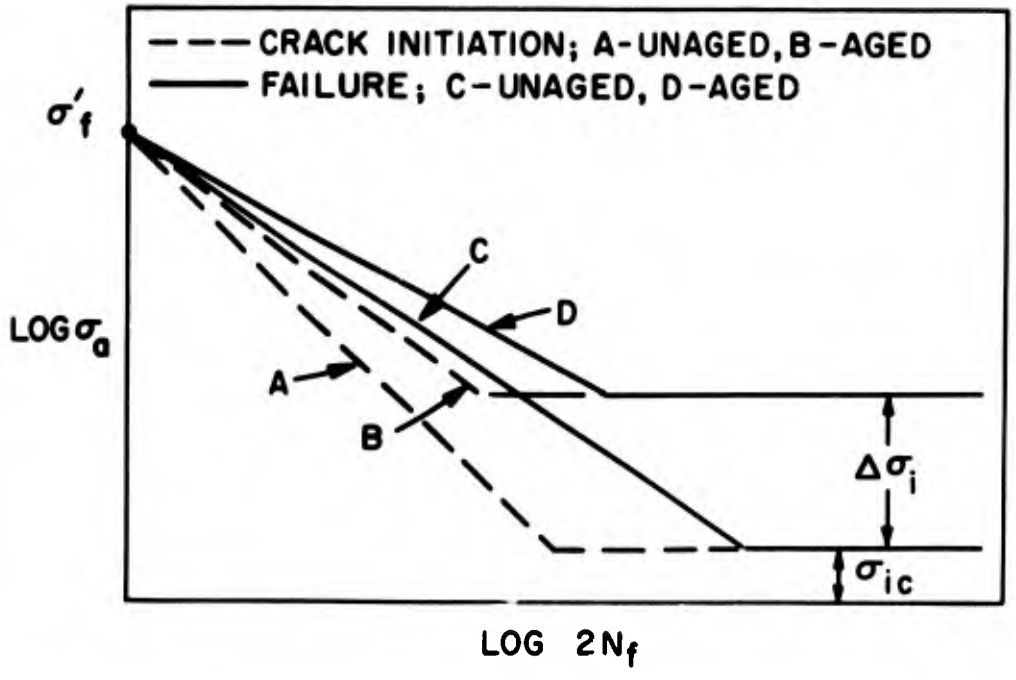

Fig.3 Schematic influence of ageing reaction on stress-life behaviour. (Ref.12)

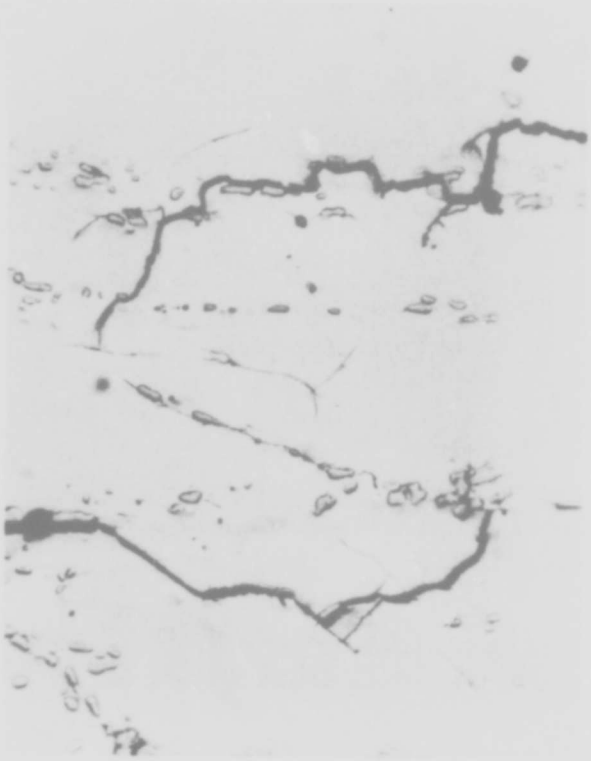

Fig.4 Transversely fatigue stressed RR 58 alloy showing initial cracks. X250

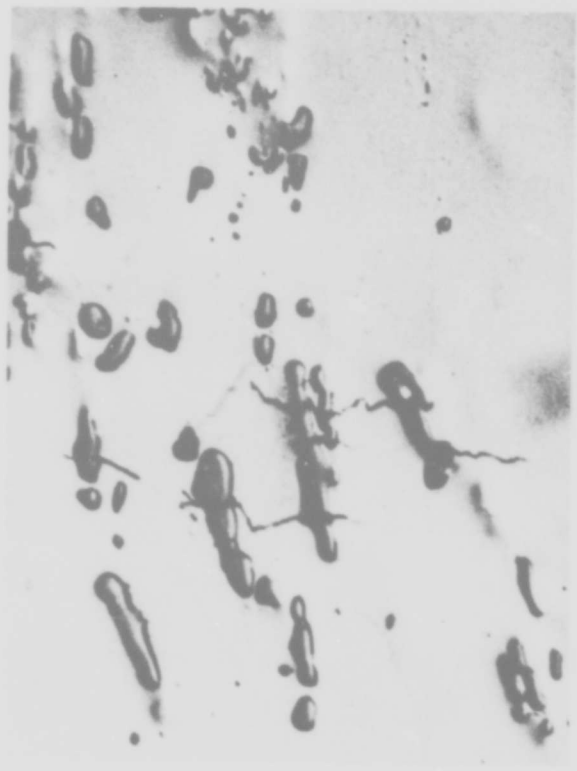

Fig.5 Cracks growing from previously cracked $FeNiAl_9$ alloy. X1000

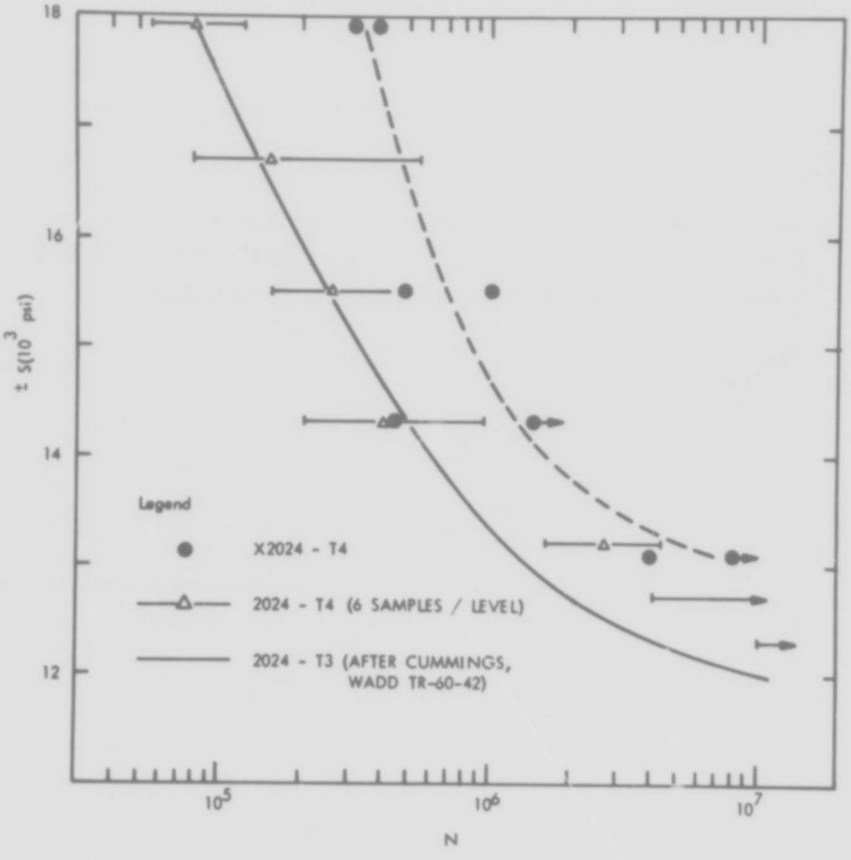

Fig.6 S/N curves for 2024 alloy (Ref.19)

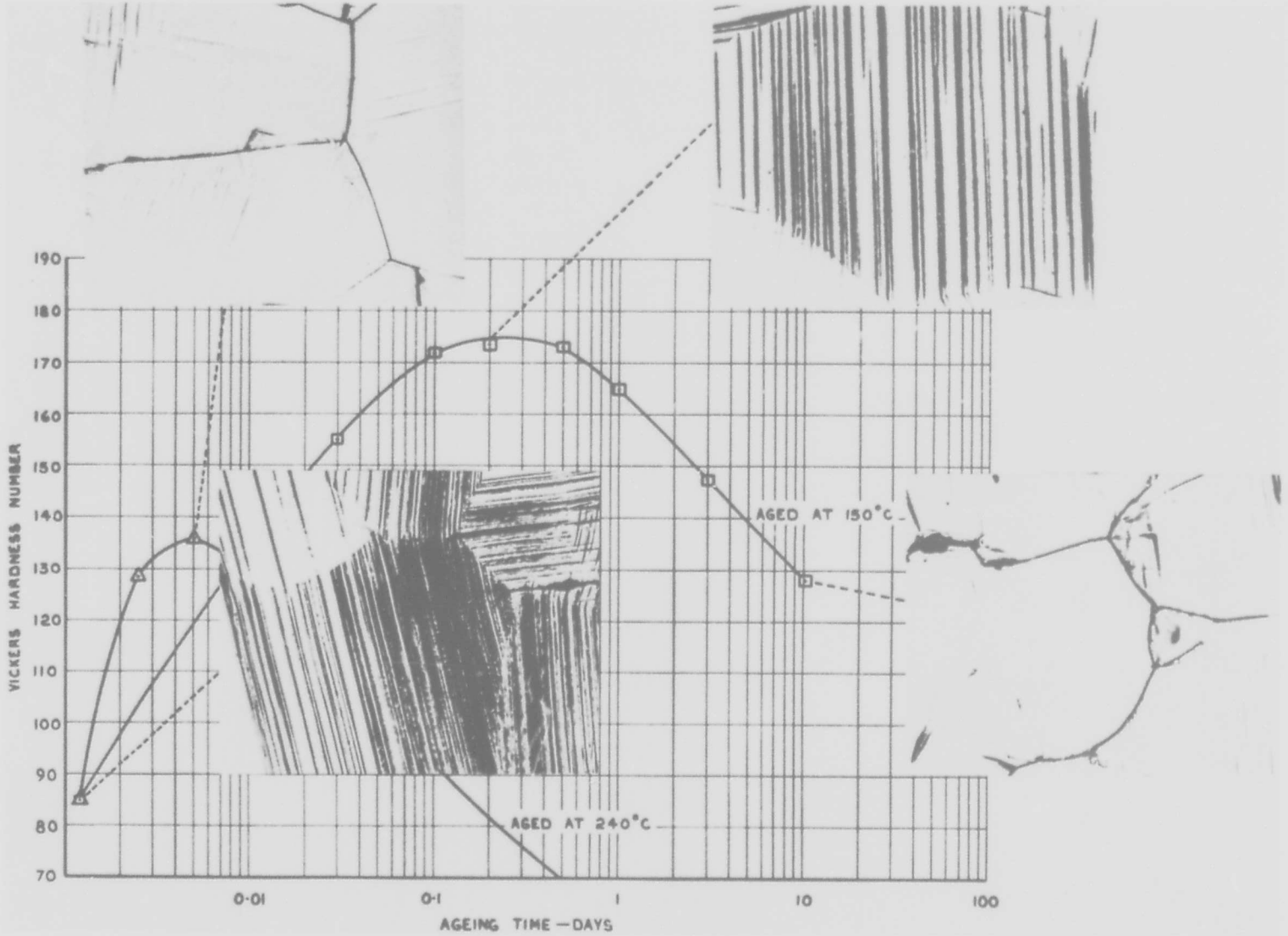

Fig. 7 Ageing curves for aluminium–7.5% zinc–2.5% magnesium alloy, solution treated at 450°C, cold water quenched and aged at 150°C and 240°C, with example of deformation produced by torsional fatigue on specimens tested in various conditions of heat treatment

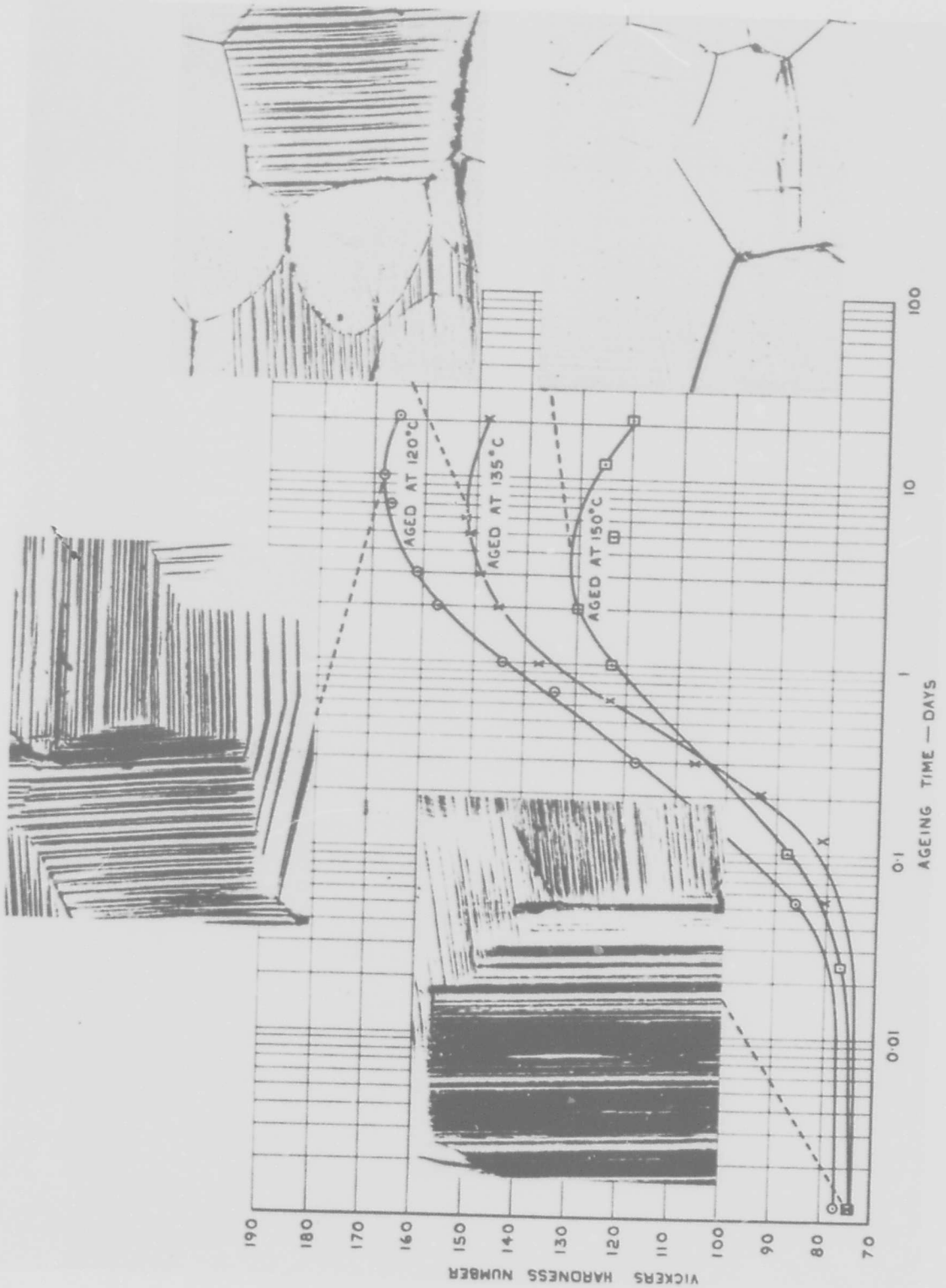

Fig.8 Ageing curves for aluminium–4% zinc–5% magnesium alloy, solution treated at 470°C, cold water quenched and aged at 120°C, 135°C and 150°C, with example of deformation produced by torsional fatigue on specimens tested in various conditions of heat treatment

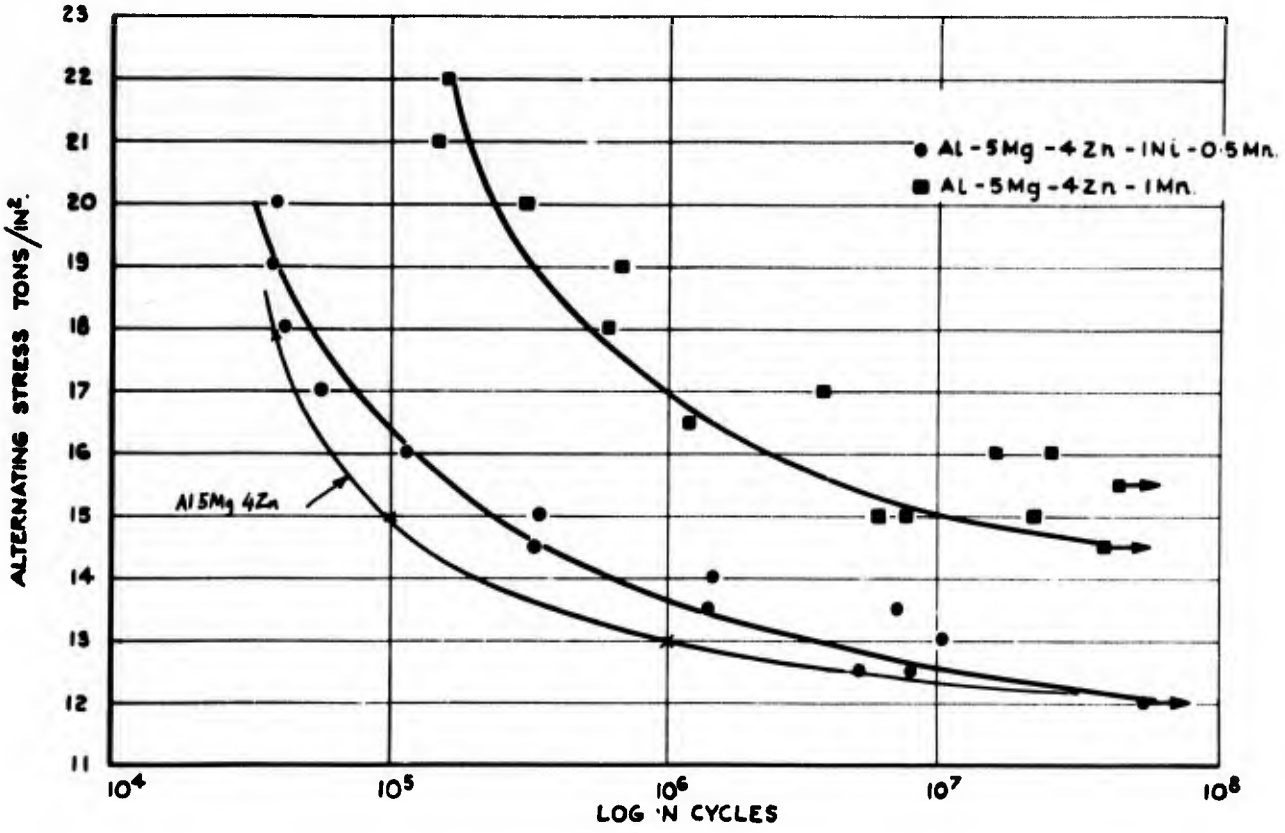

Fig.9 Fatigue curves for alloys based on the ternary alloy Al-5Mg-4Zn

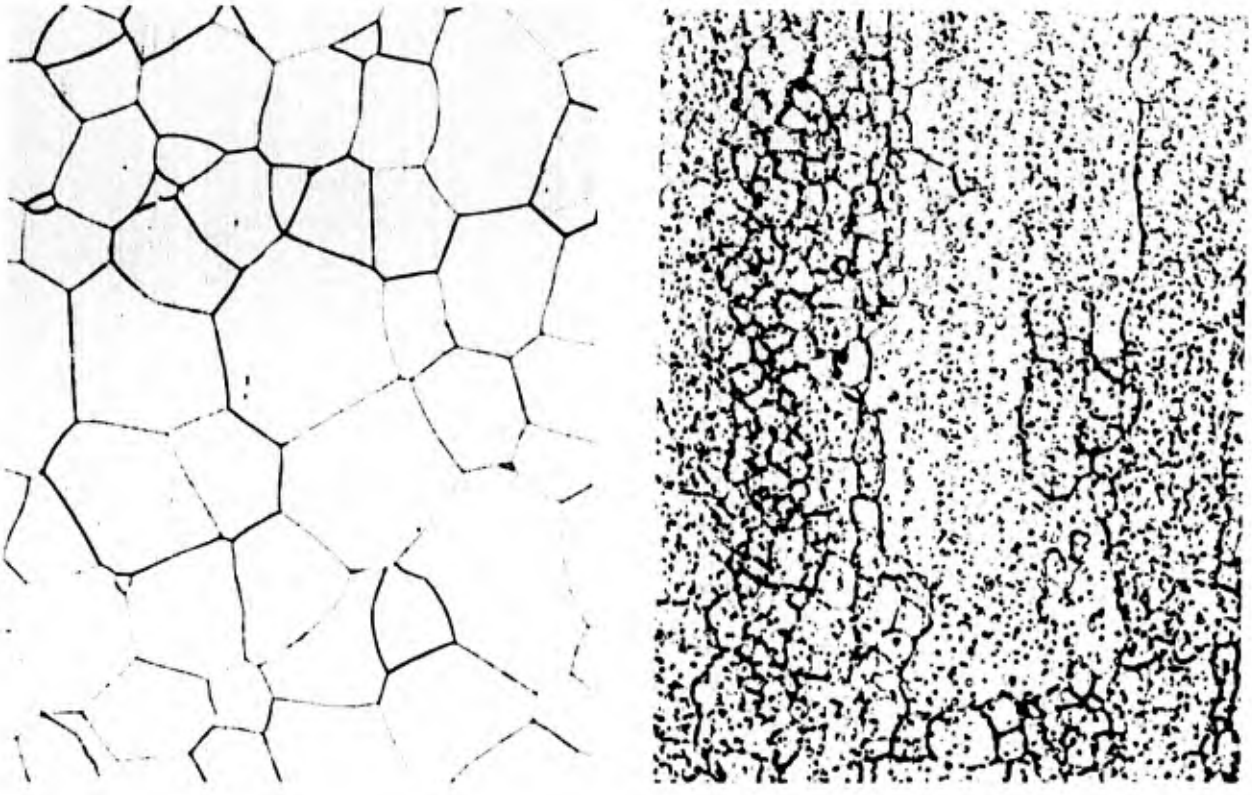

(a) (b)

Fig.10(a) Microstructure of Al-5Mg-4Zn alloy. X500
(b) Microstructure of Al-5Mg-4Zn-1Mn alloy. X500

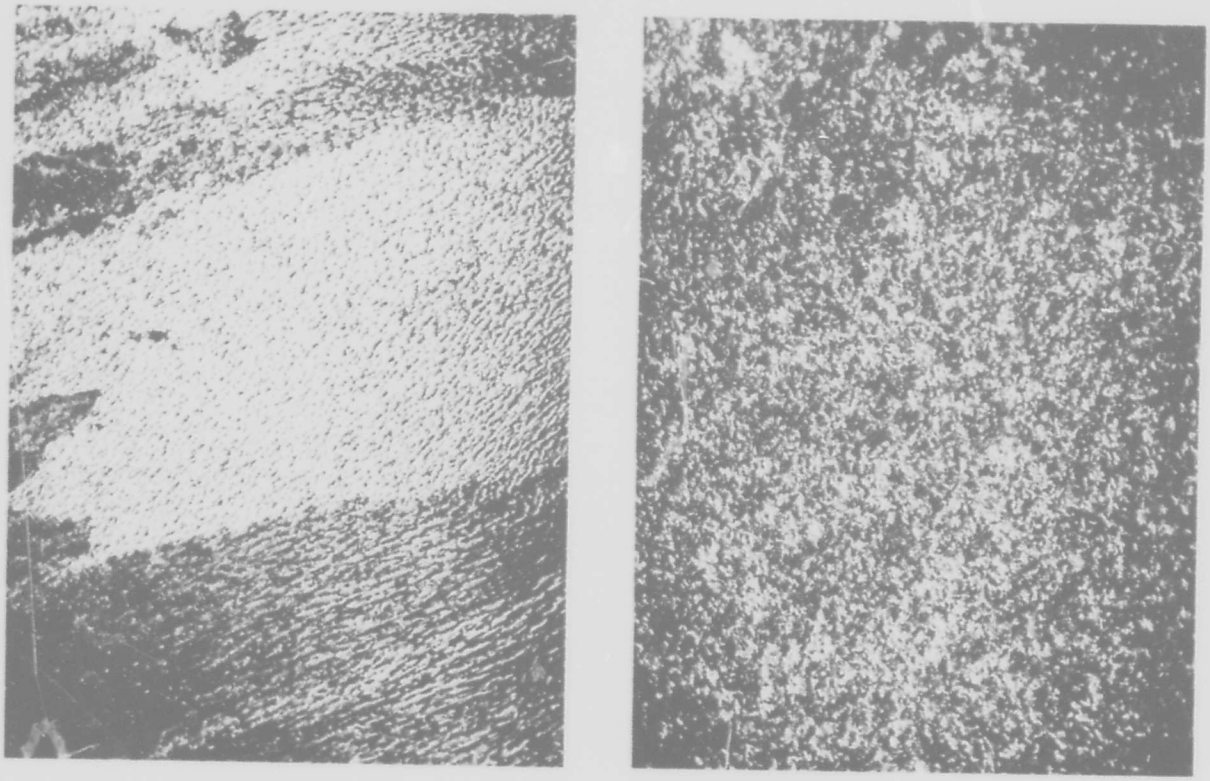

(a) (b)

Fig.11(a) Microstructure of Ti-6Al-4V alloy, large bar. X100
(b) Microstructure of Ti-6Al-4V alloy, small bar. X100

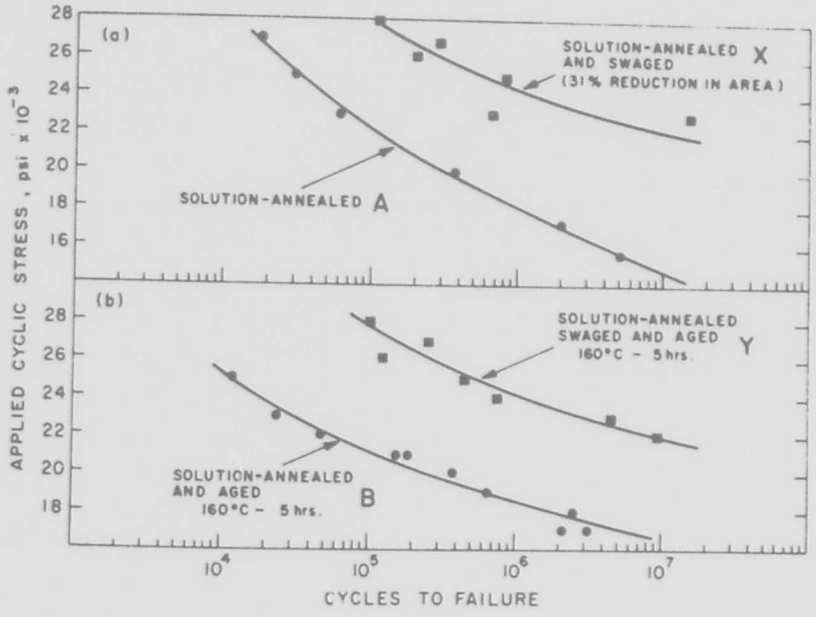

Fig.12 S-N curves showing the effects of various thermomechanical treatments on the fatigue properties of Al-4Cu alloy. (Ref.25)

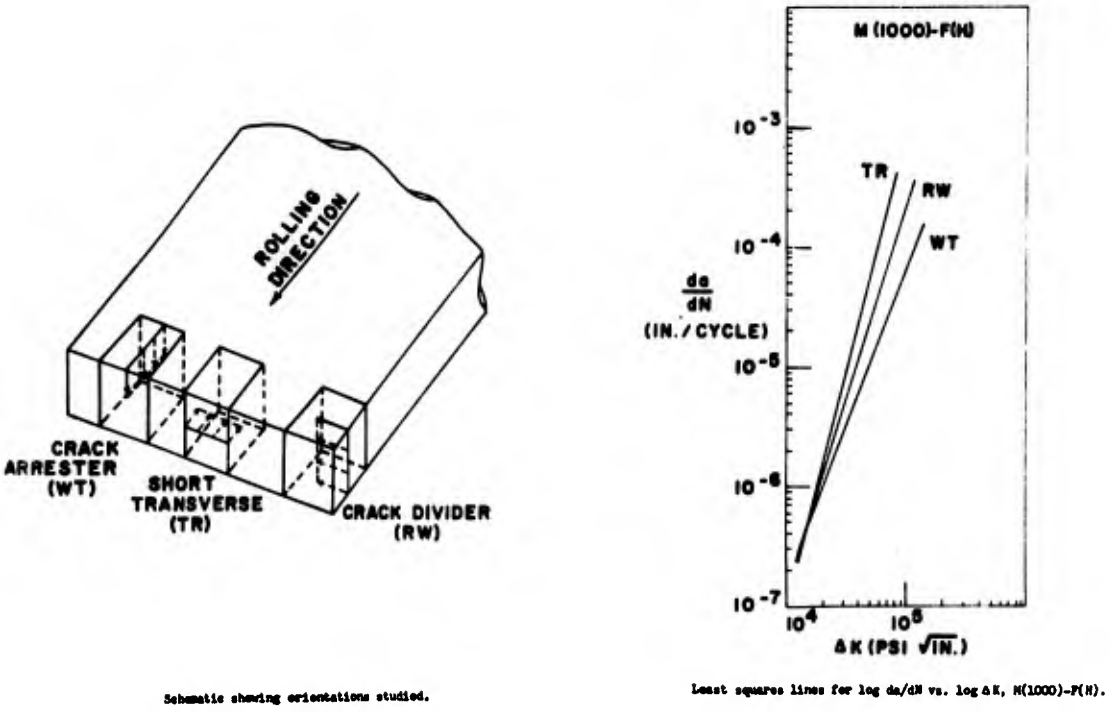

Fig.13 Fatigue crack growth curves for rolled steel plate. (Ref.F.Heiser Ph.D. Thesis, Lehigh Univ.)

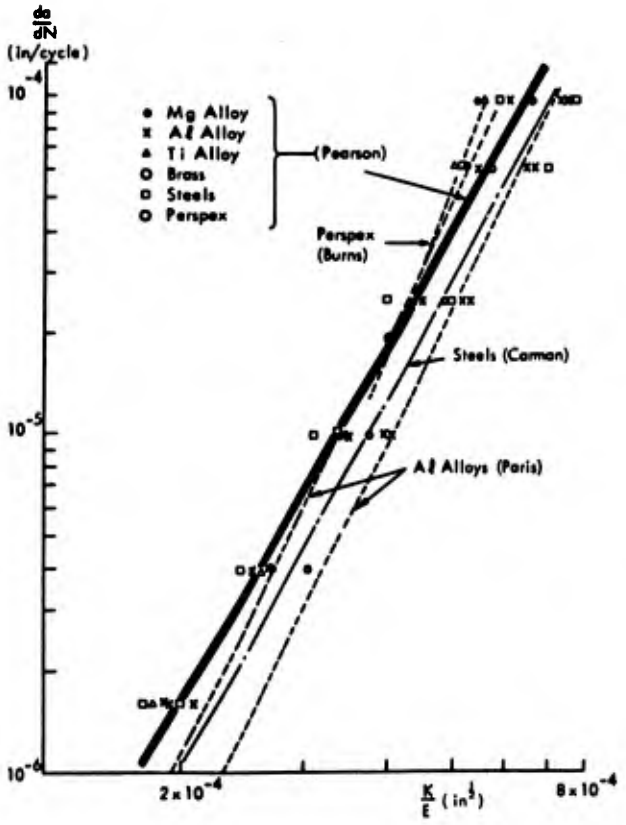

Fig.14 Crack propagation rates as a function of K/E for various materials. (Ref. S.Pearson)

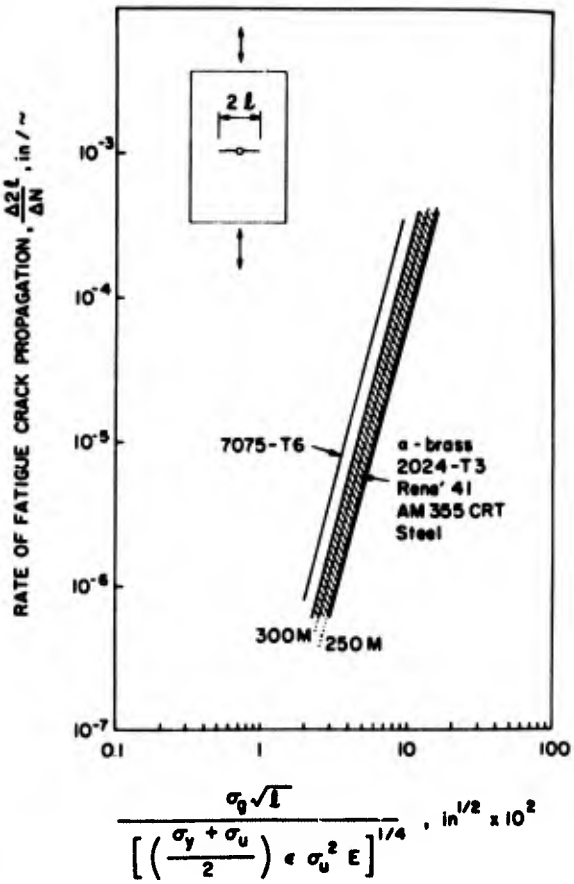

Fig.15 Normalized fatigue crack growth rates for 18Ni (250) maraging steel, 18Ni (300) maraging steel, and other alloys. (Ref.32)

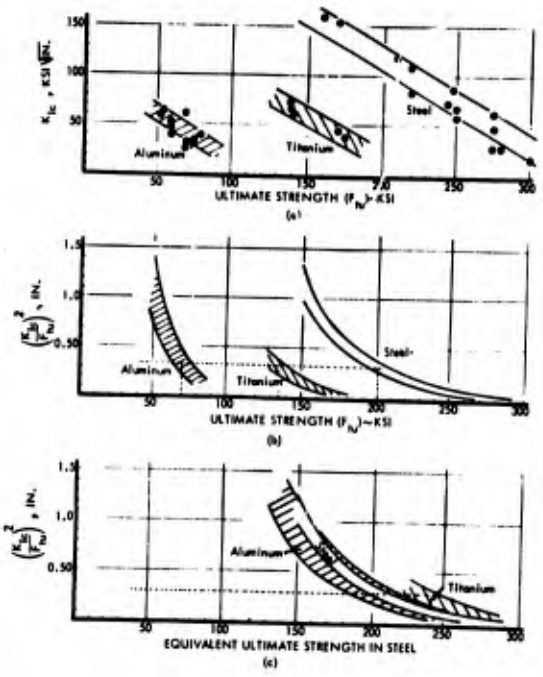

Fig.16 Material comparisons (base metal, room temperature trends) (Ref.33)

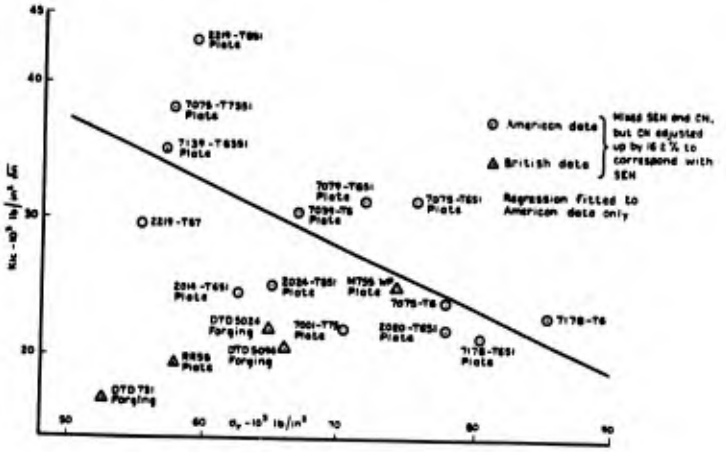

Fig.17 Fracture toughness versus yield strength. British and American data. Transverse tests. Valid data only $\left[2.5\left(\frac{K_{IC}}{\sigma_y}\right)^2 \geq \text{thickness} \right]$.

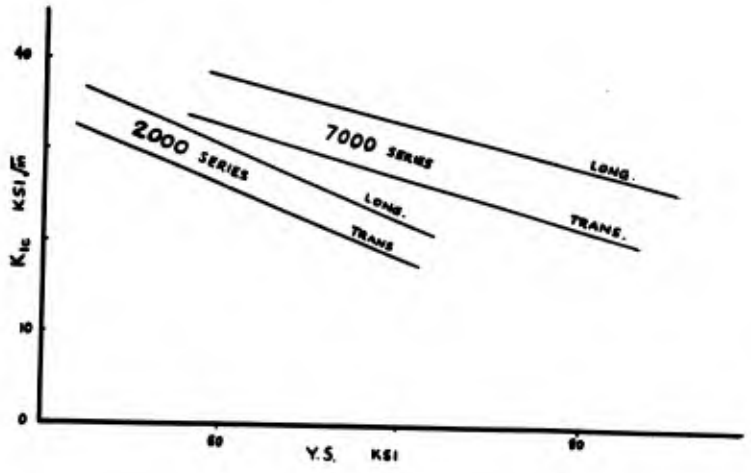

Fig.18 2000, 7000 series alloys, K_{IC} – yield strength

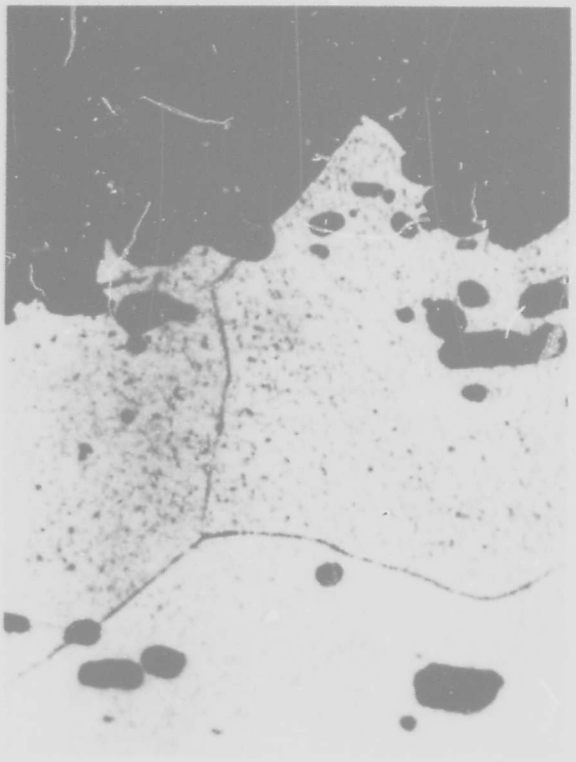

Fig.19 Part intergranular tensile fracture, RR 58 alloy. X1750

Fig.20 Maraging steel, cleavage and intergranular fracture. X1000

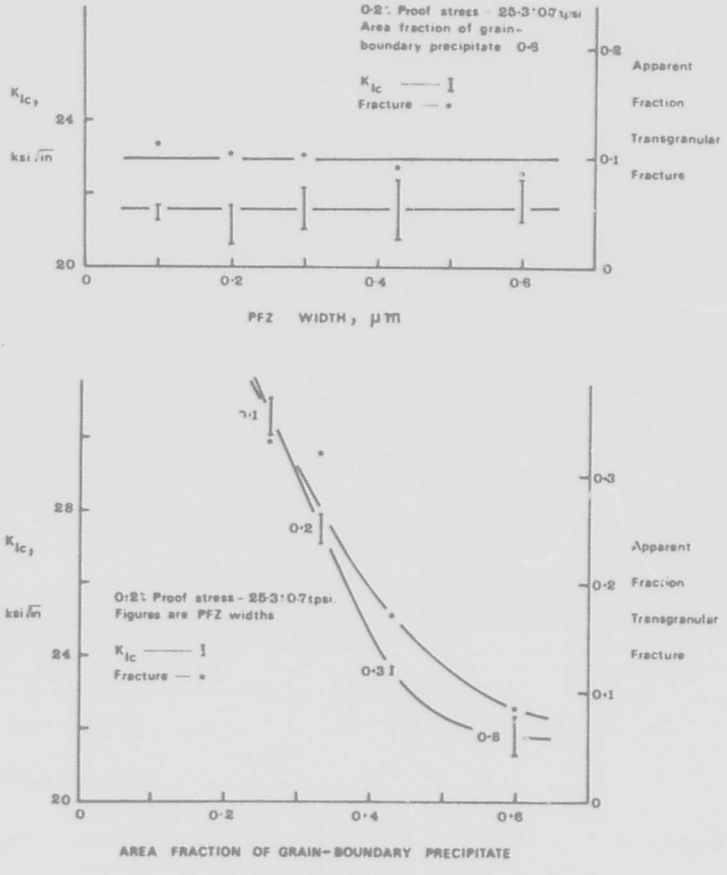

Fig.21 K_{IC} versus area fraction of grain boundary precipitate. (Ref.37)

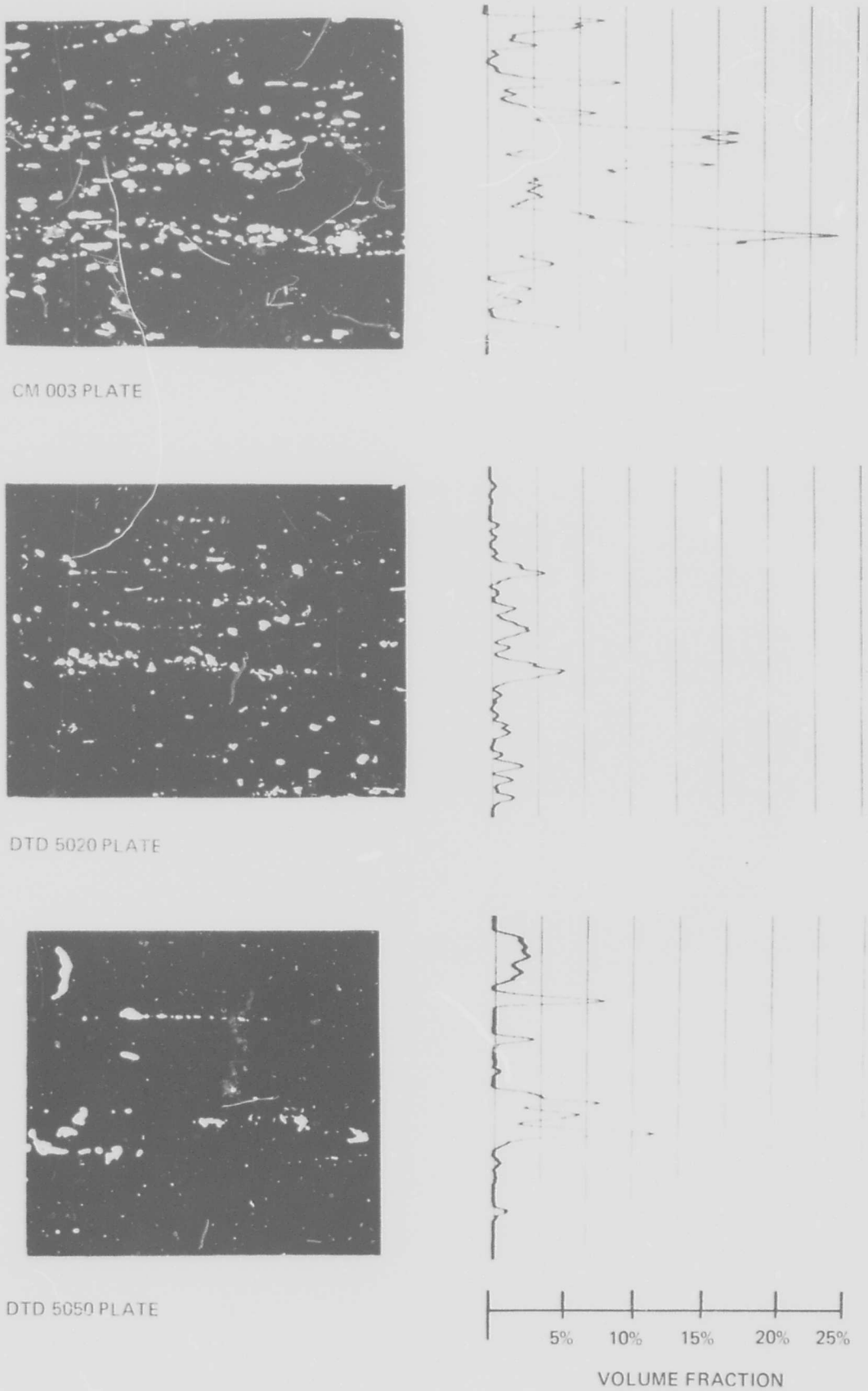

Fig.22 Volume fraction distribution curves with associated microstructures, matrix black, particles white

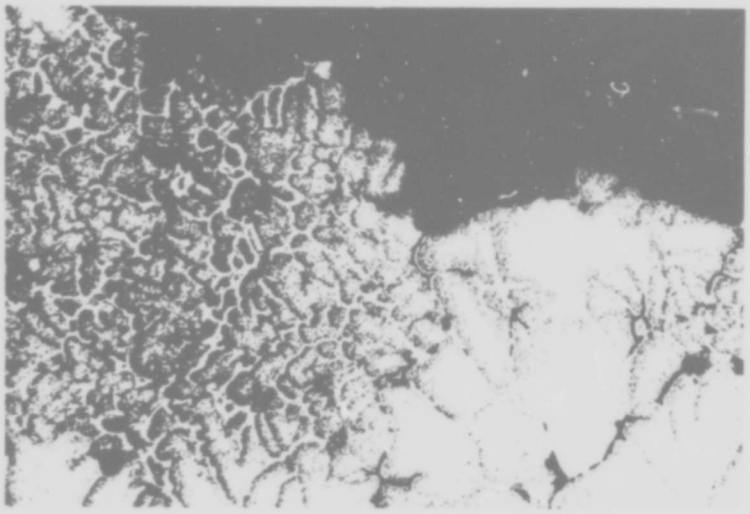

(a) "as cast"

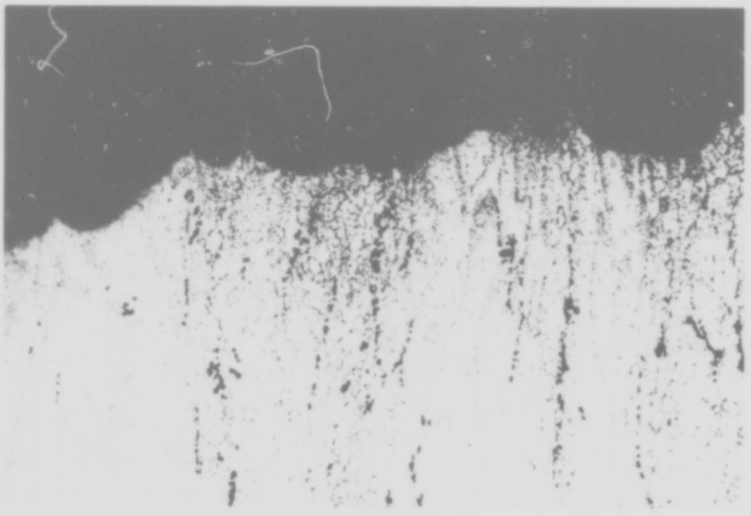

(b) longitudinal

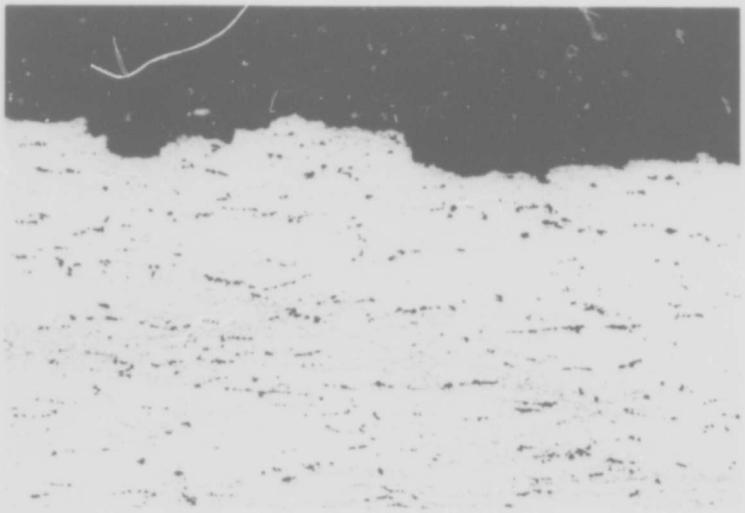

(c) transverse

Fig.23 Tensile fractures from K_{Ic} specimens DTD 5024. X100

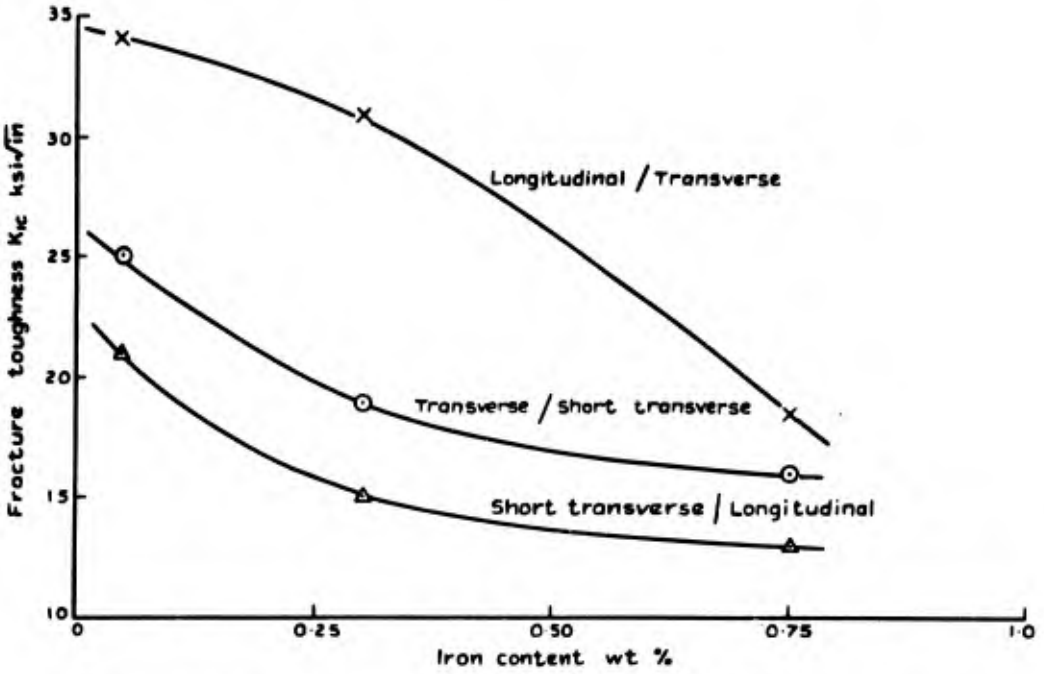

Fig.24 The effect of iron content upon fracture toughness DTD 5024. (Ref.40)

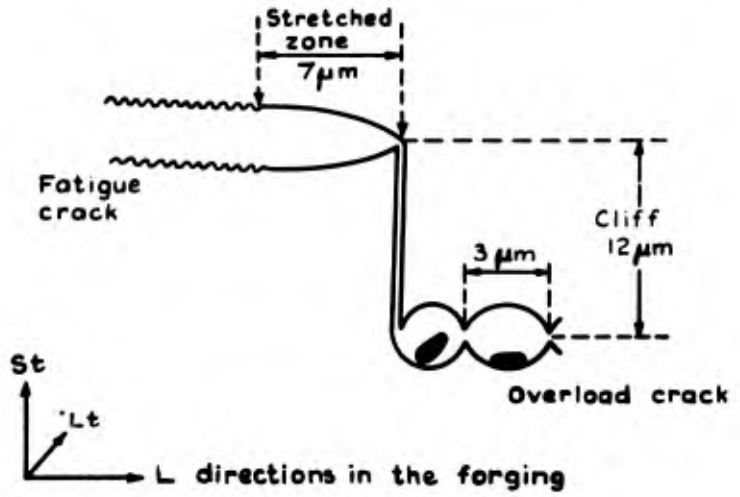

Fig.25 Schematic diagram of a section through a fracture-toughness test piece at the fatigue/overload transition. Feature sizes relate to alloy 2. See Table II. (Ref.41)

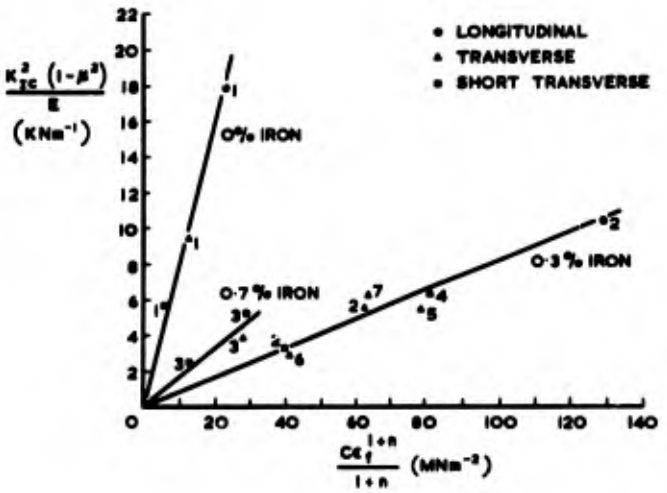

Fig.26 G_{IC}/C_{ϵ_f} plots for alloys specified in Table II. (Ref.43)

SOME RECENT DEVELOPMENTS IN FATIGUE AND FRACTURE

by

A.R.Rosenfield
University of Connecticut
Storrs, Connecticut
United States

and

A.J.McEvily
Battelle Columbus Laboratories
505 King Avenue
Columbus, Ohio 43210
United States

1. INTRODUCTION

The metallurgical factors affecting fatigue and fracture have received increasing study in recent years. Particular attention has been focused on high strength alloys of interest in aerospace applications. The major problem is that whereas high strength alloys need to be used at high stresses to maximize performance, their tolerance for flaws under both monotonic and cyclic loading as well as in both inert and agressive environments is often less than that of lower strength materials. These problems were touched upon during both the Munich Fracture Conference* and the Cambridge Strength Conference.† A sattelite meeting of the Munich Conference was also held at Cambridge and was devoted to slow crack growth.†† This paper discusses the developments at these three meetings and supplements the information presented with recent research on microstructural origins of the fracture resistance of high-strength alloys. Other topics, which received large attention, such as COD evaluation of fracture toughness of structural steels, are beyond the scope of this paper.

To provide a unified basis for discussion, schematic crack growth versus stress intensity curves are presented in Figure 1-1. Two mechanisms are considered: fatigue and stress corrosion cracking. Both phenomena exhibit three stages of crack growth.

(a) A threshold below which crack growth is not detected. Note that the threshold is much higher for stress corrosion than for fatigue.

(b) A steady-state region, constant velocity for environmental attack and power-law behavior for fatigue.

(c) An instability characterized by the fracture toughness, K_c (or K_{Ic} for plane strain, thick section behavior).

We will discuss each of these stages individually and then provide some general comments.

2. FATIGUE

At the three recent conferences covered in this review well over 100 papers were presented which dealt with the topic of fatigue. Despite this large effort much more remains to be done as indicated by the following listing (Grosskreutz 1973) of important research areas:

(a) The development of a quantitative theory of fatigue hardening.

---

* III International Conference on Fracture, April, 1973.

† *The Microstructure and Design of Alloys*, the III International Conference on Strength of Metals and Alloys, August, 1973, herein referred to as C2.

†† British Steel Corporation Conference, *Mechanics and Mechanisms of Crack Growth*, Cambridge Univ., April, 1973, herein referred to as C1.

(b) Understanding and predicting the stability of metallurgical and dislocation microstructures under cyclic loading.

(c) Documentation of the effects of strain rate and temperature on cyclic stress-strain response.

(d) The development of a model for crack initiation in high strength materials, particularly in long-life fatigue.

(e) The determination of the effects of environment on the rate of fatigue crack initiation.

(f) The determination of the mechanisms and rates of Stage I fatigue crack growth as a function of temperature, environment and materials properties.

(g) The prediction of the effect of environment-material couples on Stage II crack growth rates.

(h) The definition of the structure-sensitive aspects of Stage II crack growth rates.

(i) The study of load interaction effects on the fundamental mechanisms of the fatigue sequences.

(j) The study of creep-fatigue interactions and their effect on fundamental mechanisms of fatigue.

In this review the topics of alloy modification, thermal-mechanical processing (TMP), and fatigue crack growth will be emphasized. Additional topics are covered in the first paper of this report by Forsyth (1973).

2.1 Alloy Microstructural Modifications

In high strength aluminium alloys fatigue cracks often nucleate at relatively large second phase particles ($\sim 5\ \mu$ in size), and it seems reasonable that a reduction in the number and size of such particles should have a beneficial effect on fatigue lifetimes. Figure 2-1 illustrates the improvement obtained with 2024-T4 by a reduction in the volume fraction of second phase particles from 0.09% to 0.00016% (Grosskreutz 1970). The reduction in inclusion content has much less effect on fatigue crack propagation; experiments with RR 58 have shown that reducing the number of cracked particles did not reduce the crack rate (Forsyth 1973). Extended homogenization times prior to forging of Al-Zn-Mg-Cu-Cr alloys have been used to dissolve the nonequilibrium phase $CuAl_2$ as well as the impurity phases $FeAl_3$ and Cr_2Al (Mulherin and Rosenthal 1971). Figure 2-2 indicates the improvement obtained in this instance. (Fe and Si were much less than 0.01%.) Although some improvement has been noted in the cases cited, in other studies the reduction in particle content has been without effect on fatigue life (Thompson 1973). Further, the comparisons cited are based upon polished specimen data where the presence or absence of particles may have greatest effect; for surfaces characteristic of manufactured components, any differences due to reduction in particle content may be less apparent. Reduction in particle content may therefore have its greatest practical effect on some other property such as fracture toughness.

Attention has also been directed at the effect of finer particles or dispersoids on fatigue, and Figure 2-3 indicates the improvement obtained in one case (Forsyth 1973). Dispersoids in this material result from the addition of nickel and manganese and they are about $1\ \mu$ in size. Their presence also brings about a beneficial reduction in grain-size. The effect of small inclusions ($0.1-0.2\ \mu$) in 2024 aluminum has also been investigated (Lüterjing, et al. 1973). The composition of the commercial version of this alloy is 4.6 Cu, 1.7 Mg, 0.77 Mn, 0.36 Fe, and 0.28 Si. A pure version (X2024) contained 4.7 Cu, 1.5 Mg, 0.006 Mn, 0.04 Fe, and 0.03 Si. Large inclusions with a size of about $5\ \mu$ were present in each alloy; these particles belong to the equilibrium S-type phase of the Al-Cu-Mg system which could not be dissolved by the homogenization treatment. Figure 2-4 indicates the difference in fatigue life for these two alloys. The observed difference in lifetimes involved the crack initiation stage since studies of crack growth behavior showed the rates of crack growth to be similar. The beneficial influence of the $0.1\ \mu$ inclusions on fatigue lifetime was attributed to their effect on slip dispersal. In the pure alloy slip was heavily concentrated in narrow bands, whereas in the commercial alloy slip was more uniformly distributed.

2.2 Thermal-Mechanical Processing (TMP)

In an effort to improve the fatigue resistance of aluminum alloys TMP procedures continue to be explored. The objective of the approach is to provide a more homogeneous microstructure and to disperse the slip which occurs during cyclic loading. A recent innovation (Paton and Sommer 1973) involves aging to peak hardness and then deforming above the GP solvus to obtain a more uniform initial dislocation distribution. A compilation of published TMP procedures for aluminum alloys is given in Table 2-1.

TABLE 2-1

Thermal-Mechanical Processing Treatments Aluminum Alloys*

(1) Thomas (1960–61)

(a) Alloy – DTD687 (2.9 Mg, 5.9 Zn, 0.5 Cu, 0.1 Cr, < 0.48 Fe + Si + Ti)

(b) TMP – 460°C/12 hr – WQ 80°C–150°C/1/2 hr – deform 5–10% – age up to 24 hrs at 150°C

(c) Effect – stress corrosion life (unnotched) improved in averaged condition.

(2) Ostermann (1971)

(a) Alloy – commercial 7075 (0.11 Si, 0.04 Mn, 0.26 Fe) – X7075 (< 0.015, < 0.01 Mn, 0.01 Fe)

(b) TMP – 460°C/1 hr – WQ – 100°C/1 hr – Swage; alloy C 30%, alloy X 10% – 120°C/16 hrs.

(c) Effect – improvement in smooth bar fatigue lifetimes.

(3) Reimann and Brisbane (1973)

(a) Alloy – commercial 7075

TMP – 1. 7075-TMT – 465°C/WQ – 100°C/1 hr – 10% cold work – 120°C/16 hr
2. 7075-TMTII – as for (1) plus 165°C/6 hr

(b) Effect – no improvement in notched fatigue properties.

(4) McEvily, et al. (1963)

(a) Al – 10 Mg

(b) TMP – 446°C/16 hr – WQ – reduce 50 – 200°C/ 5 hr

(c) Effect – improvement in unnotched sheet fatigue lifetimes

(5) McEvily, et al. (1967)

(a) Alloy – Al–5.5 Zn–2.5 Mg

(b) TMP – 393°C/20 min. – reduce 50% – 121°C/5 hr

(c) Effect – some improvement in unnotched fatigue life, marked improvement in resistance to stress corrosion cracking.

(6) Titchener and Ponniah (1973)

(a) Alloy – extruded HE30TE (Al-Mg-Si-Mn)

(b) TMP – 505°C/25 min. – WQ 0°C–30% reduction-straighten at 200 MN/m^2 – 150°C/1.5 hr (TH)

(c) Effect – improvement in unnotched fatigue properties.

(7) Paton and Sommer (1973)

(a) Alloys – 2024, 7049, 7075. high purity Al–5.5 Zn–2.5 Mg

(b) TMP – 2024 – T351 + 15% deformation at 190°C + 190°C/2 hrs
7049 – T6 + 15% deformation at 163°C + 150°C/3 hrs
+ 5% deformation at 25°C + 120°C/1 hr
7075 – T6 + 15% deformation at 193°C + 163°C/3 hrs

(c) Effect – improvement in stress corrosion resistance (K_{ISCC}) without loss of tensile or fracture toughness properties

(Continued)

* Conference papers C2-14, 19, 20, 22, 23, 126, 127, 128 deal with TMP in other alloy systems.

TABLE 2-1 (continued)

(8) Thompson, et al. (1973)

(a) Alloys – Al-Zn-Mg-Cu-Zr (5 in all)

(b) TMP – 470°C/1 hr + 480°C/1 hr + 510°C/5–16 hrs – WQ – 20°C/4 days
– 120°C/4 hrs or 120°C/4 hrs + 170°C/14 hrs
– 4 levels of cold or 165°C rolling: 120–165°C/0–16 hrs 20–30%

(c) Effect – A good combination of fracture toughness, strength and corrosion resistance could be obtained by TMP. An increase in Cu or Mg content at constant yield strength had an adverse effect on toughness.

It is clear that the unnotched fatigue properties can be improved by TMP (Ostermann 1971), Figure 2-5. However, the absence of a corresponding improvement in notched fatigue properties must be regarded as a disappointment (Reimann and Brisbane 1973), Figure 2-6. The reason underlying this increase in notch-sensitivity is a matter for further study. However, even without improvement in fatigue properties, improvements in resistance to stress corrosion and in fracture toughness provide incentives for further work in this area.

2.3 Fatigue Crack Growth

The general characteristics of the rate of fatigue crack growth, $\Delta a/\Delta N$, as a function of stress-intensity range, ΔK, are shown in Figure 2-7. Two asymtotes exist; one at low ΔK levels, ΔK_{TH}, the other at high ΔK levels corresponding to K_c. There are structure-sensitive aspects to both of these limits, and these will be discussed in more detail in subsequent sections. In the intermediate range of growth rates of 10^{-5} in/cycle or so, the crack growth process is almost structure insensitive, at least for materials of high toughness. In this range Young's modulus appears to be the most important mechanical parameter. The following sections deal with varying aspects of fatigue crack propagation in some greater detail.

Threshold Level

Fatigue crack growth near the threshold has been found (Birbeck et al. 1971) to be structure sensitive in the case of low carbon steel tested in air. At low growth rates the crack path changed direction at ferrite grain boundaries, revealing the grain structure. This transgranular structure-sensitive crack, designated Stage IIa, was further characterized by markings roughly parallel to the direction of crack propagation, representing a "hill and valley" structure on the fracture surface. A second mode, observed at higher growth rates and designated IIb, was insensitive to microstructure, and was characterized by a more featureless fracture surface with no evidence of the underlying structure. A transition from Stage IIa to Stage IIb growth was found to occur when the plastic zone size r_y, taken as $\frac{1}{5.6\pi}\left(\frac{K_{max}}{2\sigma_y}\right)$, was equal to about four times the ferrite grain diameter. It was suggested that the larger size decreased constraints on the number of slip systems operative and thereby permitted slip to proceed more uniformly so that the fracture became less crystallographic.

Somewhat similar observations were made of Ti-6Al-4V fracture surfaces tested in air (Robinson, et al. 1973). At low growth rates planar fracture surfaces developed, but at higher rates the fracture surface was characterized as being amorphous. The results of additional tests (Irving and Beevers 1973) in vacuum (10^{-5} Torr) are quite interesting. In these tests, no planar regions were found to develop during continuous growth above ΔK_{TH}. However, below ΔK_{TH} discontinuous growth was observed which did involve the creation of planar fracture facets. These results suggest that corrosion fatigue due to the presence of moisture may be contributing to the observed structure sensitivity. Intermittent growth in vacuum may be due to the low moisture content of the test chamber, so that many cycles pass before the crack tip is sufficiently embrittled for the crack to grow. This mechanism is similar to the brittle film-rupture mechanism proposed for the stress corrosion of tarnished brass. Cleavage-like crystallographic features might develop if the embrittled layer is epitaxial with the underlying substrate. As the growth rate increases the amount of new fracture surface per cycle is also increased, with the result that the amount of containment (moisture) per unit area of new fracture surface decreases, eventually to the point where the embrittled layer is inconsequential. At this point the structure sensitivity would no longer be present. A check on this view might be obtained by varying the test frequency. As the frequency decreases the transition point should occur at higher growth rates.

A comparison of growth rates in air and vacuum near the threshold is given in Figure 2-8, and a marked difference is apparent. In contrast a comparison of growth rates of Ti-6Al-4V in air and dry argon (Bucci, et al. 1972) revealed no difference in crack growth behavior near the threshold. In this study cleavage-like facets were also found, presumably for both test conditions. However, it has been observed (Wei and Ritter 1972) that growth rates in vacuum (10^{-7} torr) are but one-half those in vigorously purified argon for growth rates in the range of 10^{-5} to 10^{-4} mm/cycle. These results suggest that complete removal of moisture from argon is unlikely. Residual amounts of the order of 20 ppm may be significant.

Central questions concerning both the existence of a true threshold and the causes thereof are still being debated. It has been suggested (Paris, et al. 1972) that crack closure may be important but this has been discounted (Lindley and Richards 1973 a, b). At low stress intensities the angle which the slip bands make with the crack tip increases, and this has been advanced as a factor affecting the threshold level (Lindley and Richards 1973a). For steels the relation $\Delta K_{TH} = (7.5 - 9.0)E$ has been proposed (Harrison 1970, here length units are in mm). A dependence of ΔK_{TH} on the elastic modulus and yield strength has also been proposed. On the point of the existence of the threshold it does not seem unreasonable that in the complete absence of environmental factors a cut-off should exist which corresponds to a rate of growth equal to one interatomic spacing per cycle. The counterpart of this would be reflected in the fatigue strength in vacuum at 10^8 cycles.

A compilation of threshold values is given in Table 2-2.

Environmental Effects

In addition to the research cited on environmental effects near the threshold, a number of other recent studies have been directed at clarifying the role of environment on the rate of fatigue crack growth. It is becoming clear that a variety of responses can develop depending upon the alloy and the environment. For example, in the case of Ti-6Al-4V in air the greatest effect is observed near the threshold level, Figure 2-8. For an Al-7% Mg alloy tested in air the greatest effect of the environment appears to be at growth rates of 10^{-6} in/cycle, Figure 2-9 (Ford and Hoar 1973). In those circumstances where stress-corrosion cracking exists a large effect will be found at higher growth rates, Figure 2-10.

The effect of the environment in fatigue crack initiation can also vary depending upon the particular environment-alloy couple. For example, a considerable decrease in the long-life fatigue strength has been observed for mild steel tested in London tap water (Gough and Sopwith 1932), Figure 2-11. On the other hand, in comparing results of fatigue tests of aluminum alloys tested in air or vacuum it appears there is little effect on the long-life fatigue strength, but that an air environment decreases the intermediate-life fatigue strength, Figure 2-12 (Engelmaier 1968). A stress-independent form of pitting corrosion may have been taking place in the case of steel, but in the case of the aluminum alloy, until the protective oxide film was ruptured, environment played little effect.

TABLE 2-2

ΔK_{TH} Values*

Material	ΔK_{TH} , $MN/m^{3/2}$		
	$R = -1$†	$R \simeq 0$	$R \simeq 0.5$
Mild Steel	6.4	6.5	4.3
Mild Steel in Brine	–	–	1.2
Low Alloy Steel	6.3	6.6	4.4
Maraging Steel	–	–	3.0
18/8 Austenitic Steel	6.0	6.0	5.0
Aluminum	1.0	1.7	1.2
4–1/2% Cu-Al Alloy (BSL65)	2.1	2.1	1.5
Copper	2.7	2.5	1.5
Phosphor Bronze	3.7	4.0	3.2
60/40 Brass	3.1	3.5	2.6
Titanium	–	–	2.2
Nickel	5.9	7.9	5.2
Monel	5.6	7.0	5.2
Inconel	6.4	7.1	4.7

* Based on data of Pook (1972).

† ΔK_c values at $R = -1$ are based on tensile half of cycle only

Crack Closure

During fatigue crack growth under $R = 0$ conditions, for example, upon unloading from the peak tensile stress of a cycle, a macroscopic portion of the crack surfaces close before the load is completely reduced to zero. This phenomemon was first noticed by Elber (1970), and has been a subject of much recent interest. Lindley and Richards (1973) have recently shown that closure contact is made primarily in the plane stress region along the specimen surface where thinning and extension is more pronounced than in the interior. A similar observation has been made in the case of transparent PMMA (Pitoniak et al. 1973). The closure process has also been studied by means of ultrasonics (Buck, et al. 1973), and the finding of interest is that closure takes place at a high percentage of maximum load when testing is done in vacuum as compared to testing in air, Figure 2-13. This observation suggests that reversibility of the slip process is inhibited by the diffusion of oxygen into active slip bands during testing in air. Since crack closure has been invoked to explain effects of overload and mean stress, as well as the existence of the level, it is certainly a process in need of further understanding.

Crack Retardation

If a fatigue crack is growing at a particular rate and an overload is applied, the subsequent growth rate at the initial stress amplitude can be much reduced as shown in Figure 2-14. This phenomenon is known as crack retardation. In the case of a single overload a delay is generally observed before the minimum rate is achieved, but in the case of a series of overloads applied consecutively, the delay aspect may disappear (von Euw, et al. 1972). To account for retardation, but not the delay aspect, a number of analytical approaches are being developed. All of these models relate to the size of the plastic zone created during overload, for the retardation-effect occurs within this region.

Wheeler (1972) expresses the retarded crack growth rate as

$$\frac{\Delta a}{\Delta N} = C\left(\frac{R_y}{a_p - a}\right)^m \Delta K^n$$

where $a_p - a$ is the distance from the crack tip to the elastic-plastic interface, and R_y is the extent of the current yield zone. The quantity $\frac{R_y}{a_p - a}$ changes from a low value to unity as the crack traverses the overload plastic zone.

Willenborg, et al. (1971) reduce ΔK to ΔK_{eff} as the result of an overload by setting

$$(\sigma_{max})_{eff} = \sigma_{max} - \sigma_{red}$$

$$(\sigma_{min})_{eff} = \sigma_{min} - \sigma_{red}$$

where σ_{red} is taken to be $\sigma_{overload} - \sigma_{max}$. If either of the effective stresses is less than zero, it is set equal to zero and this appears to be the principal factor bringing about retardation. Provision is made for reduction in the retardation effect as the crack traverses the overload plastic zone. For a 100% overload this model predicts that the crack should be arrested, which is not in accord with the example given in Figure 2-14. von Euw, et al. (1972) also consider that overloads may reduce ΔK in the crack growth expression as the result of crack closure effects. However, Lindley and Richards (1973b) find that fatigue crack retardation or arrest, at least under plane strain conditions, is not due to crack closure. Evidently, conclusions differ with respect to the importance of crack closure on various aspects of fatigue crack propagation.

Analysis of Growth Rates

With respect to quantitative determination of curves of the type shown in Figure 2-7, one approach is to relate the advance per cycle in the striation mode to the crack-tip opening displacement, and to include the threshold effect. This leads to (Donahue, et al. 1972)

$$\frac{\Delta a}{\Delta N} = \frac{4A}{\pi \sigma_y E}(\Delta K^2 - \Delta K_{TH}^2). \qquad (2\text{-}1)$$

Such an expression is useful only in the lower portion of Figure 2-7, since static modes of separation are not considered. It has been found that for tests in inert atmospheres for which this type of model is only valid, that A can be expressed as $A = 2\sigma_Y/E$, a finding thought to be related to the rate of strain hardening, so that

$$\frac{\Delta a}{\Delta N} = \frac{8}{\pi E^2}(\Delta K^2 - \Delta K_{TH}^2). \qquad (2\text{-}2)$$

This equation emphasizes the lack of structure-sensitivity for ΔK values away from the threshold level. Where aggressive environments are present, the rate of growth increases and this fact is reflected by an increase in the constant A. Equation (2-2) provides a baseline for growth rates below about 1 μm per cycle under $R = 0$ conditions. If growth rates are significantly higher, then the material may be embrittled and/or the environment may be particularly aggressive.

Recent studies by Ritchie and Knott (1973), by Knott and Ritchie (1973), by Richards and Lindley (1972), and by Pearson (1972) have been concerned with effects of R ratio on the rate of crack growth. They find that as the R ratio increases at a given ΔK there is little effect on the rate of growth for tough materials. However, for alloys of low toughness there is a K_{MAX} effect due to the occurrence of static modes of failure in low-toughness materials. The absence of mean stress effects in high toughness materials may be analogous to the case of notched fatigue where the local stress state may be quite different from the applied as discussed earlier. Further, Weertman (1969) has concluded that mean stress effects should be small for stress intensities below K_c.

To account for K_{MAX} effects Richards and Lindley (1972) have found the following empirical expression to be in agreement with experiments on steels:

$$\frac{\Delta a}{\Delta N} = A\left\{\frac{\Delta K^4}{\sigma_{UTS}^2 (K_c^2 - K_{MAX}^2)}\right\}^n \tag{2-3}$$

which is somewhat similar to the widely used Forman, et al. (1967) empirical equation:

$$\frac{\Delta a}{\Delta N} = \frac{C(\Delta K)^m}{(1 - R)K_c - \Delta K} \tag{2-4}$$

In view of the fact that the sensitivity of the rate of crack growth to mean stress depends on the toughness of the alloy, the following modification to Equation (2-1) is suggested, namely that

$$\frac{\Delta a}{\Delta N} = \frac{4A}{\pi \sigma_y E}(\Delta K^2 - \Delta K_{TH}^2)\left(1 + \frac{\Delta K}{K_c - K_{MAX}}\right) \tag{2-5}$$

where K_{MAX} is given by $\Delta K/(1 - R)$. This expression distinguishes between the two components of crack advance; the ductile striation component, and the static mode component. It is noted that the number of adjustable parameters goes to zero for tests in nonaggressive environments for ΔK values which are large with respect to K_{TH}. The following empirical equation is used to estimate the dependence of the threshold level on the R value:

$$\Delta K_{TH} = \frac{1.2(\Delta K_{TH_0})}{1 + 0.2\left(\frac{1 + R}{1 - R}\right)} \tag{2-6}$$

where ΔK_{TH_0} is the ΔK value for $R = 0$.

A comparison of calculations based upon Equation (2-5) with experimental results for aluminum alloys and steels of both high and low toughness is given in Figures 2-15 to 2-17, and the agreement is seen to be reasonable. It is also noted that the L64 alloy, strengthened by GPI zones (Pearson 1972) has a high threshold level but over a certain ΔK range exhibits a higher crack growth rate than does the low toughness RR58 alloy which contains the precipitate $S(Al_2CuMg)$ (Pearson 1972). One can speculate that an instability of the GP structure may be responsible for the unusually high crack growth rates exhibited.

It should also be mentioned that Pearson (1972) has fitted his data of Figure 2-15 with an empirical equation of form

$$\frac{\Delta a}{\Delta N} = \frac{C K_c (\Delta K)^3}{[(1 - R)K_c - \Delta K]^{1/2}} \tag{2-7}$$

which resembles Equation (2-3) and (2-4), but has only one adjustable parameter. In reviewing the data for Figures 2-15 to 2-17, it was of interest to find that K_{MAX} values 50% higher than K_{Ic} were reached in the case of the embrittled En30a alloy, whereas for the aluminum alloys Pearson found a much closer correspondence between static and crack growth levels of K_{Ic}, although some small variations occurred as indicated in Figure 2-15a. Pearson's results are also of interest in that 12 mm thick plate was used to insure that plane strain conditions prevailed throughout the tests.

3. STRESS-CORROSION CRACKING

Stress-corrosion cracking in Al-5.5Zn-2.5Mg alloys in 3.5% NaCl solution was studied by Ward and Lorimer (1972). A unique feature of their investigation was the use of the analytical electron microscope EMMA-4 to monitor the solute distribution adjacent to the grain boundaries. This solute distribution correlated with stress corrosion susceptibility. Aging treatments which produced a zinc concentration gradient at a boundary resulted in improved stress corrosion resistance in terms of total lifetime of unnotched specimens.

Results of another recent study on the effect of heat-treatment in the rate of stress-corrosion crack growth are shown in Figure 3-1, (Morral, et al. 1973). In this case the yield strength was constant at 40 Ksi for all treatments, and the rate of crack growth at the plateau level varied by over an order magnitude. Of the various microstructural factors involved, it appears that grain boundary precipitates were most important. The greater the volume of precipitate ($MgZn_2$) per unit of grain boundary area the greater was the resistance to stress corrosion cracking. Other factors effecting growth in the plateau region, such as the precipitate-free zones and the planar or wavy nature of the glide process appear to be much less important. The interpretation placed upon this finding is that the rate-controlling step in the plateau region is the dissolution of the $MgZn_2$ particles which act as sacrificial anodes. The greater the amount of anodic material the slower will be the rate of growth and this is consistent with Ward and Lorimer's observations. The results also appear to explain why overaged Al-Zn-Mg alloys are more resistant than underaged. However, overaging will reduce fracture toughness, and therefore an improvement in stress corrosion resistance through overaging may lead to a decrease in toughness. However, according to one model (Krafft Mulherin 1969), the K_{ISCC} level should be improved through increase in fracture toughness. Results on Ti-5Al-2.5 for example (Curtis 1968) indeed show an increase of K_{ISCC} with an increase in K_{Ic}. It may also develop that the resistance to stress corrosion in terms of fracture toughness may depend on the stress intensity level. In fact, there is one finding (Mulherin and Rosenthal 1971) that alloy modification to improve K_{Ic} does in fact raise the K_{ISCC} level but decreases resistance to stress corrosion above this level (Figure 3-2). TMP procedures can be particularly useful since they can increase the K_{ISCC} level (Paton and Sommer 1973) without loss in toughness, and such procedures can also decrease the rate of stress-corrosion cracking above K_{ISCC} (McEvily, et al. 1967).

4. FRACTURE TOUGHNESS

Compositional effects on fracture toughness may be crudely divided into those due to impurities and those due to deliberate alloy additions. Impurities are deleterious to toughness, particularly when they precipitate as large inclusions. Their effects have been discussed quantitatively elsewhere (Hahn, et al. 1972, Rosenfield and Hahn 1972, Hahn and Rosenfield 1973, Forsyth 1973) and will not be described in detail here. Suffice to say, large brittle inclusions are preferred sites for crack formation, and toughness decreases significantly with increased volume fraction. These effects are less important in high strength alloys which have low toughness to begin with. Development of alloys such as 7475 Al (low Fe and Si) and specification of low sulfur levels in steels aim at this point. In the case of temper embrittlement of steels, very low impurity levels can be disastrous. McMahon (1973) has provided an up-to-date summary of the elements that cause temper embrittlement and these are given in Table IV-1.

A more subtle problem is that of Cu in aluminum alloys. In these alloys, Cu not only strengthens by participating in the precipitation reaction, but can lower toughness by formation of large $CuAl_2$ particles. This latter effect probably dominates in the recently announced alloy, X2048*, (Levy, et al. 1973) which contains lowered Cu levels and provides higher toughness than other 2000-series alloys at the same strength level (i.e. $K_{Ic} = 33-36\ MNm^{-3/2}$ at a yield strength of $Y = 385\ MNm^{-2}$).

With regard to microstructural variations which are affected by deliverate alloying additions, considerable progress has been made in recent years. The following sections discuss those structures which produce optimum strength and toughness in steels, titanium alloys, and aluminum alloys. A basis of comparison is provided from the RAD diagram concept (Pellini 1972). We have indicated on each plot of strength versus toughness a region for which $(K_{Ic}/Y)^2 \geq 2.5$ mm. The need for such a criterion arises from a combination of fracture mechanics and nondestructive inspection (NDI). Consider a structure containing a crack of length $2a$. The structure will fail when

$$K = \sigma\phi\sqrt{\pi a} \geq K_{Ic} \tag{4-1}$$

where σ is the applied stress and ϕ is a function of geometry and loading. Let the safety factor be α, i.e., $\sigma = \alpha Y$. Thus,

$$\left(\frac{K_{Ic}}{Y}\right)^2 = \phi^2\alpha^2\pi a \quad . \tag{4-2}$$

Equation (4-2) defines the largest crack that the plate can safely contain, which should equal the largest crack that NDI will *not* detect. For aircraft structures α is often ≈ 0.8, so that $(K_{Ic}/Y)^2 \approx 2a\phi^2$ (Packman 1973). For a

* 2.8–3.8 Cu, 0.2–0.6 Mn, 1.2–1.8 Mg.

through-crack in a tensile-loaded panel $\phi = 1$ and $\left(\frac{K_{Ic}}{Y}\right)^2$ is just equal to the critical crack length which must be inspected out.

TABLE 4-1

Elements Promoting Temper Embrittlement (McMahon 1973a)

IVB	VB	VIB
C not embrittling	N apparently not embrittling	O strongly embrittling not reversible
Si weakly embrittling at 2000 ppm	P strongly embrittling	S embrittles iron but precipitated by Cr and Mn
Ge weakly embrittling at < 100 ppm	As weakly embrittling at 600 ppm	Se weakly embrittling at < 100 ppm
Sn strongly embrittling	Sb very strongly embrittling	Te very strongly embrittling
Pb ?	Bi probably like Sb, Te	Po ?

To illustrate the interplay between toughness and safety, a schematic toughness/strength diagram is show in Figure 4-1. If the criterion of inspectability is that any crack longer than 2.5 mm will be detected, alloys below the solid line will be unsafe and alloys above safe. Consider two alloys which lie at points A and B. Note first that alloy B is tougher than alloy A. However, alloy B is not as safe, because critical cracks will escape detection. The obvious goal for this alloy is to increase the toughness to some level such as B', without sacrificing strength. For alloy A, the temptation would be to increase strength at no sacrifice in toughness. The result could be as represented by point A' in Figure 4-2. In this case, the 2.5 mm line is crossed and the safety of the structure is reduced below the established level. If alloy A is to operate safely at $\sigma = 0.8Y$, the inspection capability must be improved from 2.5 mm to 2 mm. If this is not possible, as shown by Equation (4-2), the allowable stress level must be reduced to $\sigma = 0.72Y$, cancelling out the benefits of increased strength. The lines of constant safety in Figure 4-1 are the straight lines through the origin representing constant critical crack lengths. To improve alloy A and maintain its level of safety, strength and toughness must move along line A — A''. These points must be kept in mind as we discuss specific alloy and processing developments, since we must insure, above all, that any apparent improvement is not at the expense of safety.

4.1 Steels

Typical behavior of three classes of high strength steels is outlined in Figure 4-2 (Zackay, et al. 1973). The very high position of TRIP steels may be somewhat exaggerated since plane strain values have not been determined for these materials and the reported values contain a contribution from excess nonlinear crack-tip deformation. As is known, TRIP alloys contain metastable austenite and exhibit a strain-induced transformation to martensite. Since this transformation involves a dilation, it provides a mechanism for relief of local tensile stresses. Indeed, martensite is found to form preferentially at crack tips and near fracture surfaces (Antolovich and Fahr 1972).

Much attention at the International Conferences was focused on raising the levels for quenched and tempered alloys to those for 18% Ni maraging steel. One approach, exploited by Zackay, et al. (1973) involves austenitizing at 1200°C. At this temperature, the austenite is large-grained because alloy carbides are believed to be dissolved. As shown in Table 4-2, the best toughness is found in specimens quenched directly into iced brine, where the microstructure consists of self-tempered martensite. An increase of toughness with increasing austenitizing temperature and grain size in 4340 steel tempered at 200°C had been previously observed by Backofen and Ebner (1963). However, the latter authors found that austenization above 1100°C resulted in overheating and grain boundary failure. The other conditions listed in Table 4-2 plus microstructural observations suggest the following effects of microstructure:

beneficial: retained austenite and lightly-tempered martensite

deleterious: free ferrite and upper bainite.

Additional benefits of retained austenite on fracture toughness in a high carbon steel have been shown by Averbach (1973). As-quenched martensite will toughen upon tempering until the toughness minimum after 350°C tempering is approached (Robinson and Tuck, 1972, McMahon and Thomas 1973). This minimum also appears to be related to the disappearance of retained austenite and its replacement by ferrite and carbides. The role of free ferrite is complex because of its tendency to cleavage failure. For example, Robinson and Tuck (1972) find that a fine, uniform dispersion of carbides within ferrite results in higher toughness dimpled rupture compared to rod and plate carbide structures which result in cleavage.

A second method of achieving maraging toughness levels in quenched and tempered steels is by control of martensite microstructure (McMahon and Thomas 1973). Previously, Huang and Thomas (1971) had observed in Ni-Mn-C steels that dislocated martensite produces higher toughness than twinned martensite. McMahon and Thomas (1973) adjusted Cr and C levels to produce maximum strength consistent with low twin densities within the martensite. The optimum strength/toughness combination was achieved in the 4Cr-0.35 C alloy indicated in Figure 4-3. Tempering this alloy at 200°C raised K_{Ic} to its maximum level of ~ 100 $MNm^{-3/2}$ and lowered its yield strength from ~ 1650 MNm^{-2} to ~ 1515 MNm^{-2}. In both the as-quenched and quenched- and -tempered conditions the alloy attained the maraging levels shown in Figure 4-2.

TABLE 4-2

Austenitizing Treatments, Fracture Toughness and Yield Strength of Steels, As-Quenched Condition (Zackay, et al. (1973))

Steel (Composition)	*Austenitizing Temperature*, °C	*Quenching Medium*	*0.2% Yield Strength* MNm^{-2}	*Fracture Toughness* $MNm^{-3/2}$
Laboratory heat (5Mo-0.60Mn-0.30C)	1200	Iced Brine	1475	110
	870	Iced Brine	1335	57
AISI 4130 (0.30C-0.85Cr-0.46Mn-0.20Mo)	870	Oil	1385	63
	1200→870*	Oil	1445	80
	1200	Iced Brine	1475	110
AISI 4340 (0.40C-0.72Cr-1.73Ni-0.80Mn-0.24Mo)	870	Oil	1590	39
	1200→870*	Oil	1590	69

* Specimens cooled slowly from 1200°C to 870°C before quenching to maintain quenching conditions identical with 870°C austenitized specimens.

Results such as those of both Zackay, et al. (1973) and McMahon and Thomas (1973) offer suggestions for producing high toughness in a high strength steel. These include:

(a) Elimination of trace elements such as S and P.

(b) Austenization at sufficiently high temperatures to dissolve alloy carbides.

(c) Alloying to provide sufficient hardenability to avoid formation of upper bainite and free ferrite.

(d) Providing a low enough C content to insure high Ms temperatures and to avoid microtwinning of the martensite that is formed. Retention of austenite and some self-tempering of martensite during quenching are both beneficial.

(e) Limiting tempering temperatures to below ~ 300°C to avoid decomposition of any retained austenite.

The bulk of available data tend to support these guidelines.

Lower bainite, formed by isothermal transformation above the Ms temperature, can also be produced with combined strength and toughness equivalent to maraging steels. While there is some controversy (Huang and Thomas 1971), the bulk of the data indicate that lower bainite is tougher than martensite. There is no question that lower bainite has superior toughness to twinned martensite, but the possibility exists that it is inferior or equal to lath martensite (McMahon and Thomas 1973). Figure 4-4 illustrates the results of Liu (1969) comparing toughness of

bainitic and martensitic structures on a single alloy*, isothermally transformed or tempered at various temperatures. In the martensitic condition about 20% of microtwins were observed. Liu (1969) ascribes the toughness difference mainly to the difference in carbide precipitation. In lower bainite the precipitates are quite uniformly distributed and dimpled rupture is observed. Within Liu's martensitic materials, the dislocated regions appear to fail by dimpled rupture while the internally twinned regions, which exhibit more heterogeneous carbide precipitation, appear to fail by quasi-cleavage. It is likely this alloy would be tougher in the tempered martensite condition if none of the martensite were twinned. The question remains open whether lower bainite is superior to tempered lath martensite. In any event, strength levels of bainitic structures appear to be limited and very high strengths appear to be attainable only with martensitic structures.

When considering maraging steels, we are dealing with 100% lath or dislocated martensite hardened by fine precipitates of intermetallic compounds (Floreen 1968). Viewed in this light, it is not surprising that quenched and tempered steels can attain comparable strength and toughness to maraging steels. Unlike the case for quenched and tempered steels, the effect of austenite on toughness is not clear. Claims have been made that reverted austenite raises toughness (Floreen 1968), lowers toughness (Steffans and Seifert 1973), or has no effect (Pampillo and Paxton 1972), and this point needs further investigation. An interesting observation is the result (Strawley 1969, Pampillo and Paxton 1972) that overaged alloys are less tough than underaged alloys, analogous to a well-known effect in aluminum alloys (see below). They ascribe this decreased toughness partly to increased nucleation of voids by the hardening precipitate.

4.2 Titanium Alloys

The isothermal phase transformation and martensitic reaction in titanium appear to offer similar opportunities as for steel to improve toughness. Figure 4-5 shows the results of several authors (Coyne 1970, Crossley, et al. 1973, Judy, et al. 1973, Peterson 1973, Rogers 1973) and indicates definite trends depending on microstructure. The superiority of metastable β alloys (e.g., Ti-15% Mo) is quite marked although the mechanism is not clear. Suggestions that have been made of a TRIP effect (Crossley, et al. 1973), Hall and Hammond 1973) are plausible and deserve further study. Within the $(\alpha + \beta)$ alloys, acicular structures are tougher than equiaxed structures. The behavior of this alloy family is partially determined by the α/β interface which is a preferred site for void nucleation under stress. Greenfield and Margolin (1971) report evidence that toughness increases linearly with decreasing grain size in alloys containing equiaxed α. For acicular structures they claim a toughness improvement of $\sim 30\ MNm^{-3/2}$ over equiaxed structures arising from the grain boundary α film provided that the film thickness is greater than $\sim 5\ \mu m$. Finally, near α alloys, although they tend to be quite tough, do not exhibit high strength.

In sum, optimization of strength and toughness in titanium alloys appears to depend on the presence of non-equilibrium components. Metastable β is better than acicular α which, in turn, is better than equiaxed α. The fiducial line of $(K/y)^2 = 2.5$ mm suggests that adequate toughness is attainable in thick sections up to yield strengths in excess of $1200\ MNm^{-2}$ ($\sim 0.12E$). Optimization of toughness seems to lie with development and exploitation of β alloys, but there are no clear guidelines as to how to proceed.

4.3 Aluminum Alloys

Until very recent years, much of the attention in the aluminum alloy systems has been focused on purification and aging. The effects of removing Fe and Si have been discussed in an earlier paper (Hahn and Rosenfield 1973). It is found, for example, that K_{Ic} is increased from 30 to 40 $MNm^{-3/2}$ at a strength level of 500 MNm^{-2} by reducing Fe and Si from levels characteristic of 7075 to those characteristic of 7475. The aging effects are well-known and are illustrated in Figure 4-6. It is believed that the superiority of the 7000 series (Al-Zn-Mg-Cu) over 2000 series (Al-Cu-Mg) is due to the larger particle sizes in the latter system while the superiority of underaged alloys appears to be due to an increased tendency towards grain boundary failure as aging proceeds.

Lately, thermal-mechanical processing (TMP) has aroused considerable interest because of the improved strength levels produced and indications of better stress corrosion and unnotched fatigue behavior. Thompson, et al. (1973) have examined the effect of TMP on a series of sheet alloys based on 7475 + Zr.† After a preliminary hot rolling, specimens were preaged, either warm rolled at 165°C or cold rolled, and reaged. Strengths as high as 540 MNm^{-2} were attained and adequate corrosion resistance would be expected on the basis of electrical conductivity measurements. Table 4-3 gives the toughnesses for one of their alloys as a function of the processing conditions. Note that overaging followed by warm working results in the highest toughness. For comparison, a similar alloy conventionally worked has almost the same toughness but 8% lower strength (Rosenfield, et al. 1973).

---

* The reported data were Charpy energy values. These were converted into fracture toughness using an empirical formula of Ault, et al. (1971) $K_{Ic} = \frac{Y}{6.28}\left[(3.81CVN + 319)/Y - 0.18\right]^{1/2}$, where the units are $K_{Ic} = MNm^{-3/2}$, CVN = J, and $Y = MNm^{-2}$.

† 7475 + Zr = 7475 with 0.12% Zr replacing the Cr.

TABLE 4-3

Fracture Toughness of 4-mm Thick Aluminum Alloy Sheet (Al-5.5Zn-2.5Mg-1.9Cu-0.12Zr-0.08Si-0.07Fe) as a Function of Thermal-Mechanical Treatment. Thompson, et al. (1973)

Preage Treatment	K_c ($MNm^{-3/2}$)	
	Worked 30% at 165°C	*Cold worked 30%*
Underage	103	78
Overage	148	121

In general, it appears that TMP of aluminum alloys does not provide major toughness improvements but that higher strengths can be produced with no loss in toughness. Sommer, et al. (1972) recommend processing temperatures above 160°C. Lower temperatures result in inhomogeneous slip which leads to inhomogeneous precipitations during the final aging and degradation of all properties.

Effects on toughness of grain size and shape are also beginning to emerge. A current study (Rosenfield, et al. 1973) of conventionally processed material includes a series of alloys based on 7075 (including 7475, 7475 + Zr, etc.). In the overaged condition, these alloys have a marked tendency towards grain boundary failure. Thus, the results of Figure 4-7 are not surprising. It appears that more attention needs to be paid to the effects of alloying additions on the retention of the wrought structure and the suppression of recrystallization and grain growth. Additional study is needed on segregation of impurities to grain boundaries or whatever other mechanism is lowering the toughness of recrystallized alloys. For reference, Figure 4-7 also contains the range of Thompson, et al.'s (1973) TMP data on similar alloys. Since metallographic and fractographic evidence were not presented, it is not clear how these results correlate with those on conventionally processed material.

A final problem, which is not limited to Al alloys but also occur in steels and Ti alloys, is the occurrence of superbands (Hahn and Rosenfield 1973). These bands are localized regions of very heavily concentrated deformation and have a greater tendency to form in higher strength materials. Thus, the decrease in toughness with increase in strength level can be correlated with superband occurrence. Figure 4-8 shows an example of superband formation on on the surface of a bent sheet in an Al-Mg-Cu-Zn quartenary alloy in the peak-aged condition. With further deformation the major band of Figure 4-8(b) develops into a crack. Apparently, a similar mechanism attains at the tip of a notch, the highly concentrated deformation limiting the toughness. At lower strength levels, the deformation is much less concentrated as shown in Figure 4-9. Presently, there is no information on the metallurgical factors controlling superband formation. However, there is good reason to believe that their elimination would enhance toughness, by producing less intense local strain concentration at the tip of a crack.

5. CONCLUDING REMARKS

After considering the various crack growth processes in fatigue, stress corrosion and fracture, it appears that the dominant structure-sensitive material property is the fracture toughness. In fatigue crack growth the K_{Ic} value determines the point of final failure, but other regions of the crack growth curve are relatively structure insensitive so long as K_{MAX} is well below K_c (Equation 2-2). It is noted that the ΔK_{TH} value is relatively structure insensitive. In stress corrosion K_{Ic} not only determines the point of final failure, but there is also evidence that it is simply related to the threshold for stress corrosion cracking, K_{ISCC}. If it were not for the plateau part of the stress corrosion crack growth curve, the maximization of K_{Ic} would be a complete remedy for improving not only stress corrosion but all forms of fracture. However, at least in the case of Al-Zn-Mg curves, those heat treatments which increase fracture toughness unfortunately also increase the plateau growth rates. Thus some sort of trade-off may be required.

Upon examination of typical rates of stress corrosion crack growth and times to failure it is seen that stress corrosion lifetimes are very short in many cases. When such materials are used it is imperative the combination of flaws and applied or residual stresses do not exceed the K_{ISCC} level. Alternately, it is possible that even if the K_{ISCC} level is exceeded that the plateau growth rates can be lowered to acceptable values through thermo-mechanical processing. However, the critical crack lengths determined from fracture toughness measurements of TMP Al alloys suggest that not all of the strength of these alloys can be utilized.

Improvement of resistance to environmental failure also should result in lowered fatigue crack growth rates in practical situations.

19. Greenfield, M.A. Margolin, H. — Met. Trans., Vol.2, 841.

20. Grosskreutz, J.C. — Proc. Air Force Conf. on Fatigue and Fracture, AFFDL-TR 70-144, 47, 1970.

21. Grosskreutz, J.C. — PLV-212*, 1973.

22. Hahn, G.T. et al. — Annual Reviews of Material Science, Vol.2, 381, 1972.

23. Hahn, G.T. Rosenfield, A.R. — Met.Trans. (in press), 1973.

24. Hall, I.W. Hammond, C. — *Titanium Science and Technology*, R.I.Jaffee and H.M.Burte, eds, Plenum, N.Y., p.1365, 1973.

25. Harrison, J.D. — Metal Construction, Vol.2, 93, 1970.

26. Huang, D.H. Thomas, G. — Met. Trans., Vol.2, 1587, 1971.

27. Irving, P.E. Beevers, C.J. — Research Report, U. of Birmingham, Dept of Physical Metallurgy and Science of Materials, 1973.

28. Judy, R.W. et al. — *Titanium Science and Technology*, R.I.Jaffee and H.M.Burte, eds, Plenum, N.Y., p.1393, 1973.

29. Knott, J.F. Ritchie, R.O. — C-1, Paper 12*, 1973.

30. Krafft, J.M. Mulherin, J.H. — Trans. ASM, Vol.62, 64, 1969.

31. Levy, S.A. et al. — AIAA, Paper 73-385, 1973.

32. Lindley, T.C. Richards, C.E. — V-431/A*, 1973a.

33. Lindley, T.C. Richards, C.E. — CERL Report, 1973b.

34. Liu, Y.H. — Trans. ASM, Vol.62, 55, 1969.

35. Lütjering, G. et al. — C-2, Paper 87*, 1973.

36. McEvily, A.J. et al. — Trans. ASM, Vol.60, 661, 1967.

37. McEvily, A.J. et al. — Trans. AIME, Vol.227, 453, 1963.

38. McMahon, C.J., Jr — III-323*, 1973a.

39. McMahon, C.J., Jr — Trans. ASME, Vol.H95, 142, 1973b.

40. McMahon, J.A. Thomas, G. — C2-36*.

41. Morral, J.E. et al. — To be published, 1973.

---

* Key to coding:
C-1 = British Steel Corp. Conference on Mechanics and Mechanisms of Crack Growth
C-2 = III International Conference on Strength of Metals and Alloys
All others = III International Conference on Fracture.

42. Mulherin, J.H. Rosenthal, H. — Met. Trans., Vol.3, 427, 1971.

43. Ostermann, F. — Met. Trans., Vol.2, 2897, 1971.

44. Packman, P. — Air Force Materials Lab., private communication, 1973.

45. Pampillo, C.A. Paxton, H.W. — Met. Trans., Vol.3, 2895, 1972.

46. Paris, P.C. et al. — ASTM STP Vol.513, 141, 1972.

47. Paton, N.E. Sommer, A.W. — C-2, Paper 21*, 1973.

48. Pellini, W.S. — NRL Report 7406, 1972.

49. Pearson, S. — Eng. Fract. Mech., Vol.4, 9, 1972.

50. Peterson, V.C. et al. — *Titanium Science and Technology*, R.I.Jaffee and H.M.Burte, eds, Plenum, N.Y., p.1969, 1973.

51. Pitoniak, F.J. et al. — To be published, 1973.

52. Pook, L.P. — ASTM STP Vol.513, 106, 1972.

53. Reimann, W.H. Brisbane, A.W. — Eng. Fract. Mech., Vol.5, 67, 1973.

54. Richards, C.E. Lindley, T.C. — Eng. Fract. Mech., Vol.4, 951, 1972.

55. Ritchie, R.O. Knott, J.F. — V-434A*, 1973.

56. Robinson, J.L. et al. — V-343*, 1973.

57. Robinson, J.N. Tuck, C.W. — Eng. Fract. Mech., Vol.4, 377, 1972.

58. Rogers, D.H. — *Titanium Science and Technology*, R.I.Jaffee and H.M.Burte, eds, Plenum, N.Y., p.1719, 1973.

59. Rosenfield, A.R. Hahn, G.T. — Colloquie sur la Rupture des Materiaux, Grenoble, France, Societe Francaise de Metallurgie, Section Regionale du Sud-Est, 1972.

60. Rosenfield, A.R. et al. — Tech. Rept AFML-TR-72-199, Part II, Wright-Patterson AFB, Ohio, 1973.

61. Sommer, A.W. et al. — Report AFML-TR-72-5, Wright-Patterson AFB, Ohio, 1972.

62. Speidel, M.O. et al. — ASTM STP Vol.520, 1973.

63. Srawley, J.E. — *Fracture 1969*, P.L.Pratt, et al. eds, Chapman and Hall, London, p.131, 1969.

64. Tichener, A.L. Ponniah, C.D. — C-2, Paper 88*, 1973.

---

* Key to coding:
C-1 = British Steel Corp. Conference on Mechanics and Mechanisms of Crack Growth
C-2 = III International Conference on Strength of Metals and Alloys
All others = III International Conference on Fracture

65. Thomas, G. — J. Inst. Metals, Vol.89, 287, 1960–61.

66. Thompson, D.S. — Reynolds Aluminum Company, Private communication, 1973.

67. Thompson, D.S. et al. — C-2, Paper 24*, 1973.

68. van Leeuwen, H.P. — Aluminum, Vol.48, 719, 1972.

69. von Euw, E.F.J. et al. — ASTM STP Vol.513, 230, 1972.

70. von Elber, W. — Eng. Fract. Mech., Vol.2, 37, 1970.

71. Ward, D.E. Lorimer, G.W. — C-2, Paper 100*, 1973.

72. Weertman, J. — Int. J. Fract. Mech., Vol.5, 13, 1969.

73. Wei, R.P. Ritter D. — J. of Materials, Vol.7, 240, 1972.

74. Wheeler, O.E. — J. of Basic Eng., Trans. ASME, 181, 1972.

75. Willenborg, J., et al. — Air Force Flight Dynamics Laboratory, TM-71-1-FBR, 1971.

76. Zackay, V.F. et al. — C2-35*.

* Key to coding:
C-1 = British Steel Corp. Conference on Mechanics and Mechanisms of Crack Growth
C-2 = III International Conference on Strength of Metals and Alloys
All others = III International Conference on Fracture.

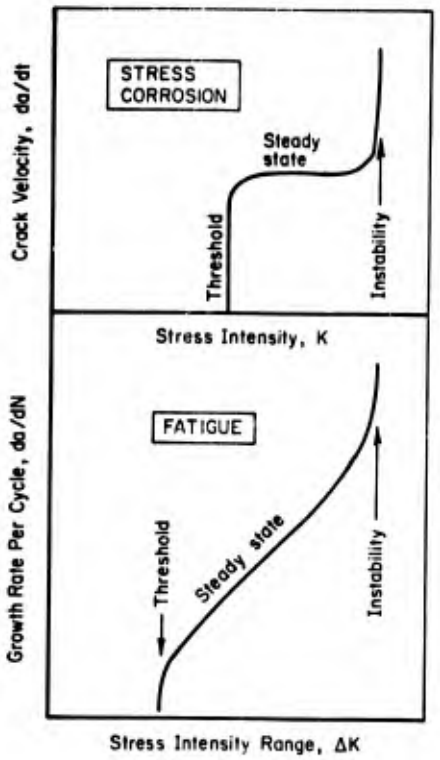

Fig.1.1 Schematic diagram of stable crack growth behavior of high strength alloys. All scales are logarithmic

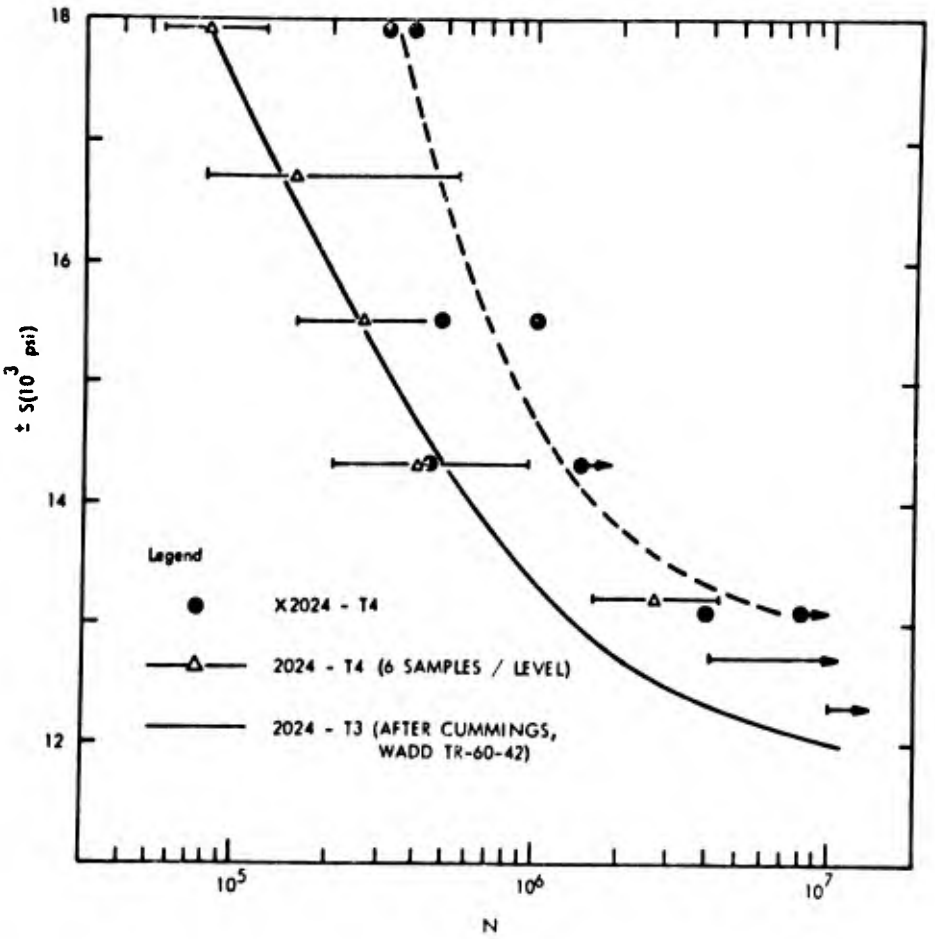

Fig.2.1 The effect on fatigue of reducing the concentration of undissolved second-phase particles in 2024-T4 aluminum. Volume percent of "inclusions": X2024, 1.6×10^{-4}; commercial 2024, 9×10^{-2}. (Grosskreutz 1970)

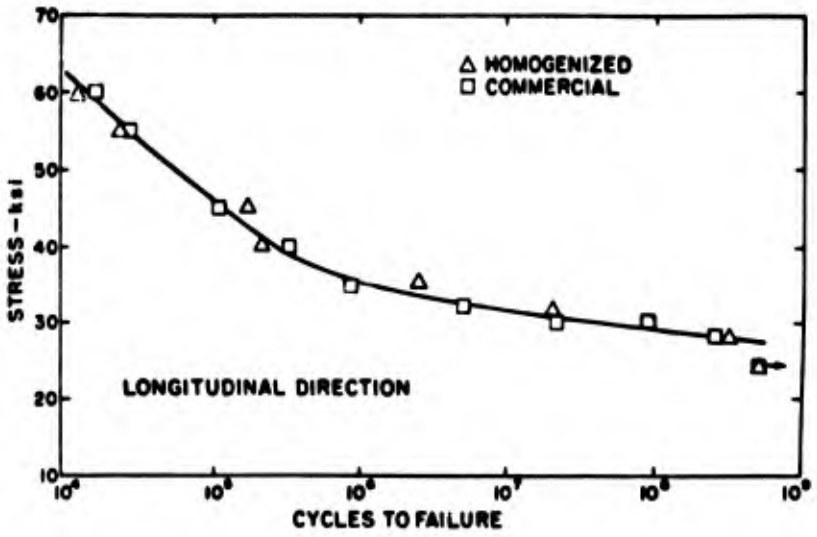

Fig.2.2(a) Longitudinal fatigue characteristics of commercial and low second phase 7075-T6 aluminum alloy. (Mulherin and Rosenthal 1971)

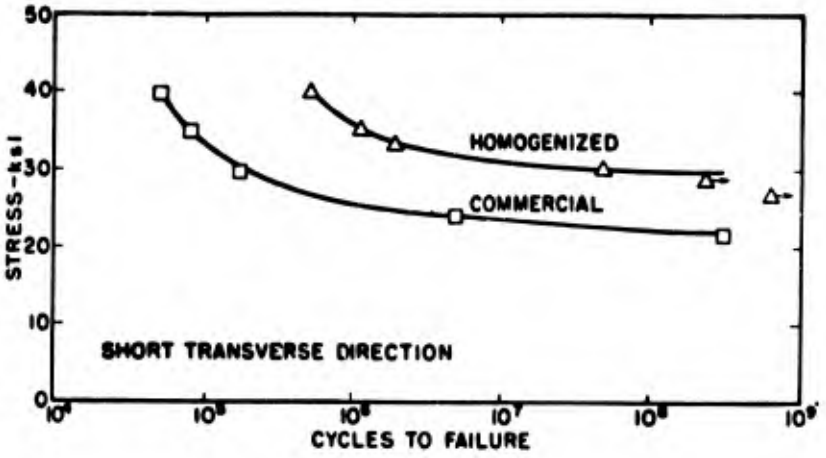

Fig.2.2(b) Short transverse fatigue characteristics of commercial and low second phase 7075-T6 aluminum alloy. (Mulherin and Rosenthal 1971)

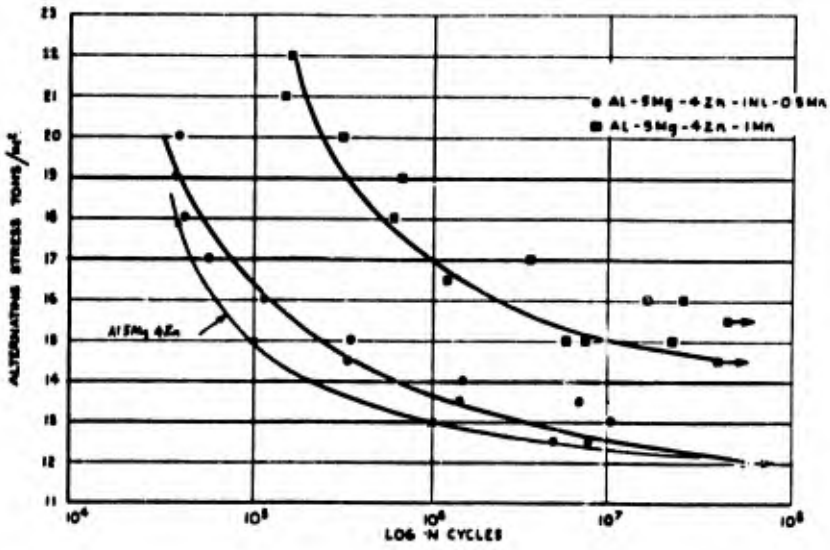

Fig.2.3 Fatigue curves for alloys based on the ternary alloy Al-5Mg-4Zn. (Forsyth 1973)

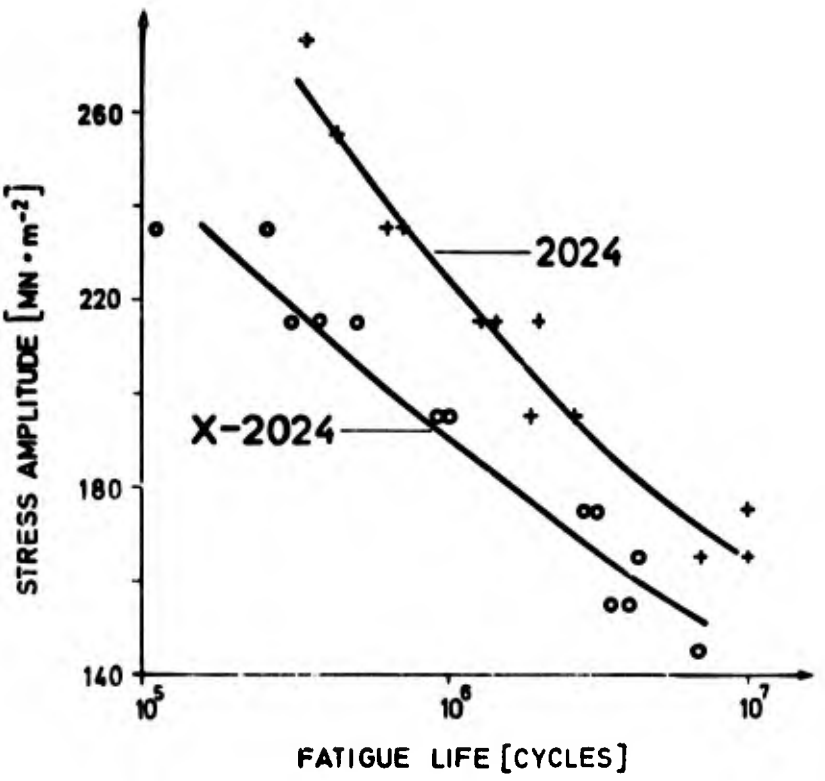

Fig.2.4 Fatigue life vs. stress amplitude for two Al-alloys. X-2024 contrained reduced amounts of Mn, Si, and Fe (Lütjering, et al. 1973)

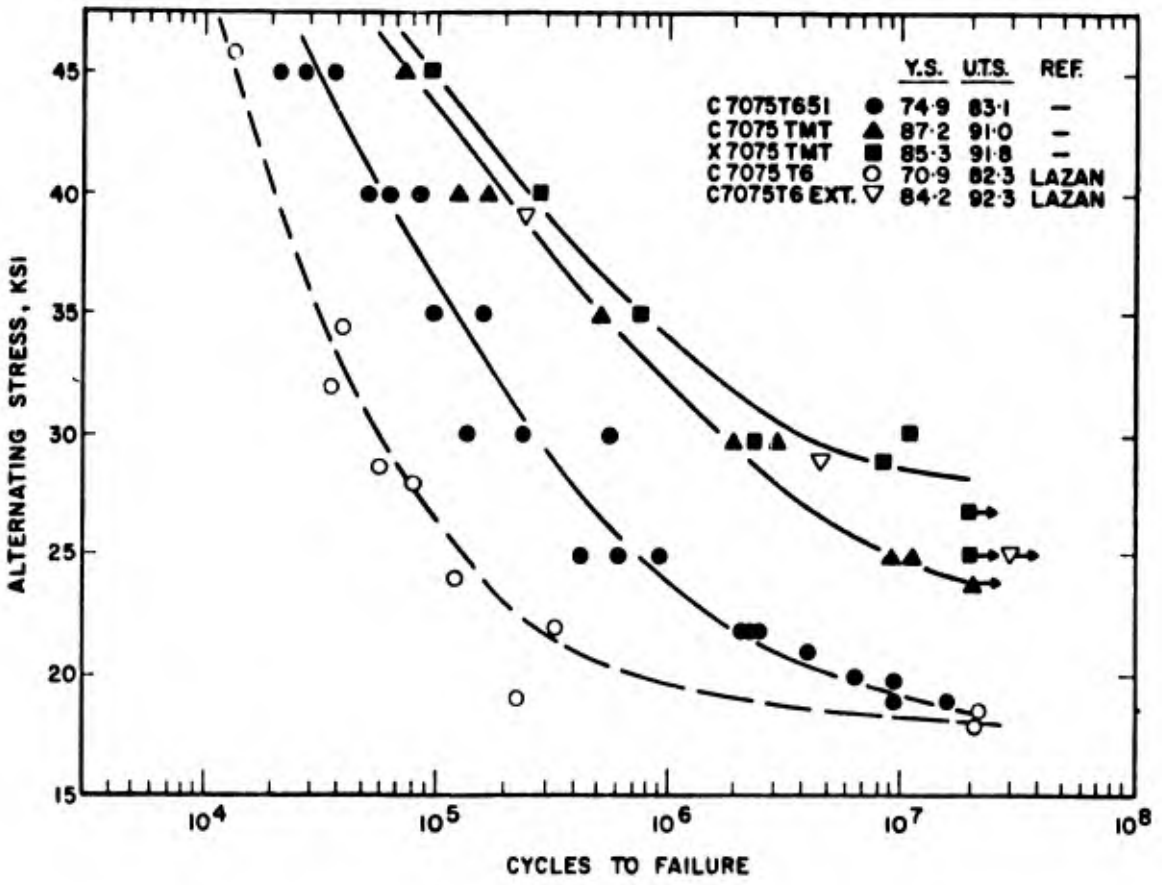

Fig.2.5 Smooth bar S-N curves of 7075 aluminum alloys with and without thermal-mechanical treatments. Axial loading with R = −1 . (Ostermann 1971)

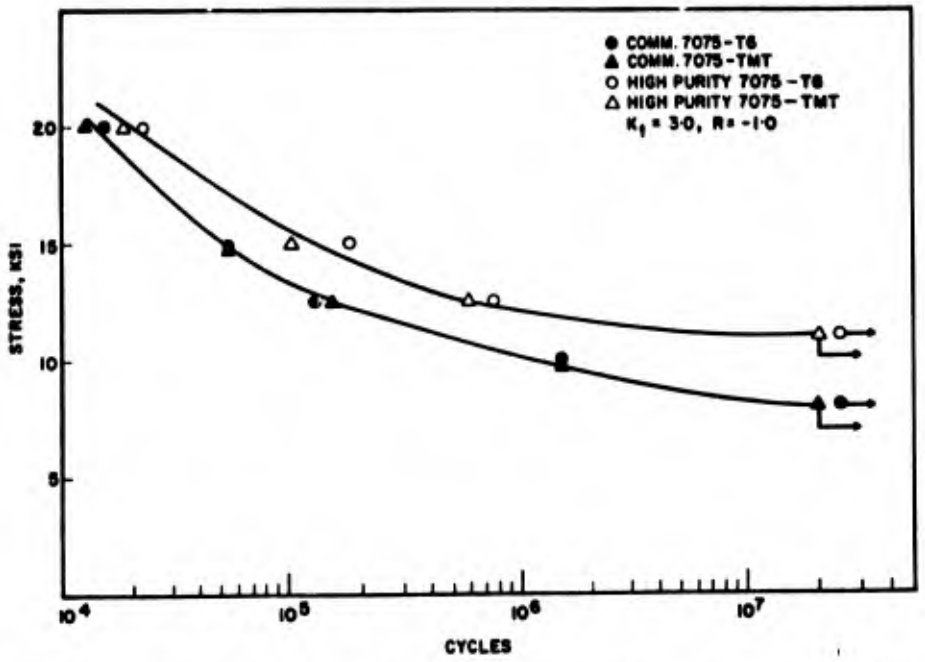

Fig.2.6 Notched fatigue properties of thermomechanically processed 7075. (Reimann and Brisbane 1973)

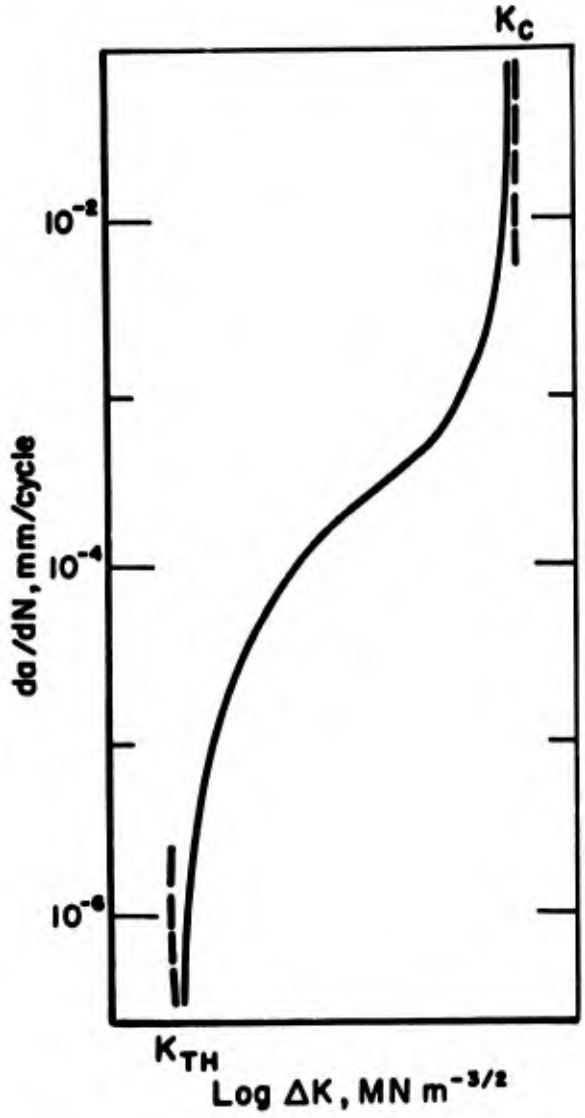

Fig.2.7 Schematic variation of fatigue crack growth rate, da/dN , with alternating stress intensity, ΔK

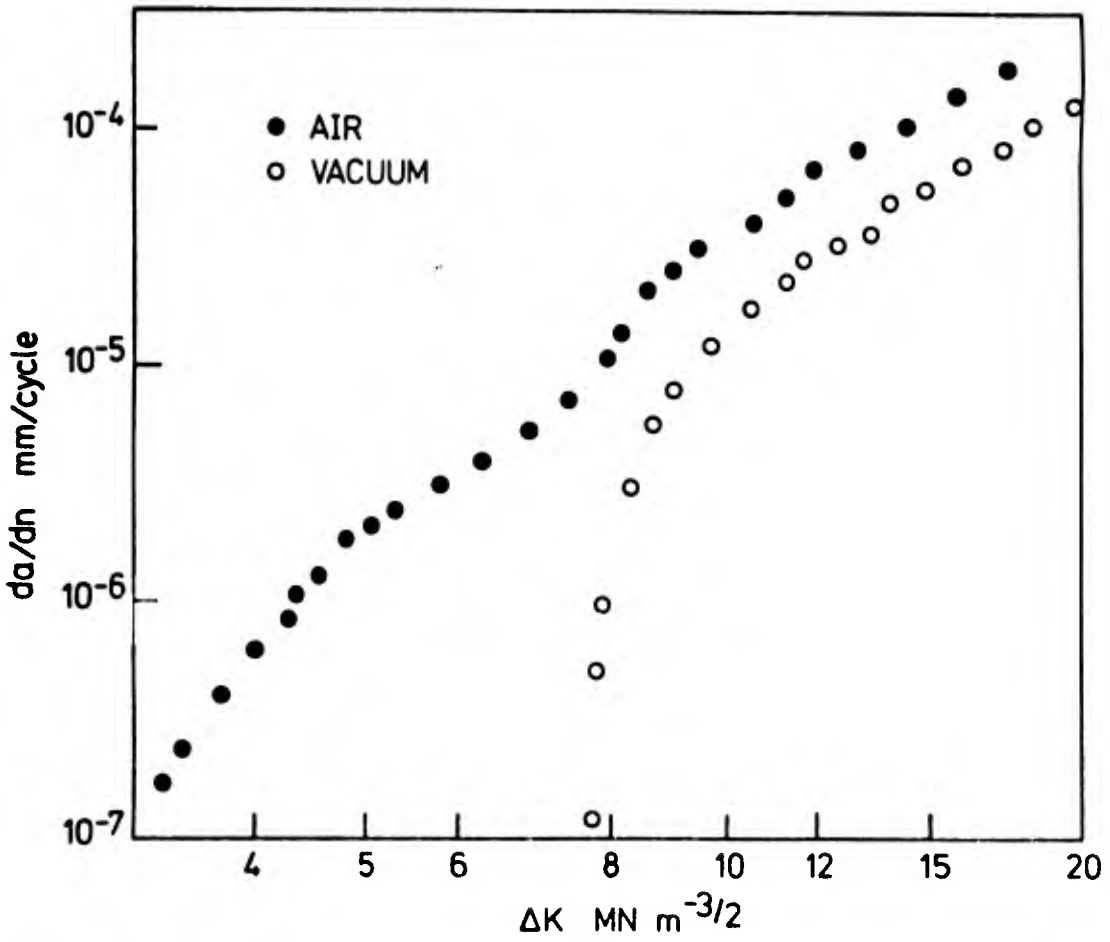

Fig.2.8 Comparison of growth rates in air and vacuum for Ti-6Al-4V at R = 0.35 . (Irving and Beevers 1973)

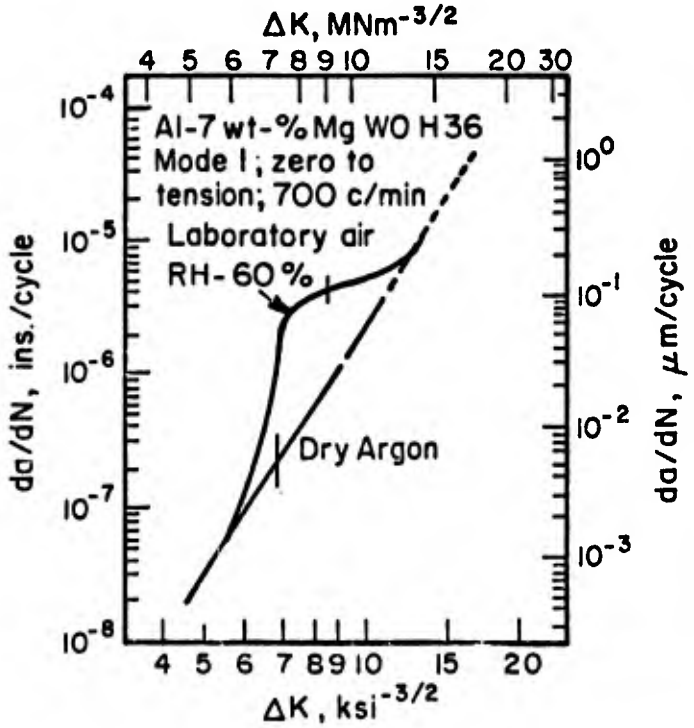

Fig.2.9 Comparison of crack growth rates in laboratory air and dry argon (Ford and Hoar 1973)

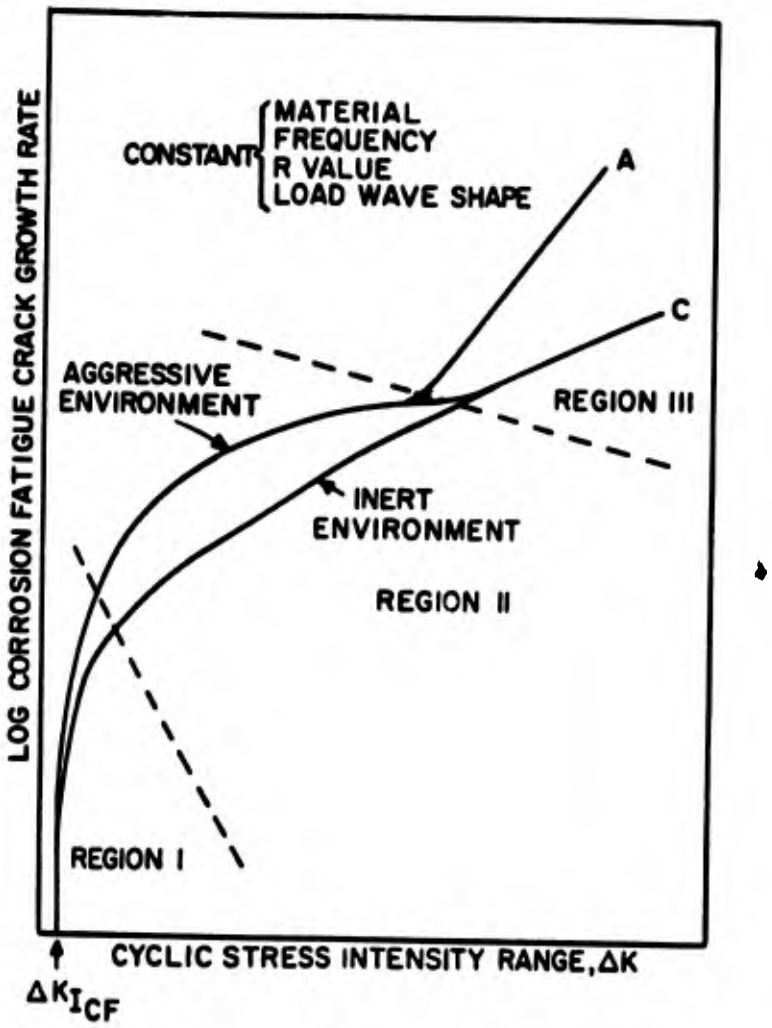

Fig.2.10 Schematic representation of the influence of stress intensity on the growth rate of corrosion fatigue cracks. After McMahon (1973b)

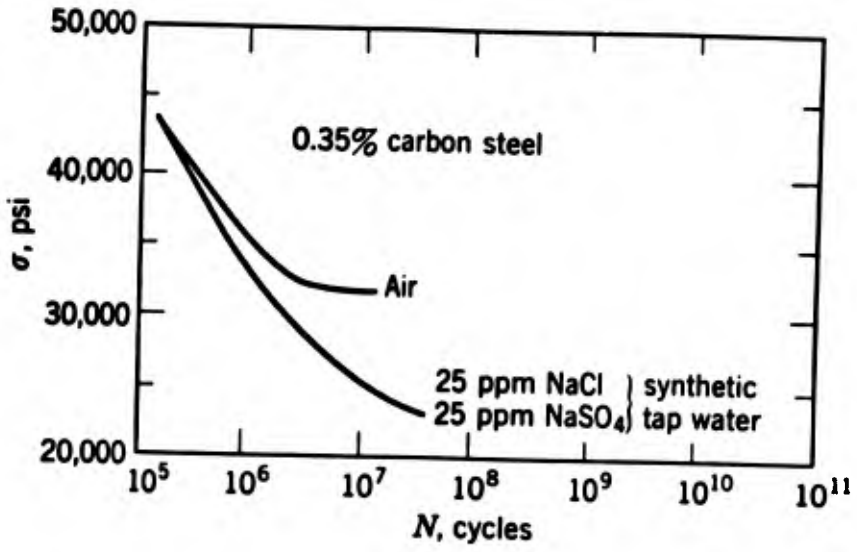

Fig.2.11 Effect of environment on fatigue properties of a 0.35% carbon steel. (Gough and Sopwith 1932)

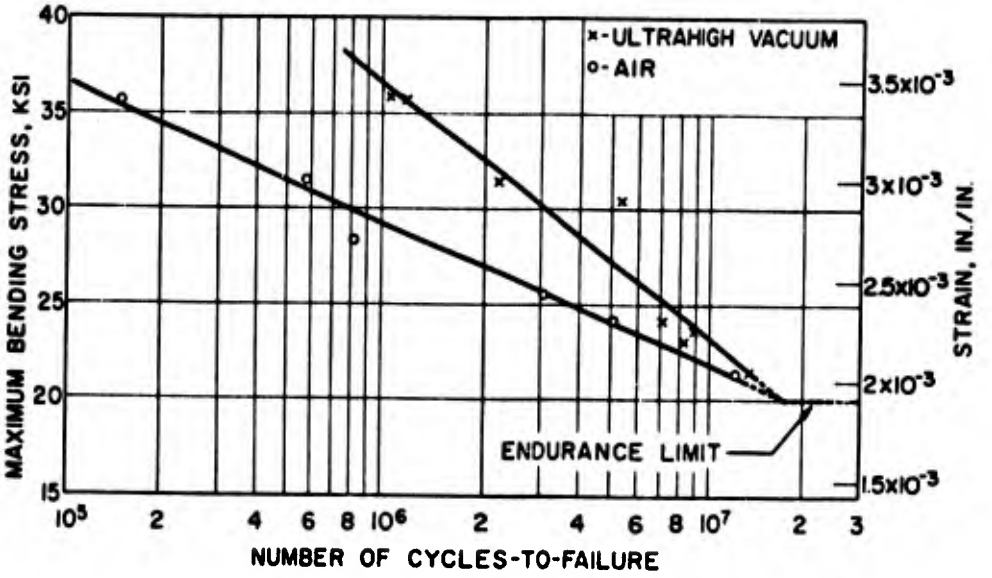

Fig.2.12 Fatigue life in air and vacuum for 2024-T3 aluminum alloy. (Engelmaier 1968)

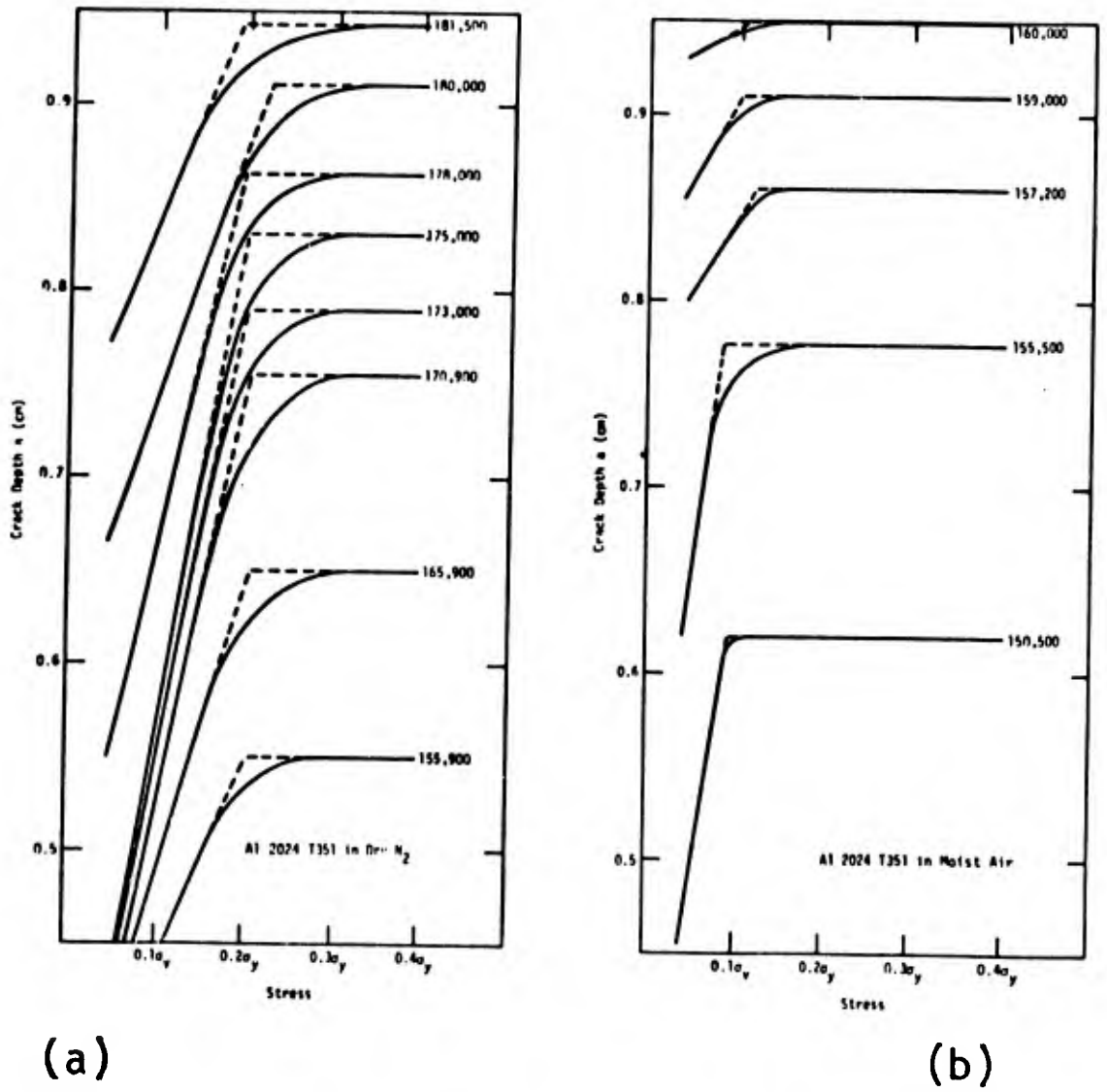

Fig.2.13 Crack closure effect in Al 2024; (a) in dry N_2; (b) in moist air. (Buck, et al. 1973)

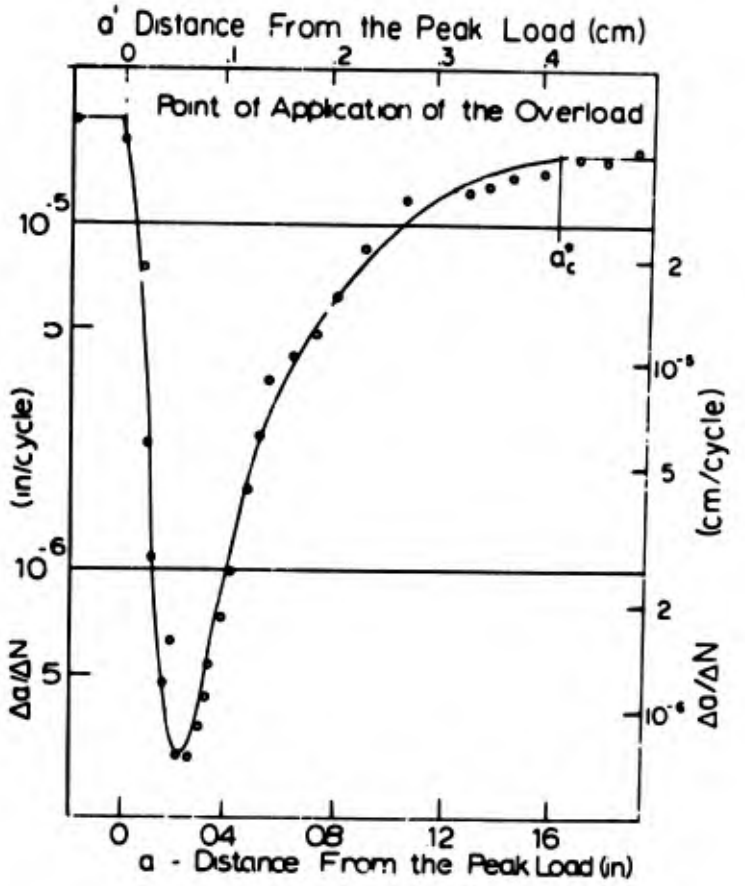

Fig.2.14 Growth rate through the delay region after a 100% overload. Material 2024-T3. Overload K_{MAX} = 39.6 $MNm^{-3/2}$, steady state ΔK = 19.8 $MNm^{-3/2}$. (von Euw, et al. 1972)

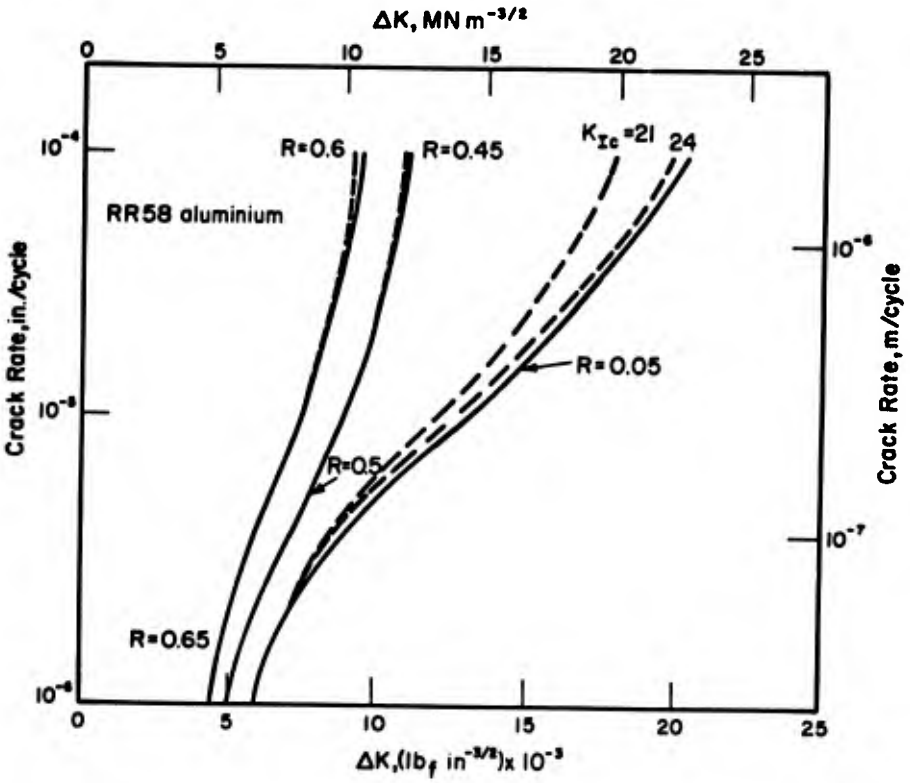

Fig.2.15(a) Comparison of experimental (Pearson 1972) and calculated (dashed curves) growth rates for a low toughness aluminum alloy, RR58. ΔK_{TH_0} taken as 5 Ksi$\sqrt{in.}$, σ_y as 60 Ksi, E as 10.7 x 10^6 psi, and the constant A as 0.02, K_c as 21 Ksi$\sqrt{in}$ except as noted

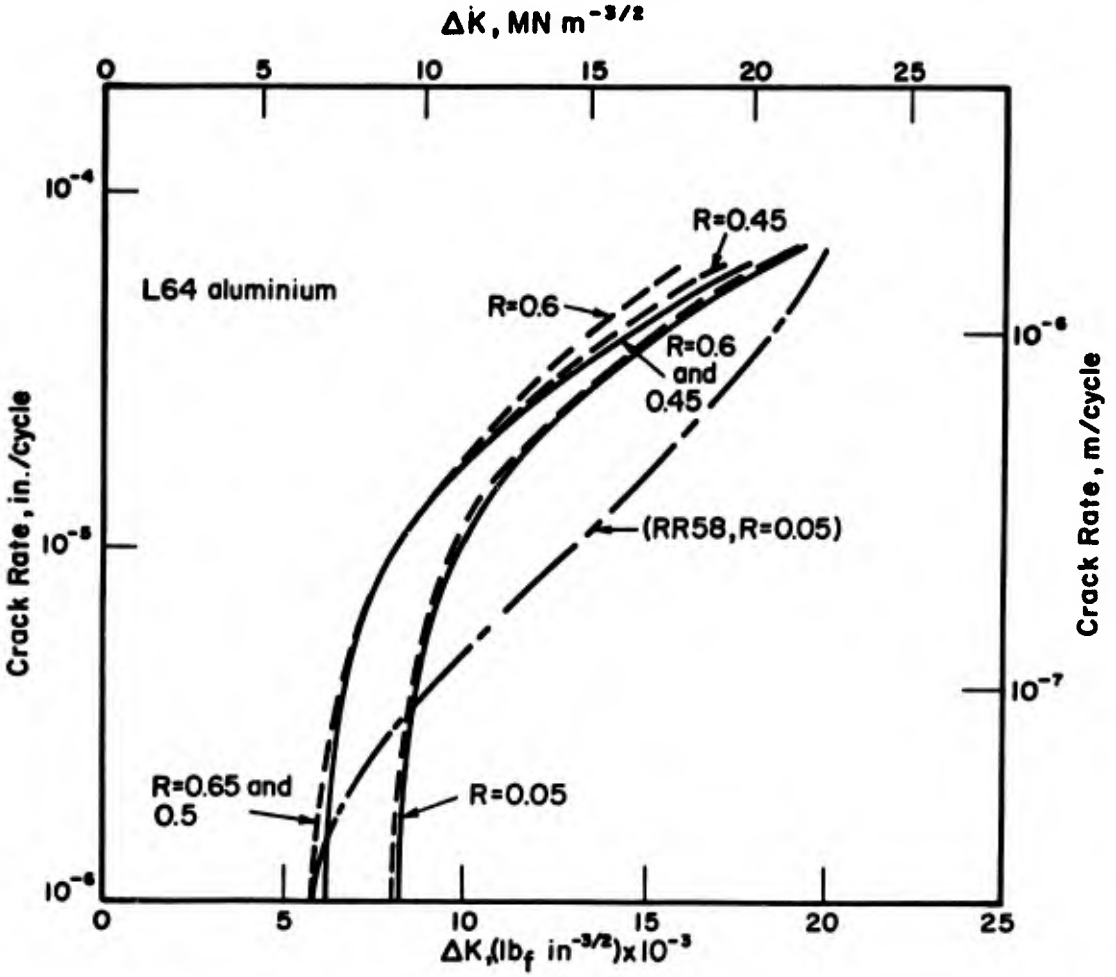

Fig.2.15(b) Comparison of experimental (Pearson 1972) and calculated (dashed curves) growth rates for a high toughness aluminum alloy, L64. ΔK_{TH_0} taken as 7 Ksi$\sqrt{in}$., σ_y as 52.5 Ksi, as 10.6 x 10^6 psi, K_c = 60 Ksi$\sqrt{in}$. RR58 test results shown for comparison

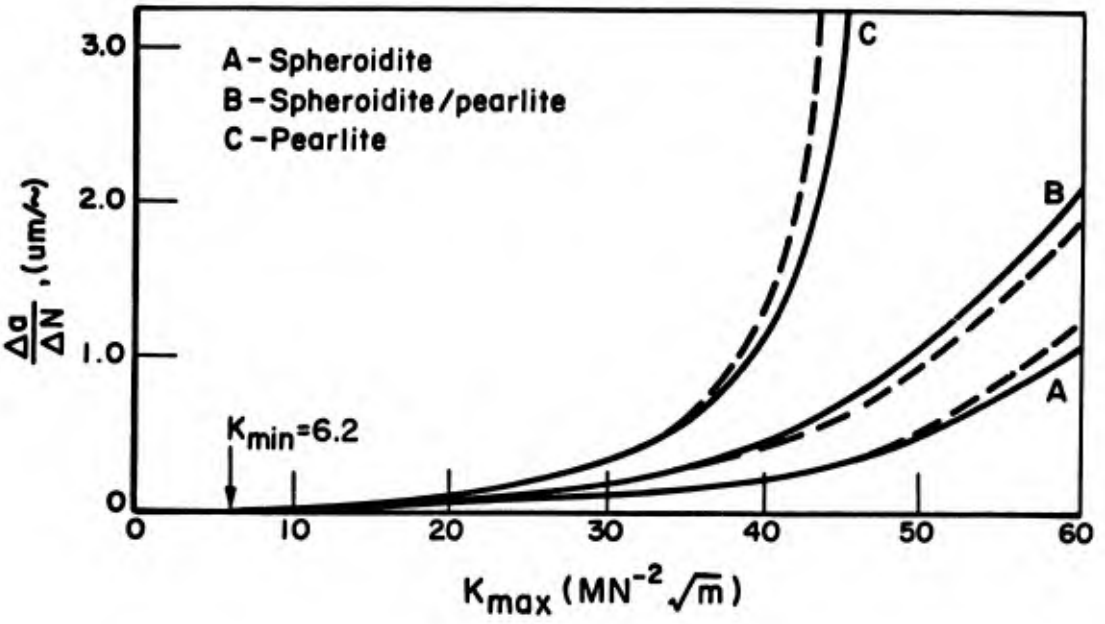

Fig.2.16 Comparison of experimental (Richards and Lindley 1972) and calculated (dashed curves) growth rates for a 1% carbon steel heat treated to give three different microstructures. K_c values: A-200 $MNm^{-1/2}$; B-90 $MNm^{-3/2}$; C-50 $MNm^{-3/2}$. Constant A taken to be 0.015, ΔK_{TH} = 11 $MNm^{-3/2}$. E = 20.7 x 10^4 MNm^{-2}; σ_y = 415, 455 and 380 MNm^{-2} for A, B, and C, respectively

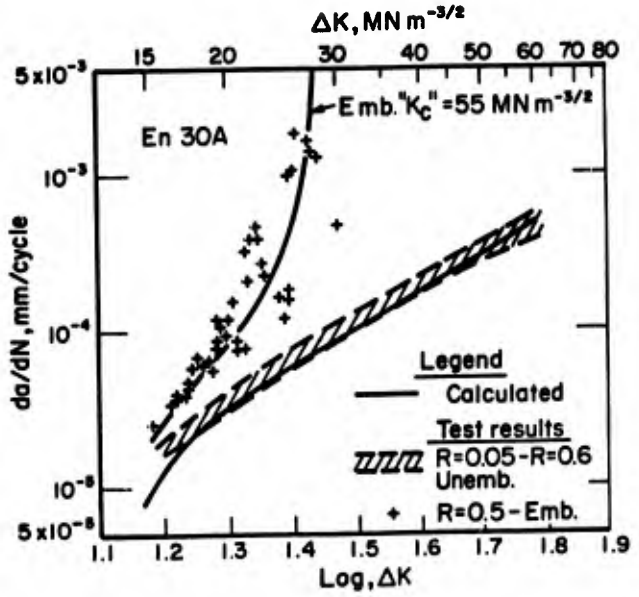

Fig.2.17 Comparison of experimental (Ritchie and Knott 1973, Knott and Ritchie 1973) and calculated growth rates for En30a steel in unembrittled and embrittled conditions. σ_y unembrittled 743 MNm^{-2} embrittled 735 MNm^{-2}, constant $A = 0.015$, $\Delta_{TH} = 11\ MNm^{-3/2}$, K_c embrittled = 55 $MNm^{-3/2}$, K_c unembrittled large with respect to K_{MAX}

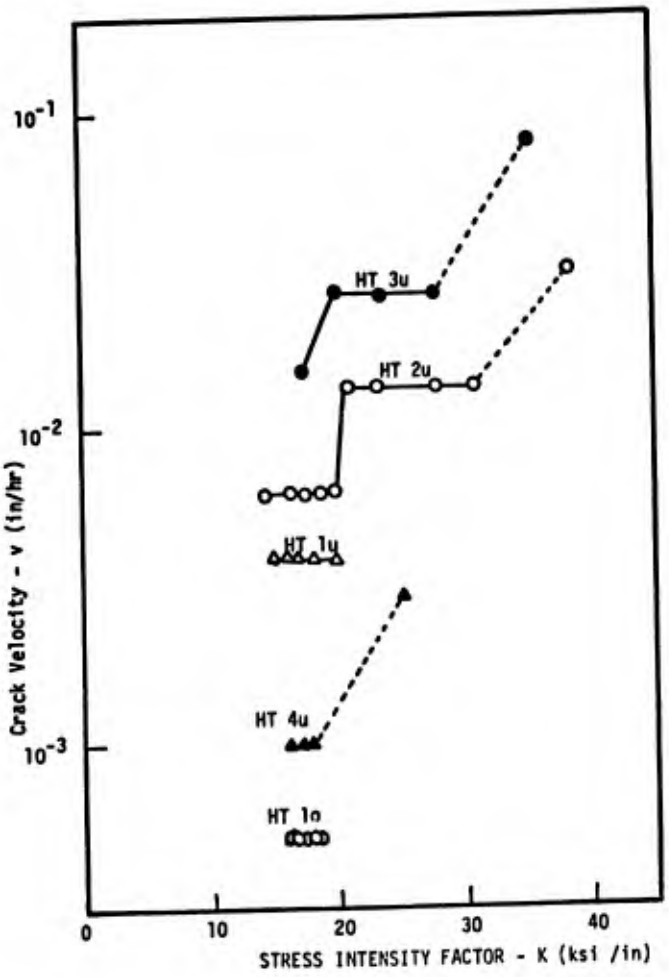

Fig.3.1 Stress corrosion crack velocity as a function of stress intensity for different heat treatments of an Al-5.5Zn–2.5 Mg alloy. The yield strength in each case was over 40 Ksi. Designation u, underaged; o, overaged. Volume of grain boundary precipitate increases monotonically with decrease in plateau level. (Morral, Poulose, McEvily 1973)

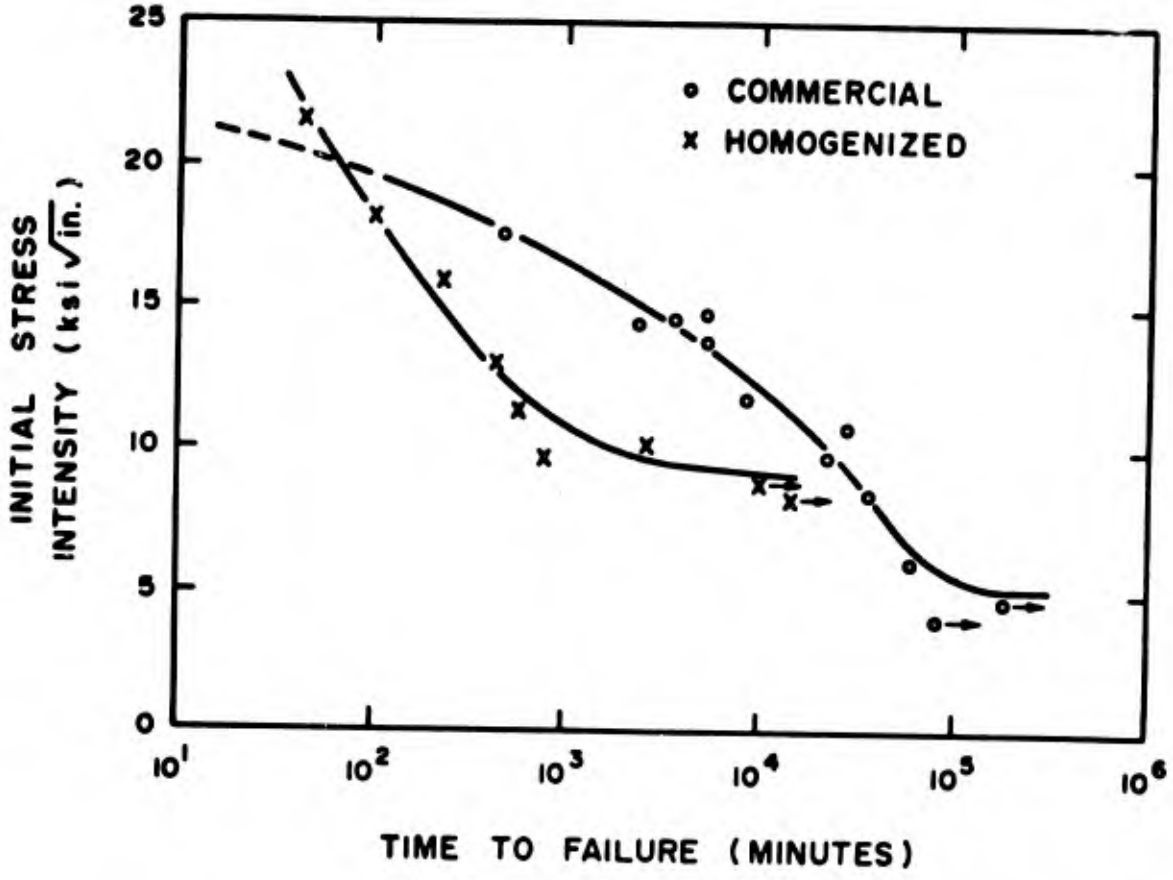

Fig.3.2 Stress corrosion crack propagation characteristics of commercial and experimental homogenized 7075 Al on the short transverse direction when exposed to salt water.
(Mulherin and Rosenthal 1971)

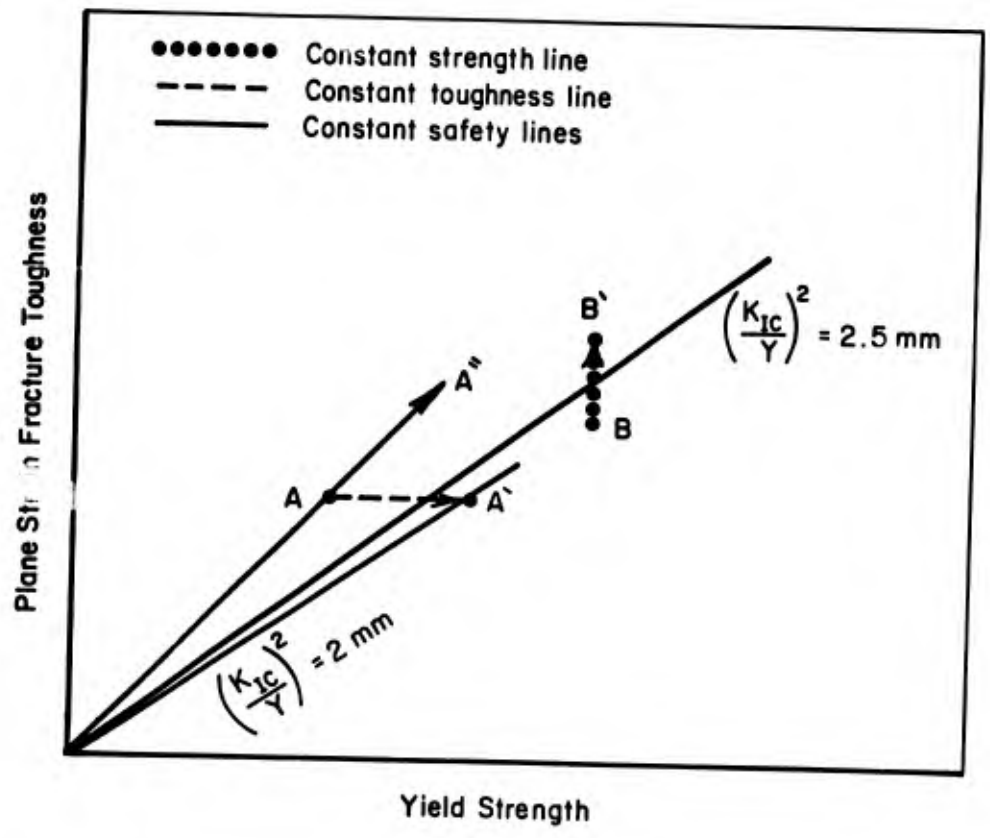

Fig.4.1 Schematic toughness/strength diagram illustrating the concept of constant safety

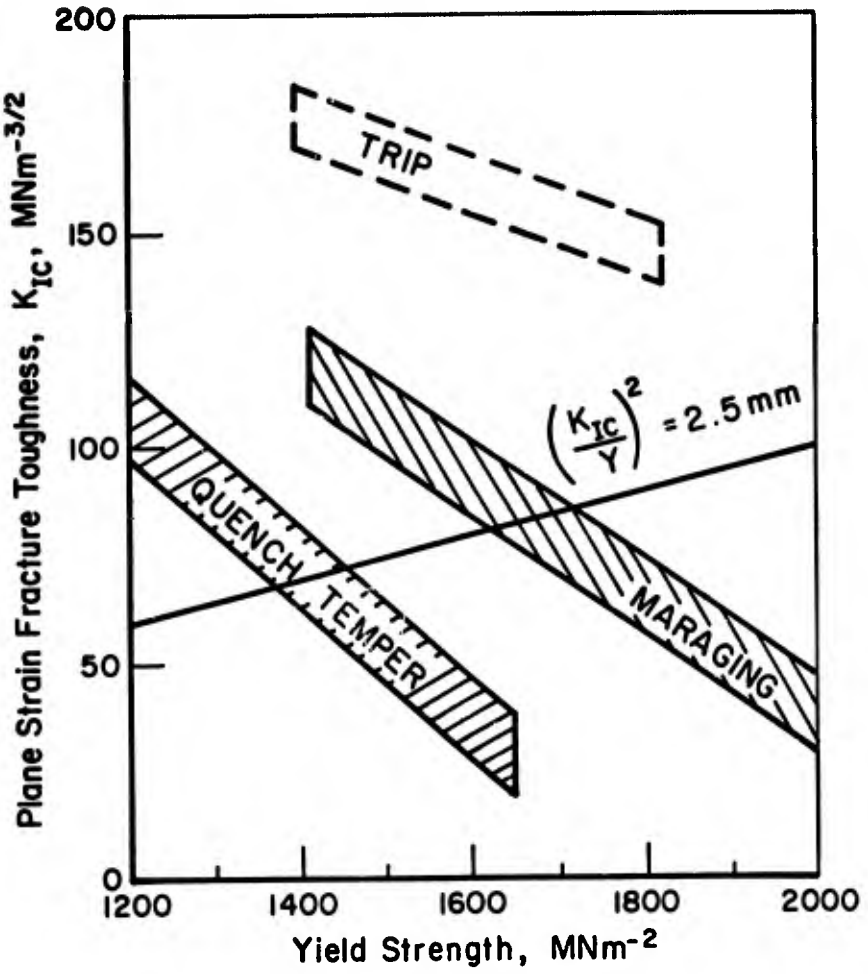

Fig.4.2 Toughness-strength relations for steels. After Zackay, et al. (1973)

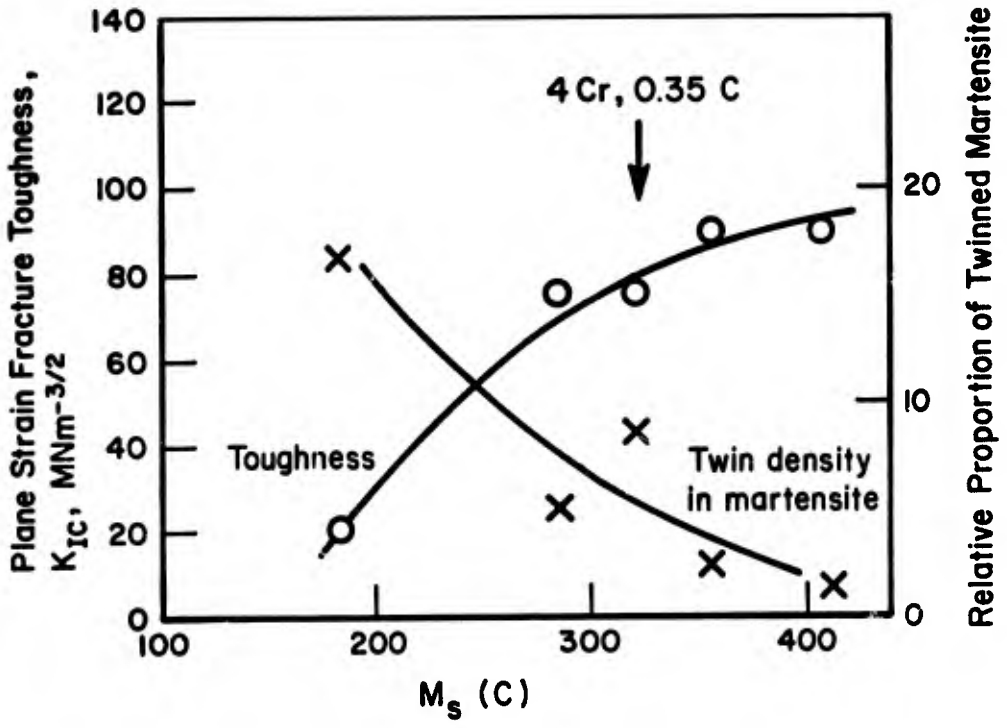

Fig.4.3 Toughness and microtwin frequency as a function of martensite start temperature for a series of Fe-Cr-C alloys. Data of McMahon and Thomas (1973)

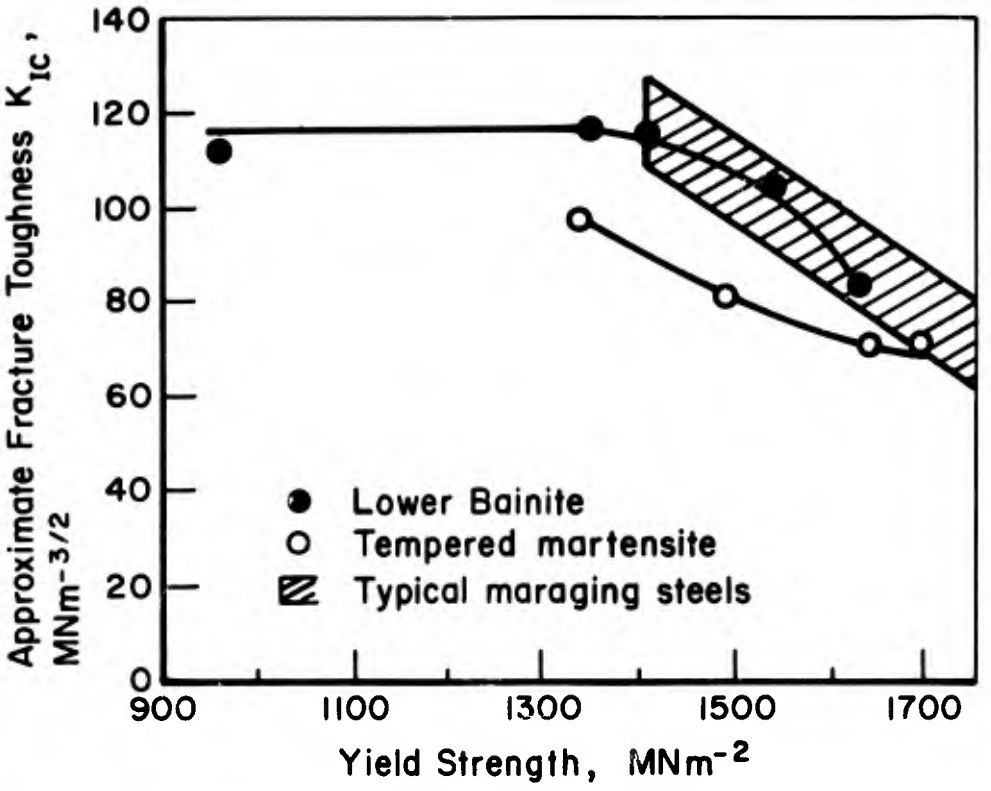

Fig.4.4 Fracture toughness as a function of yield strength and microstructure for steel HP-9-4-45 (8% Ni, 3.8% Co, 0.43% C). Data of Liu (1969)

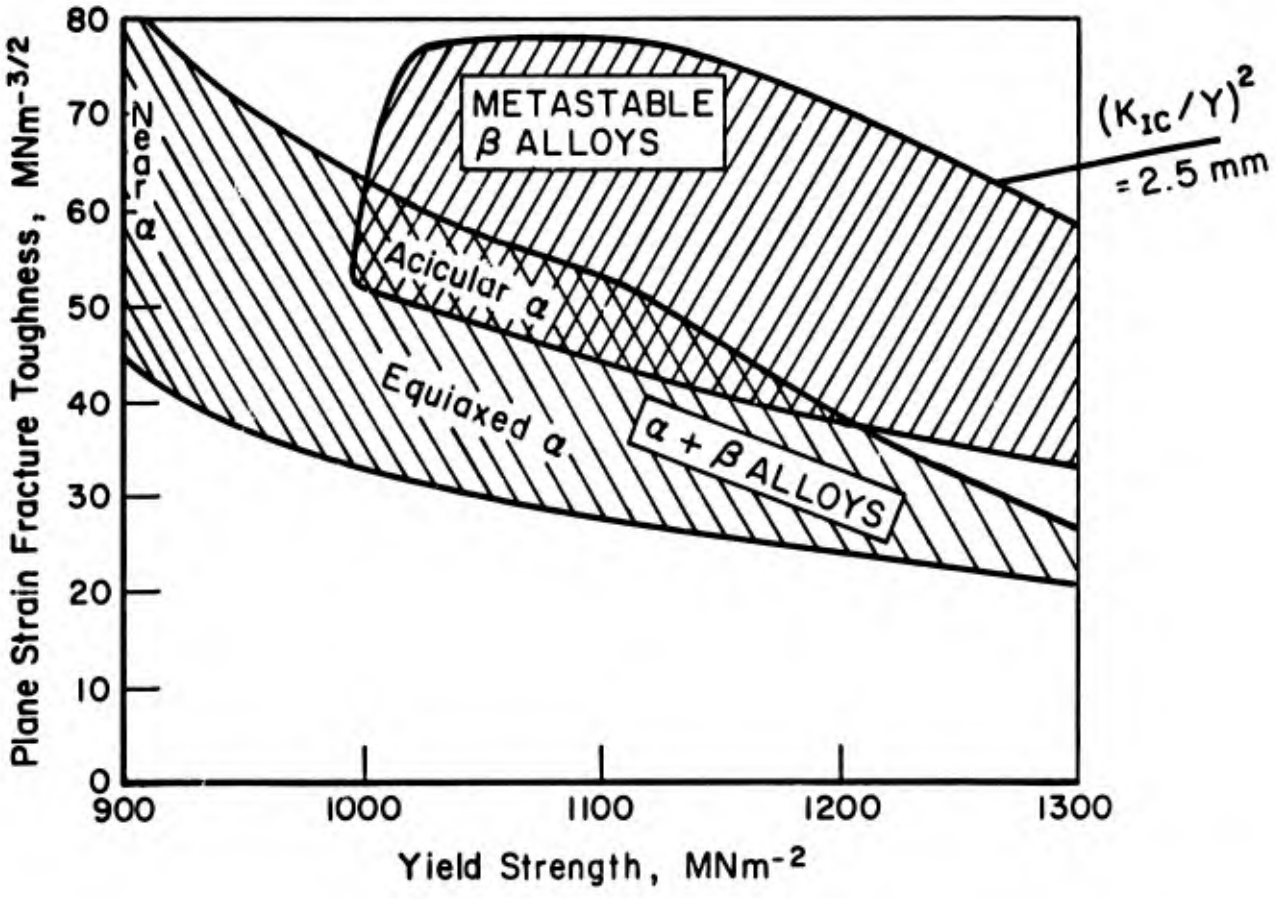

Fig.4.5 Schematic diagram of the strength-toughness relation for titanium alloys. (Coyne 1970, Crossley, et al. 1973, Judy, et al 1973, Rogers 1973)

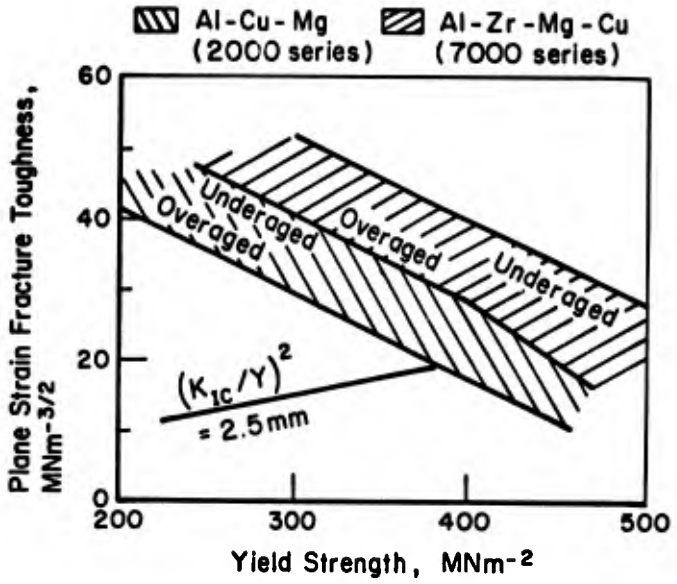

Fig.4.6 Schematic diagram of the strength-toughness relation for aluminum alloys. (Develay 1972)

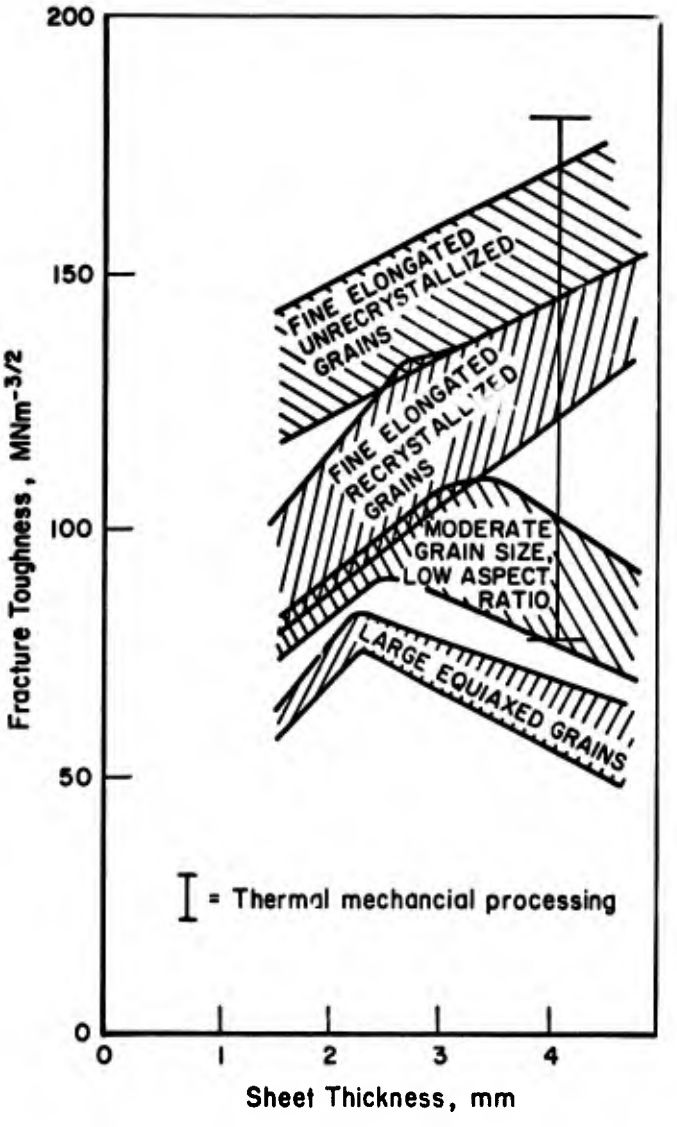

Fig.4.7 Fracture toughness of overaged 7000 series aluminum sheet

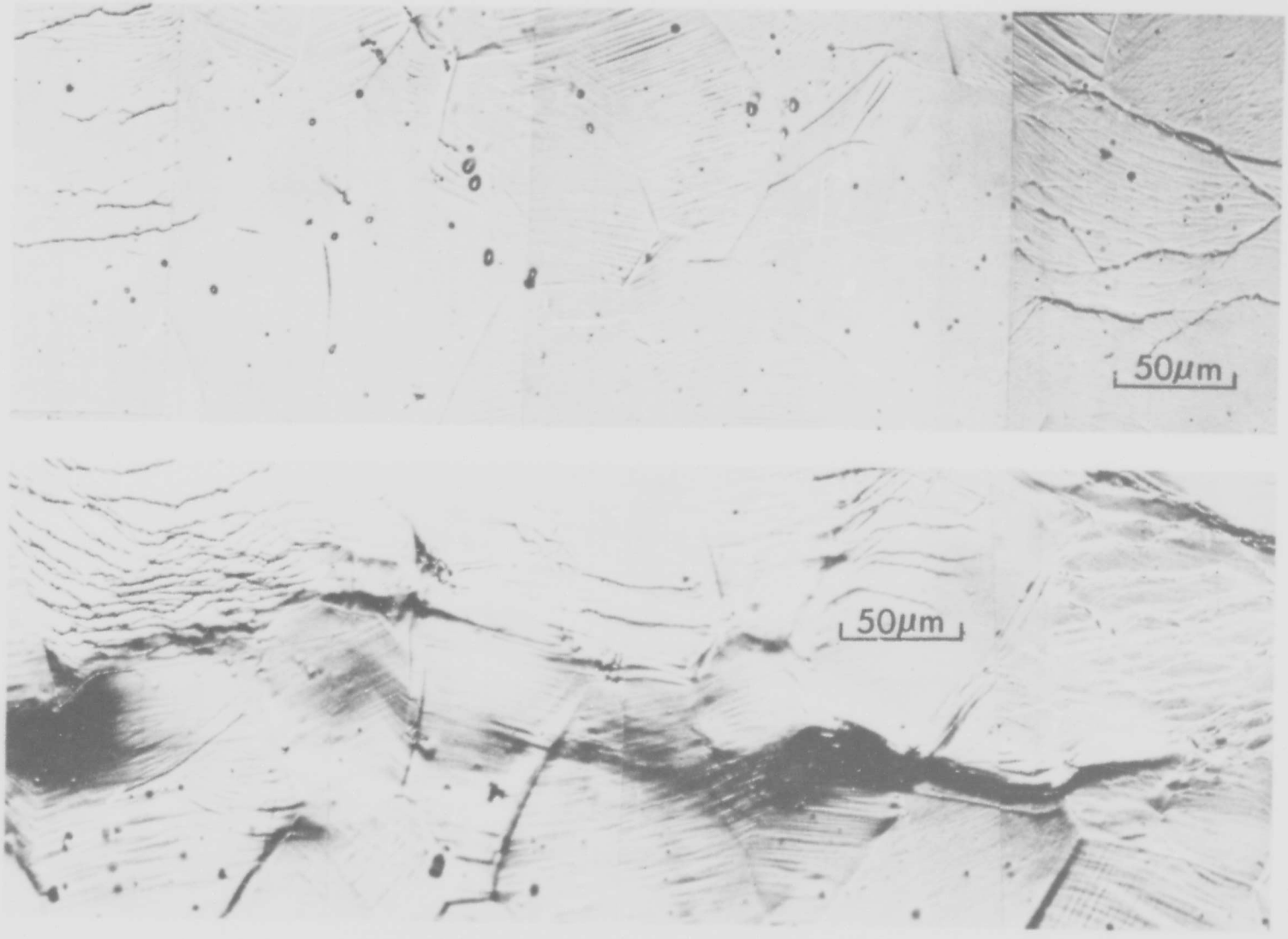

Fig.4.8 Optical micrographs of replicas of the same region of the surface of a plastically bent strip showing the progressive development with plastic strain of a super band in a 7000-series alloy in the peak aged condition. The tensile direction is vertical. (a) plastic strain 0.08, (b) plastic strain 0.17

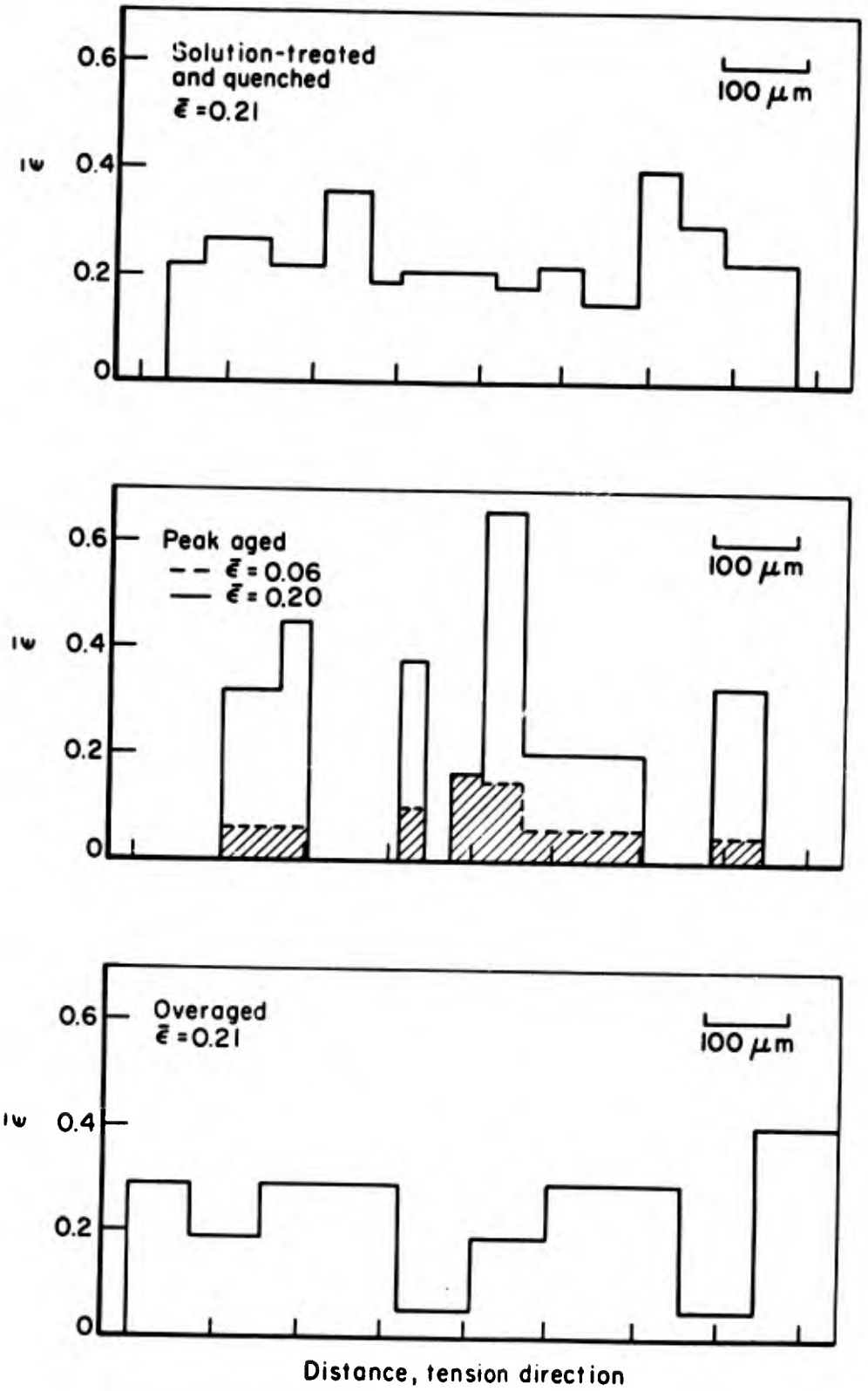

Fig.4.9 Influence of heat treatment on the plastic strain distribution on the microscale for "plane strain" deformation. The true strain measurements were derived from replicas of the type shown in Figure 4.8, taken on the surface of plastically bent strips of a 7000-type alloy (alloy X): (a) solution treated and quenched condition, (b) the peak aged condition and (c) overaged. The average grain boundary intercept is 90 μm. (Hahn and Rosenfield 1973)

IMPROVEMENT OF THE PROPERTIES OF HIGH STRENGTH Al-Zn-Mg-Cu ALLOYS BY THERMOMECHANICAL PROCEDURES

by

E. Di Russo
Istituto Sperimentale dei Metalli Leggeri
Via del Lavoro, 2
C.P. 129
Novara, Italy

and

S.Signoretti
Direzione Laboratori, Aeronautica Militare
Via Tuscolana, 473
00181 Roma, Italy

1. INTRODUCTION

This paper describes a new thermomechanical processing technique, developed at ISHL, for producing plates and forgings of 7000 series alloys (7075, 7049, 7475, 7050, etc.) showing a less transverse effect than similar conventionally processed materials. This procedure, called Intermediate Thermomechanical Treatments (ITMT), is based on a combination of warm deformations and heat treatments which involve the recrystallization of the ingot in small equiaxed grains in an intermediate (or final) stage of the working.

As a result of the processsing, the alloys exhibit better ductility, toughness and stress-corrosion properties, for a given strength, than conventionally processed materials, mainly in the short transverse direction. Moreover, it has been found that the contemporary application of ITMT and final (FTMT) thermomechanical treatments of T-AHA type, which, as is known, cause a super-hardening effect with an acceptable loss in ductility, may lead to decidedly "new" products with properties that are much superior to those of commercial traditional products.

2. DESCRIPTION OF THE PROCESS

Research work is being carried out at Experimental Institute of Light Metals (Novara) on medium and high strength age hardenable aluminum alloys, for obtaining wrought products with improved primary and/or secondary properties compared to those of industrially produced material. This work is sponsored by the Italian Ministry of Defence and the US Dept of the Army under a US/Italy Cooperative Research and Development Project on Aluminum Alloys.

Two different routes are followed: both are based on the application of combined cycles of plastic deformation and thermal treatment. These cycles have been indicated schematically intermediate (*ITMT*) and final (*FTMT*) thermomechanical treatments, according to their "position" in the production schedule of the alloy. The ITMT process may be considered as a new fabrication technique of plates and forgings; the FTMT process represents a particular final super-hardening heat treatment. The ITMT process was aimed at improving the secondary properties, such as ductility, toughness, stress-corrosion and fatigue resistance in the transverse directions (and above all in the short transverse direction) without decreasing the typical strength levels of the conventionally produced alloys in the traditional tempers. The FTMT process was aimed at increasing the strength of wrought products such as sheets, plates and extrusions, while maintaining the other properties at satisfactory levels.

Our investigations have been mainly devoted to the *Al-Zn-Mg-Cu alloys*, since they represent the most attractive materials for applications requiring a high strength to weight ratio. On the other hand, the potential of the Al-Zn-Mg-Cu system for alloy development to attain higher strengths and more favourable combinations of strength and toughness appears to be greater than that of any other aluminum alloy system.

As has been said previously, the ITMT process was designed essentially for reducing the short transverse effect of some types of wrought products. As is known, this transverse effect is related to several structural features, e.g.:

(i) *second phase particles*, inherited from the original cast ingots (oxide inclusions, unsoluble and undissolved intermetallic compounds) which are disposed in layers parallel to the metal flow direction (stringers);

(ii) *preferential orientation*; however this feature seems to play a marginal role;

(iii) *grain size and morphology*; the plastic processing of the ingots yields to unrecrystallized "grains" (composed of sub-grains of a few microns in diameter) elongated in the working direction. This "pancake" structure is typical for the plates of 7000 group alloys, and is to be ascribed to the presence of chromium.

The boundaries of the elongated grains, which correspond to the original cast grain boundaries, are *weak* regions. In fact when the wrought product is mechanically stressed in the short transverse direction, the fracture path preferentially follows such boundaries[1]. A possible explanation of this behavior could account for a geometrical factor, and for the localization of the second phase particles along the primary grain boundaries. Secondary particles may be more or less avoided by careful control of the melting and casting conditions; in this line, the most important approaches towards the reduction of the transverse effect are:

- lowering of the impurity level,
- advanced homogenization of the ingot,
- high solidification rate.

These processings improve the ductility and toughness, primarily as a consequence of a reduction of volume percentage of secondary phases[2,3,4,5].

No specific research work has been devoted to the elimination of the original cast grain boundaries and the modification of the "pancake" structure. Therefore it has been essential to develop new fabrication techniques that could ensure that the product's final structural features are related in the least possible way to the original structure of the ingot. The ITMT process was based on the assumption that the influence of the original cast structure could be minimized by *an intermediate recrystallization* of the ingot during the working cycle; in addition, in order to have the most effective recrystallization structure, *it appeared necessary to produce fine and equiaxed grains*[6].

A preliminary investigation performed on h.p. 7075 alloy, showed that the recrystallization of the ingot was possible only through procedures based on peculiar combinations of plastic deformation and heat treatment. In more detail, these tests showed that among the main factors controlling the recrystallization process, i.e. the deformation temperature and the degree of deformation, the latter depends on the initial disposition of both chromium and solute elements (Zn, Mg and Cu). The more pronounced the Cr-rich particles precipitation, the greater must be the deformation for recrystallizing the material, whereas the deformability of the alloy increases when Zn, Mg and Cu are out of solution as not-coherent precipitates. As has been demonstrated elsewhere, Cr precipitation is a function of the temperature and of the holding time of the homogenization treatment of the ingot[7]. In addition, it is to be stressed that when the recrystallization occurs in the presence of a copious precipitation of Cr-rich compounds, the recrystallized grains are not equiaxed, but they appear to be more or less elongated in the metal flow direction.

An important role is also exerted by the *heating rate* up to the recrystallization temperature; increasing the heating rate produces a higher degree of recrystallization and a greater number of grains per unit area. Figure 1 shows, in a qualitative manner, how the processing variables may control the intermediate recrystallization of a high purity 7075 alloy. It appears that deformation is more difficult when the material is only partially homogenized; on the other hand, recrystallization has a less equiaxed character when the ingot is fully homogenized, i.e. when the matrix shows a copious precipitation of Cr-bearing compounds.

From these early investigations, tentative conditions for obtaining an equiaxed grain structure in high purity 7075 type alloys were determined and the complete fabrication cycle of plates (or forgings) based on the ITMT technique was scheduled as shown in Figure 2. Two ways are indicated: one is based on intermediate recrystallization followed by a conventional hot working cycle; the other one is based on a recrystallization process which represents the final step of the plastic working. It is to be noted that the (intermediate or final) recrystallization is produced on a partially homogenized ingot (where Cr is prevailingly distributed in solid solution) subjected to deformation at medium temperature. After recrystallization, the ingot is fully homogenized. This treatment causes a fine and homogeneous precipitation of Cr-rich particles, and this precipitation prevents any grain boundary migration during the subsequent operations.

A simple scheme of the structural transformations occurring during a conventional and ITMT processing of 7075 alloy plates is illustrated in Figure 3. This model has been based on optical and electron microscopy observations. The main structural parameters considered are the original boundaries of the cast grains, the interdendritic segregations, the precipitation of the chromium dispersoids and the formation of both the equiaxed recrystallized grain and sub-grain structures. The wrought product so obtained may then be subjected to a conventional heat treatment or to FTMT treatment, as indicated in Figure 2.

As reported elsewhere, the FTMT cycle is a peculiar type of heat treatment (consisting of a pre-aging at low temperature followed by a cold or warm plastic deformation and by a final aging step) which provides a strong hardening effect due to the synergistic action of dislocations and age precipitation[8,9,10,11,12,13]. This sequence

permits a reduction of the inhibiting effect on the aging reactions exerted by the dislocations, so that it is possible to attain a further hardening in the final aging stage.

Figure 4 gives an overall view of the different contributions to the *maximum* hardening produced by aging and deformation in the following cycles: T-AH, T-HA and T-AHA* as a function of the degree of deformation. The advantage of applying the deformation after a first step of artificial aging appears evident. Obviously the sequence T-AH, where H is produced after the peak aging, was neglected because in this case, instead of disjoint, an excessive decay of elongation occurs because of the difficulty of producing deformation.

3. EXPERIMENTAL RESULTS

One of the first applications of ITMT techniques was made in the fabrication of 10 mm - thick rolled plates of h.p. 7075 alloy (Al – 5.78%Zn – 2.65%Mg – 1.64%Cu – 0.22%Cr – 0.0024%Ti – 0.0013%Fe – 0.004%Si). The working schedule is given in Table I. Process A is a conventional hot rolling cycle and it is characterized by full initial homogenization. Processes B, C and D are of ITMT type; they differ from one another for the intermediate working procedure and for the degree of reduction in thickness in the final stage of working.

Figure 5 shows the microstructures of the ingot in the as cast state and after pre-homogenization at 400°C x 10–24 h. The structure produced by the pre-homogenizing cycle is characterized by a hardly detectable precipitation of Cr-rich particles and by a partial solution of the eutectic network. The microstructures of the samples (longitudinal section) at the end of the working cycles, after quenching and aging, are illustrated in Figures 6, 7 and 8.

After the conventional working cycle (process A), the plate exhibits coarse, elongated "grains", consisting in turn of sub-grain aggregates (Fig.6); such "grains" correspond to the original primary grains. The thermomechanical process B, free from subsequent final conventional working, produces a plate with very small, mostly equiaxed recrystallized grains (Fig.6). The thermomechanical processes C and D, with hot rolling subsequent to the recrystallization stage, cause a structure composed of small elongated "grains", consisting in turn of sub-grain aggregates (Fig.7).

Figure 8 shows the microstructures of the plates produced respectively by conventional cycle and by thermomechanical procedure (process C), observed by transmission electron microscopy. As a main structural feature, the different morphology of Cr-rich precipitated particles induced by the two different processes must be noted. In the traditionally fabricated material one can observe an inhomogeneous distribution of coarse Cr-particles, while in the thermomechanically processed material the Cr-precipitates are finer and more evenly distributed within the matrix.

The tensile properties of the samples produced as above, and T6 treated, are given in Table II. The materials have also been subjected to a final thermomechanical treatment (T-AHA); the tensile properties in this new temper are given in the same table. These results indicate clearly that the ITMT processes increase markedly the elongation and above all the reduction in area values, compared to the conventional cycle. Such improvement is achieved without appreciable changes in strength. The combination of ITMT + FTMT processes produces plates with very high strength and good ductility.

Another application of the ITMT technique was made in the production of 25 mm - thick plates of c.p. 7075 (Al – 5.80%Zn – 2.66%Mg – 1.68%Cu – 0.22%Cr – 0.23%Fe – 0.06%Si) and c.p. 7050 (Al – 5.78%Zn – 2.24%Mg – 2.24%Cu – 0.16%Zr – 0.029%Ti – 0.0018%Fe – 0.0064%Si) alloys; the working schedule is indicated in Table III. For each alloy, two cycles, one of conventional type and the other of ITMT type were tested. The characteristics of our rolling mills did not permit deforming the ingot samples (height = 175 mm) only by rolling; the rolling was limited to a final stage of working, while the first stage down to approximately 40 mm was accomplished by hand forging, providing the metal could flow preferentially in one direction.

The microstructures of the pre-homogenized ingots are illustrated in Figure 9. As commonly found, the contemporary addition of Zr + Ti has caused a high refinement of the primary grains. The application of the previously described ITMT process to c.p. 7075 has caused significant variations in structure with respect to the conventional cycle (Fig.10). In this case, however, the combined effect of a low degree of purity and of a greater thickness of the plate, has not allowed us to obtain a grain structure as fine as that produced on 10 mm - thick plates of higher purity alloy (Fig.7). Also on the Zr-bearing alloy an ITMT process analogous to that applied to c.p. 7075, has cause substantial changes in the grain structure (Fig.10).

The tensile properties of the T6 plates, determined in the longitudinal direction, are indicated in Table IV. The same table also gives the short transverse fracture toughness properties of the plates in T651 temper, determined on DCB specimens, pre-cracked in fatigue. On both alloys the experimented ITMT process causes a small decrease in strength and an increase in elongation, reduction in area and fracture toughness. It is worthwhile noting that the decrease in strength occurs in the longitudinal direction, while the improvement in toughness (10–20%) is in the short transverse direction.

* where A = aging and H = deformation

As has been previously emphasized, the goal of the ITMT processing is to increase ductility and toughness in the short transverse direction; therefore some decrease of strength in the other working directions may be accepted. Table V shows the tensile properties of the alloys in the long transverse direction after a two-step aging cycle; the conclusions which may be drawn are analogous to those concerning the T6 state.

Results of alternate immersion standard stress-corrosion tests performed on "U" shaped smooth specimens, taken from the short transverse direction of the two-step aged plates, are given in Table VI and Figure 11. The data indicate clearly that the ITMT process improves the stress-corrosion resistance of both alloys.

Conclusions similar to those for the influence of the ITMT process may be drawn from the examination of the curves of crack growth rate versus crack-tip stress intensity factor obtained using DCB specimens (taken from the short transverse direction), according to the procedure suggested by Hyatt (Figures 12 and 13). In particular the ITMT processed materials exhibit, after two-step aging, not only higher K_{ISCC} values, but also higher fracture toughness indexes (K_c) in the short transverse direction than the convetionally produced plates (Table VII).

The results achieved by the application of ITMT processes point out that our assumption was correct since through the described modifications of the grain structure it is really possible to reduce the transverse effect. It is obvious however that further investigations are needed in this area and the parameters involved in this new processing technique must be defined according to *the composition of each alloy, the nature of the addition elements and the thickness of the final product*. With reference to the FTMT cycles, described in detail elsewhere, in this paper it is sufficient to give a general view of the combination of strength/elongation achievable on sheets of various 7000 series alloys using the T-AHA sequence (Figure 14 – Table VIII).

Other works are in progress for optimizing the FTMT and ITMT processing parameters; it is reasonable to expect from the contemporary application of ITMT + FTMT the obtaining of "new" products with a combination of properties significantly better than that of the industrially produced materials

ACKNOWLEDGEMENTS

The authors are grateful to the ISML technicians for their valuable assistance in performing this work.

REFERENCES

1. Di Russo, E. Giarda, A. — *Risultati de indagini strutturali eseguite su estrusi di leghe Al-Zn-Mg-Cu: considerazioni sull'effetto di pressa".* Alluminio e Nuova Metallurgia, XL, n.11, pp.539-549, (1971).

2. Bower, T.F. et al. — *Development of High Strength Wrought-Aluminum Base Alloys.* Metallurgical Trans., I, pp.191-197, (1970).

3. Di Russo, E. — *Ricerche sull'impiego di aluminio iperpuro nelle leghe leggere Al-Zn-Mg-Cu a resistenza meccanica elevata.* Alluminio e Nuova Metallurgia, XXXVI, n.1, pp9-15, (1967).

4. Singh, S.N. Flemings, M.C. — *Solution Kinetics of a Cast and Wrought High Strength Aluminum Alloy.* Trans. A.I.M.E., CCXLV, pp.1803-1809, (1969).

5. Antes, H.W. Markus, H. — *Homogenization Improves Properties of 7000 Series Aluminum Alloy.* Metals Engineering Quarterly, X, n.4, pp9-11, (1970).

6. Di Russo, E. et al. — *Thermomechanical Process for Improving the Toughness of the High Strength Aluminum Alloys.* Ital. Pat. n.918, 387 (1971), US Filed 7.6.71, Ser. No.150, 501.

7. Conserva, M. et al. — *Cr Precipitation in a High Purity Al-Zn-Mg-Cu Alloy.* To be published in Metallography.

8. Conserva, M. et al. — *A New Thermomechanical Treatment for Al-Zn-Mg type Alloys.* Alluminio, Nuova Metallurgia, XXXVII, pp.441-445 (1968).

9. Di Russo, E. Conserva, M. — *Thermomechanical Treatment Procedures for Heat Treatable Aluminum Alloys.* Ital. Pat. 886, 185 (1970) (US Filed 14.470, Ser. No.28, 514).

10. I.S.M.L. — *Improvements of the Properties of High Strength Aluminum Alloys by Means of Complex Thermomechanical Treatments* (CTSD-32). Final Technical Report n.71/21 311 – Contract CTSD-32 (1971).

11. Buratti, M. et al. *Super-indurimento di leghe Al-Zn-Mg mediante trattamenti termomeccanici.* Alluminio, XLI, pp.414-418 (1972).

12. Conserva, M. et al. *Age Hardening Behavior of TMT Processed Al-Zn-Mg-Cu Alloy.* Mat. Sci. Engng XI, pp.103-112, (1973).

13. Di Russo, E. et al. *Thermomechanical Treatments on High Strength Al-Zn-Mg(Cu) Alloys.* Met. Trans., IV, pp.113-1144, (1973).

TABLE I

Working Schedule of ~ 10 mm – Thick Rolled Plates of h.p. 7075

Process Designation	*Homogenization of Ø 110 mm Ingot*	*Plastic Pre-heating (*)*	*Plastic Working*	*Intermediate or final thickness*	*Recrystallization treatment (in salt bath)*	*Full homogenization*	*Plastic Pre-heating*	*Plastic working*	*Final thickness*
Conv. cycle (A)	450°C x 8 h + 480°C x 24 h	430°C x 1 ÷ 2 h	Hot rolling	10 mm (r.t. = 72%)	–	–	–	–	10 mm
ITMT Cycle (B)	400°C x 24 h	330°C x 1 ÷ 2 h	Continuous warm rolling (†)	10 mm (r.t. = 72%)	475°C x 2 h	480°C x 24 h	–	–	10 mm
ITMT + conv. cycle (C)	400°C x 10–24 h	330°C x 1 ÷ 2 h	Continuous warm rolling (†)	15 mm (r.t. = 57%)	475°C x 2 h	480°C x 24	430°C x 1 h	Hot rolling	10 mm (r.t. = 34%)
ITMT + conv. cycle (D)	400°C x 10 h	330°C x 1 ÷ 2 h	Continuous warm forging (†)	15 mm (r.t. = 57%)	475°C x 2 h	480°C x 24 h	430°C x 1 h	Hot rolling	10 mm (r.t. = 34%)

(*) Thickness of the ingot samples = 35 mm

(†) Cold water cooling at the end of the working

h.p. 7075: Al – 5.78% Zn – 2.65% Mg – 1.64% Cu – 0.22% Cr – 0.0024% Ti – 0.0013% Fe – 0.004% Si

TABLE II

Tensile Properties in the Long Transverse Direction of 10 mm – Thick Rolled Plates of h.p.7075 Alloy, Produced by Different Processings, in Various Tempers

Process designation	T (N3) A 120°C x 24 h (T6)				T (N3) A 105°C x 6 h + Hc 10 + A 120°C x 13 h			
	T.S. kg/mm²	Y.S. kg/mm²	El. %	R.A. %	T.S. kg/mm²	Y.S. kg/mm²	El. %	R.A. %
Conv. cycle (A)	62.1	55.5	8.5	17.3	66.3	63.0	4.6	13.7
ITMT cycle (B)	61.4	55.3	12.1	38.9	65.5	62.8	7.6	32.1
ITMT + conv. cycle (C)	61.5	56.0	10.5	33.6	65.9	62.5	6.9	27.6
ITMT + conv. cycle (D)	62.4	56.4	11.3	34.6	65.5	62.1	7.8	34.9

T = quenching in water at room temperature from 475°C (soaking time: ~ 2 h)

Hc 10 = degree of deformation in % given by warm rolling at ~ 180°C.

TABLE III

Working Schedule of ~ 25 mm – Thick Forged – Rolled Plates of c.p.7075 and h.p. 7050

Process designation	*Homogenization of Ø 180 mm Ingot*	*Plastic pre-heating (*)*	*Plastic working*	*Intermediate thickness*	*Recrystallization treatment (in salt bath)*	*Full Homogenization*	*Plastic pre-heating (**)*	*Plastic working*	*Final thickness*
Conv. cycle	400°C x 15 h + 463°C x 50 h	430°C x 1–2 h	Hot forging	40 mm (r.t. = 75%)	–	–	430°C x 1–2 h	Hot rolling	25 mm (r.t. = 28%)
ITMT + conv. cycle	400°C x 15 h + 280°C x 8 h	280–285°C x 1–2 h	Warm forging (†)	40 mm (r.t. = 75%)	457 ÷ 460°C x 2 ÷ 3 h	463°C x 50 h	430°C x 1–2 h	Hot rolling	25 mm (r.t. = 28%)

(*) Thickness of the ingot samples = 175 mm

(†) Cold water cooling at end of the working

(**) After machining of the forged plates down to t = 35 mm

c.p. 7075: Al – 5.80% Zn – 2.66% Mg – 1.68% Cu – 0.22% Cr – 0.23% Fe – 0.06% Si

h.p. 7050: Al – 5.78% Zn – 2.24% Mg – 2.24% Cu – 0.16% Zr – 0.029% Ti – 0.0018% Fe – 0.0064% Si

TABLE IV

Tensile and Fracture Toughness Properties of 25 mm – Thick Forged – Rolled Plates of c.p. 7075 and h.p. 7050 Alloys, Produced by Different Processings

Alloy	*Process designation*	*Longitudinal direction*					*Short transverse direct* (*)	
		temper	T.S. kg/mm²	Y.S. kg/mm²	El. %	R.A. %	*temper*	K_c (†) $kgmm^{-2/3}$
c.p. 7075	Conv. cycle	T6	63.2	58.5	8.0	21.4	T651	49.5
	ITMT + conv. cycle	T6	61.0	56.5	10.0	28.5	T651	59.5
h.p. 7050	Conv. cycle	T6	63.5	58.4	9.6	22.6	T651	67.0
	ITMT + conv. cycle	T6	60.5	55.0	12.1	37.5	T651	74.0

(*) TL crack orientation
(†) determined on DCB specimens pre-cracked in fatigue
T6 = T (N3) A125°C x 24 h
T651 = T (H1.6%) (N3) A125°C x 24 h
T = quenching in water at room temperature from 470°C (soaking time ~ 2–3 h)
H1.6% = reduction in thickness of 1.6% by cold rolling

TABLE V

Tensile Properties in the Long Transverse Direction of 25 mm – Thick Forged – Rolled Plates of c.p. 7075 and h.p. 7050 Alloys, Produced by Different Processings, in (*) T (N3) A105°C x 8 h + 160°C x 24 h Temper

Alloy	*Process designation*	T.S. kg/mm²	Y.S. kg/mm²	El. %	R.A. %
c.p. 7075	Conv. cycle	58.2	52.0	10.4	27.3
	ITMT + conv. cycle	56.5	49.5	12.0	34.2
h.p. 7050	Conv. cycle	59.3	54.3	9.7	25.6
	ITMT + conv. cycle	56.7	51.5	13.1	40.3

(*) T = quenching in water at room temperature from 470°C (soaking time ~ 2–3 h)

TABLE VI

Stress Corrosion Behavior in the Short Transverse Direction (*) of 25 mm – Thick Forged – Rolled Plates of c.p.7075 and h.p.7050 Alloys, Produced by Different Processings in (†) T(N3) A105°C x 8 h + 160°C x 24 h Temper. (Alternate immersion tests in NaCl 3.5% on "⊐" shaped smooth specimens stressed in the middle plane of the exposed surface at various % of Y.S. in bending by imposed strain (leg deflection measured at the bottom of leg)

Alloy	*Process designation*	*Hours to visible stress corrosion cracks at indicated stress level in bending*		
		75% Y.S.	50% Y.S.	25% Y.S.
c.p. 7075	Conv. cycle	80, 100, 144, 144, 72	144, 144, 144, 144	216, 216, 216
	ITMT + conv. cycle	480, 144, 1176, 144, 800	1176, 1176, 1176, OK	OK, OK, OK
h.p. 7050	Conv. cycle	144, 1176, 1512, 500	144, OK, OK	OK, OK, OK
	ITMT + conv. cycle	OK, OK, OK	OK, OK, OK	OK, OK, OK

(*) TL crack orientation
(†) T = quenching in water at room temperature from 470°C (soaking time ~ 2–3 h)
OK = specimens free from visible cracks after 2000 h of test

TABLE VII

Results of Stress-Corrosion Tests (DCB Specimens Pre-Cracked in Tension) Performed on Short Transverse Direction (*) of 25 mm – Thick Forged – Rolled Plates of c.p.7075 and h.p.7050 Alloys, Produced by Different Processings in (†) T(H1.6%) (N3) A105°C x 8 h + 160°C x 24 h Temper

Alloy		*Process*	K_c	K_{ISCC}
Type	n.		$\frac{kg}{mm^2}\sqrt{mm}$	$\frac{kg}{mm^2}\sqrt{mm}$
c.p. 7075	7	Convent.	76.8	32.0
		ITMT + Convent.	99.2	38.0
h.p. 7050	8	Convent.	106.6	32.0
		ITMT + Convent.	132.0	41.5

(*) TL = crack orientation
T = quenching in water at room temperature from 470°C (soaking time ~ 2–3 h)
(†) H1.6% = reduction in thickness of 1.6% by cold rolling
K_{ISCC}: determined after more than 5000 h of test, when the crack growth was of ~ 1.5×10^{-9} cm/sec

TABLE VIII

Composition of the Sheets Subjected to Final Thermomechanical Treatments (FTMT) (see Figure 12)

Alloy	*Number*	Zn %	Mg %	Cu %	Cr %	Mn %	Zr %	Ti %	Fe %	Si %
7005 commercial purity	1	5.07	1.04	–	0.14	0.22	0.12	–	0.12	0.09
7039 commercial purity	2	4.01	2.78	–	0.14	0.23	0.10	–	0.14	0.09
7039 high purity	3	4.09	3.04	–	0.18	0.33	0.14	0.045	0.012	0.017
7075 commercial purity	4	5.49	2.46	1.69	0.13	0.20	–	0.074	0.28	0.20
7075 commercial purity	5	5.74	2.60	1.63	0.22	–	–	0.005	0.22	0.13
7075 high purity	6	5.68	2.50	1.60	0.22	–	–	0.010	0.0016	0.005

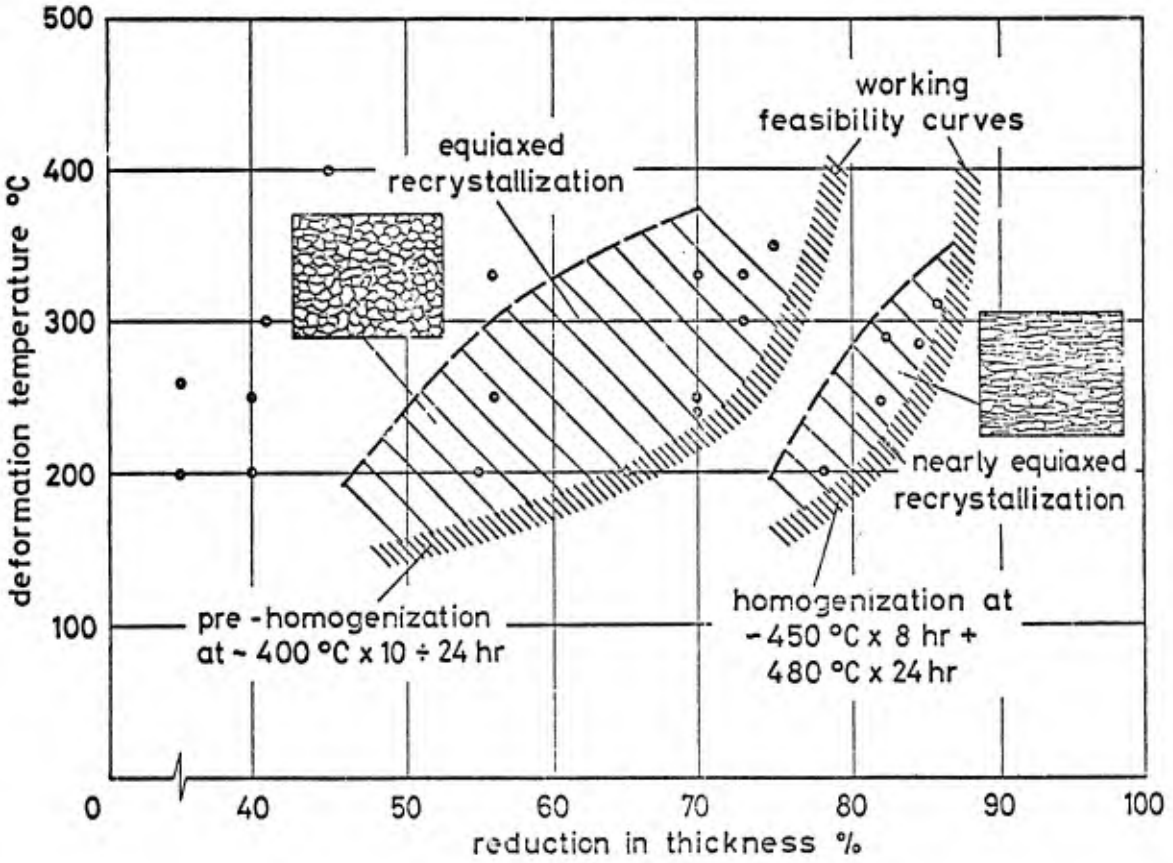

Fig.1 Effect of the processing variables on the recrystallization structure of h.p. 7075 plates. Two different homogenizing treatments are considered: 400°C for 10÷24 h (Cr in solution) and 450°C for 8 h + 480°C for 24 h (Cr in form of precipitates). The recrystallization treatment is 475°C for 2 h

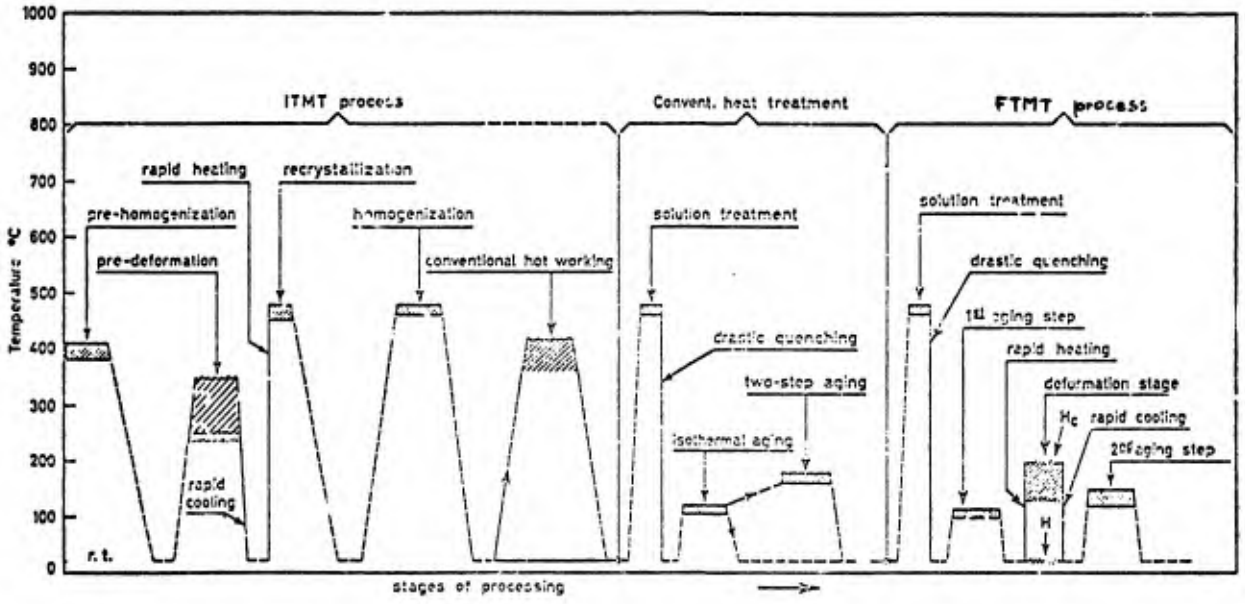

Fig.2 Scheme of the intermediate thermo-mechanical treatment

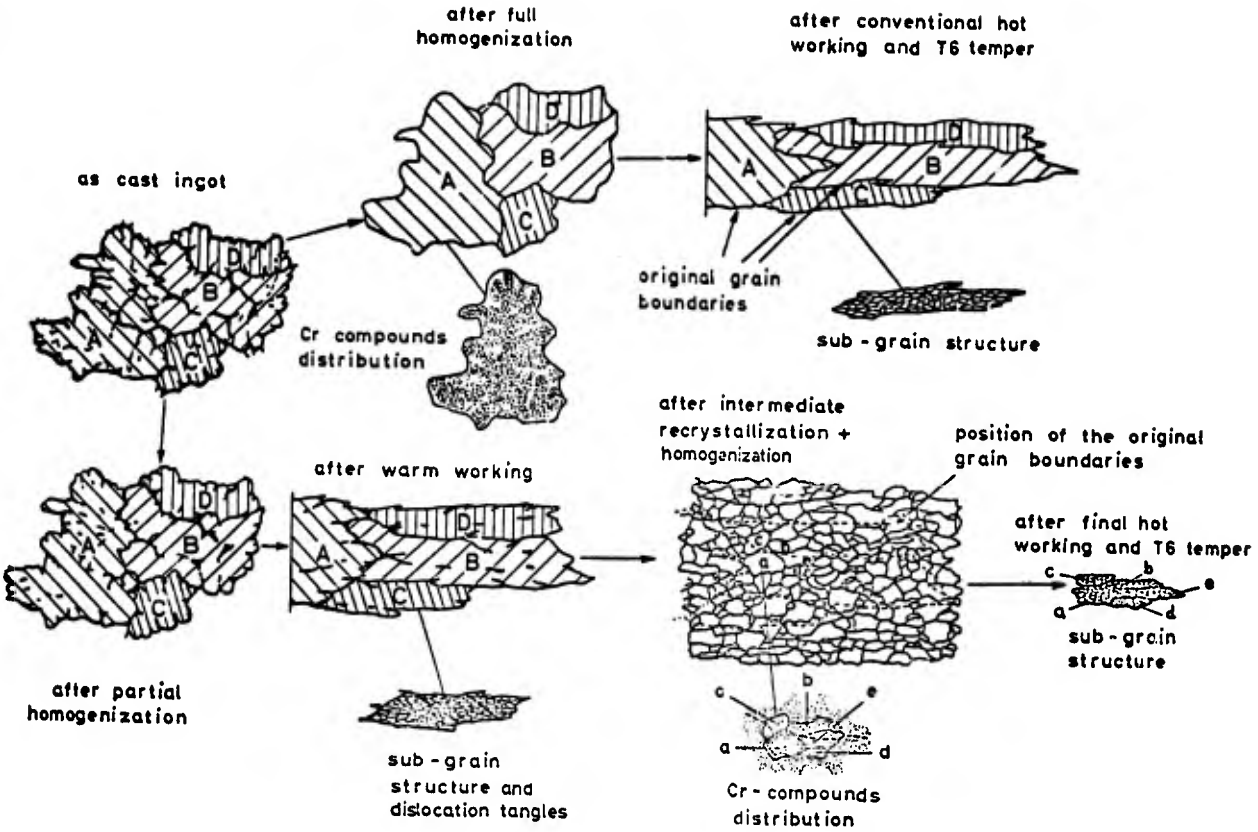

Fig.3 Schematic diagram showing the microstructural transformations of h.p. 7075 ingot processed according to conventional treatment (top) and an ITMT cycle (bottom)

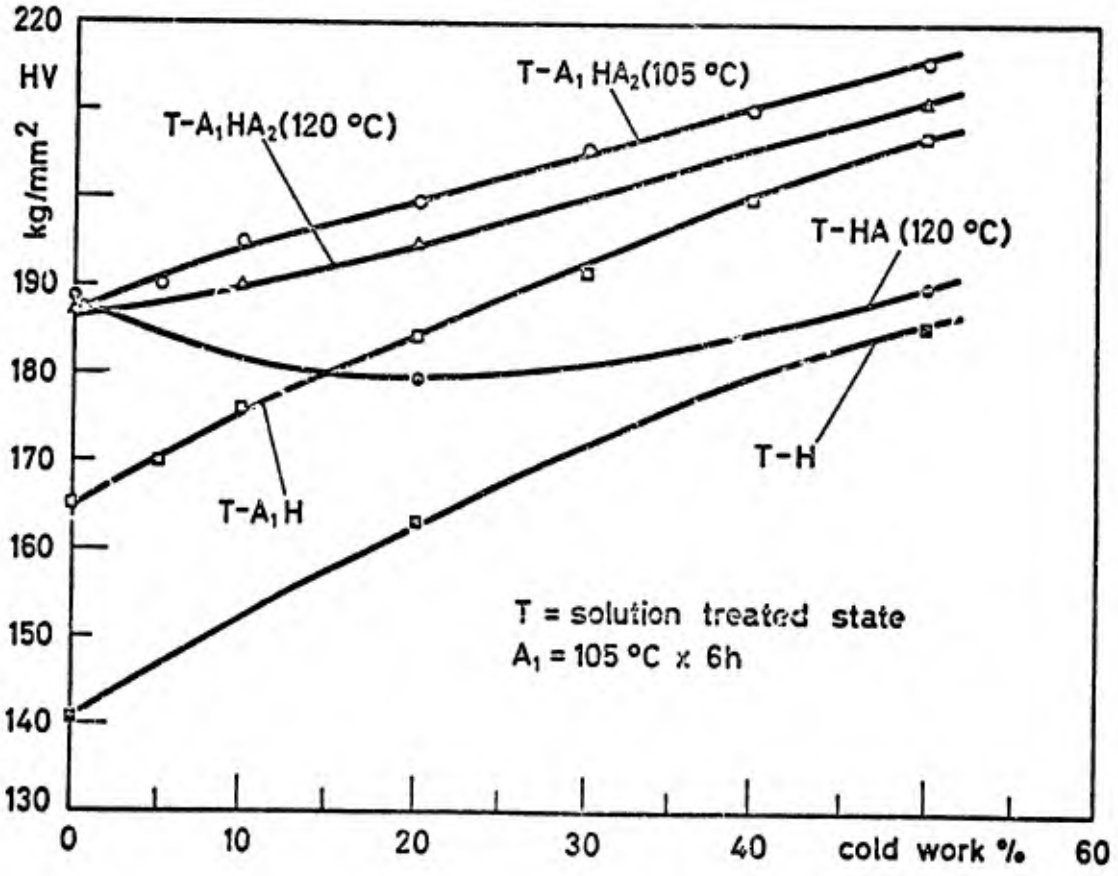

Fig.4 Hardness values versus per cent cold work of c.p. 7075 alloy samples in various thermomechanical tempers

as cast

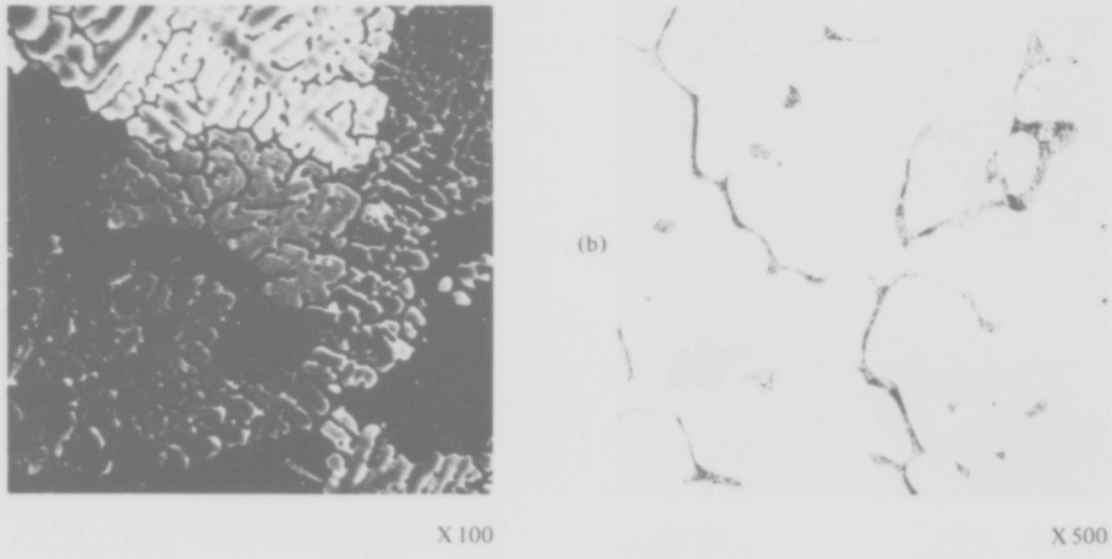

pre-homogenized at 400°C x 10–24 h

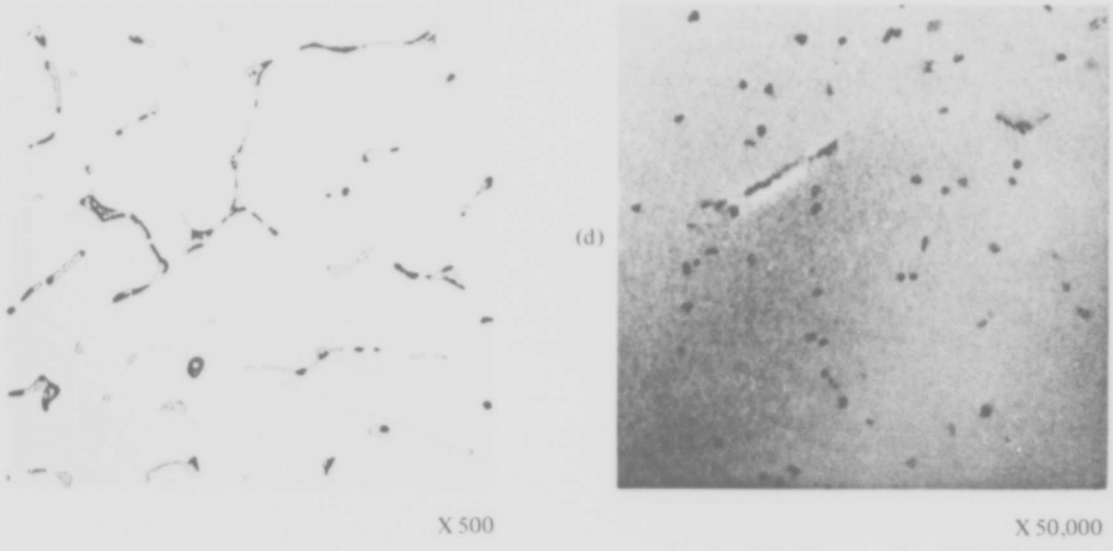

Fig.5 Typical microstructures of the ingot (Ø 114 mm) of h.p. 7075 alloy, in the as cast state and after pre-homogenization at 400°C x 10–24 h
(a), (b) and (c) optical micrographs
Magn. X 100 – Anodic etching in HF 2%
Magn. X 500 – Etching in HF 0.5%
(d) transmission electron micrograph

conv. cycle (A)

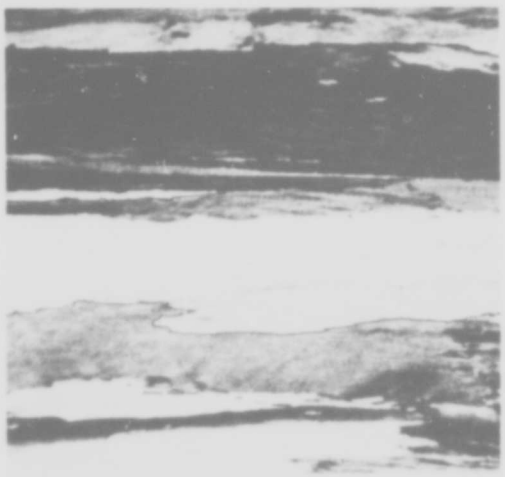

X 100

X 500

ITMT cycle (B)

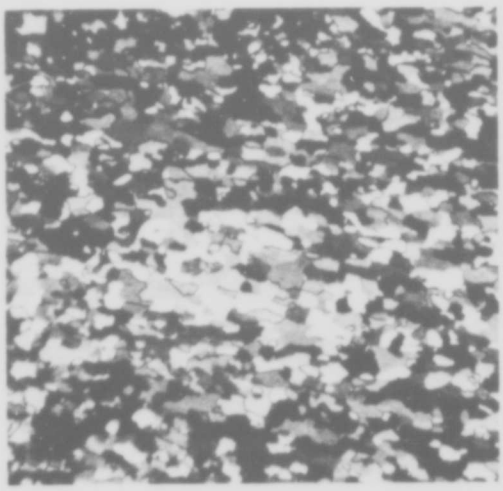

X 100

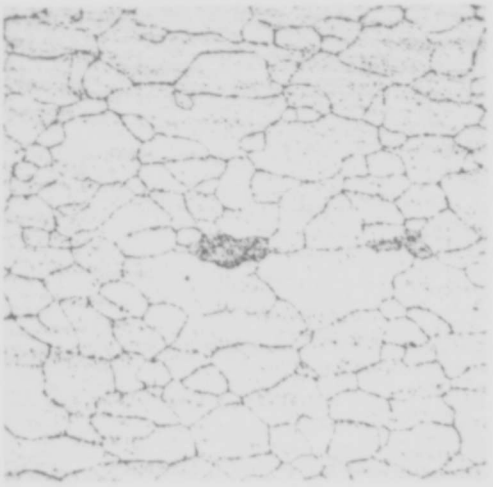

X 500

Fig.6 Typical microstructures of the rolled plates (t = 10 mm) of h.p. 7075 alloy produced by conventional and ITMT cycles (processes A and B), after TA temper. Longitudinal section
Magn. X 100. Anodic etching in HF 2%
Magn. X 500. Etching in HNO_3 25% at 70°C

ITMT + conv. cycle (C)

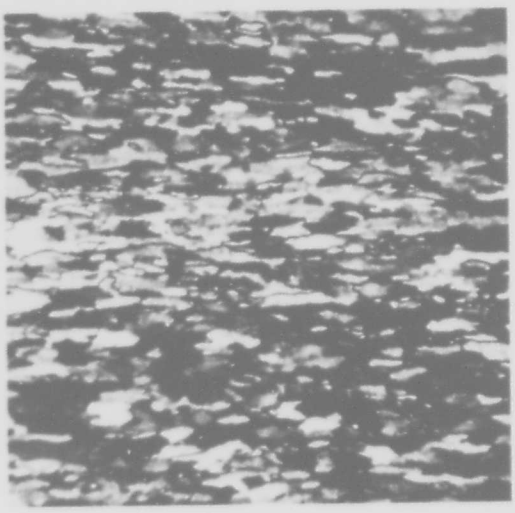

X 100

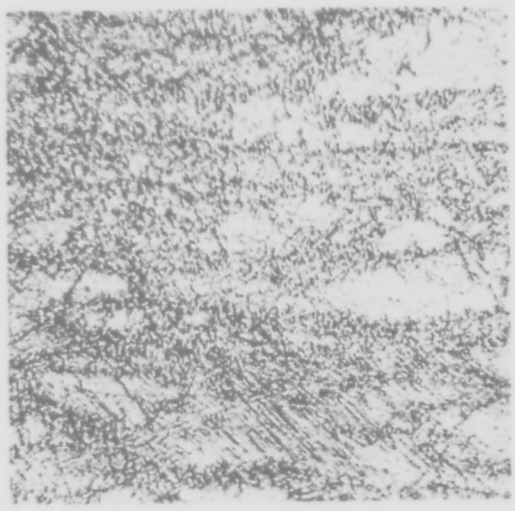

X 500

ITMT + conv. cycle (D)

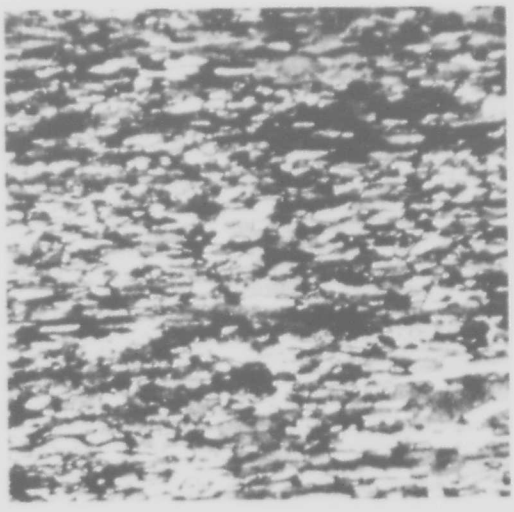

X 100

X 500

Fig.7 Typical microstructures of the rolled plates (t = 10 mm) of h.p. 7075 alloy produced by ITMT + conventional cycles (processes C and D), after TA temper. Longitudinal section
Magn. X 100 — Anodic etching in HF 2%
Magn. X 500 — Etching in HNO_3 25% at 70°C

conv. cycle (A)

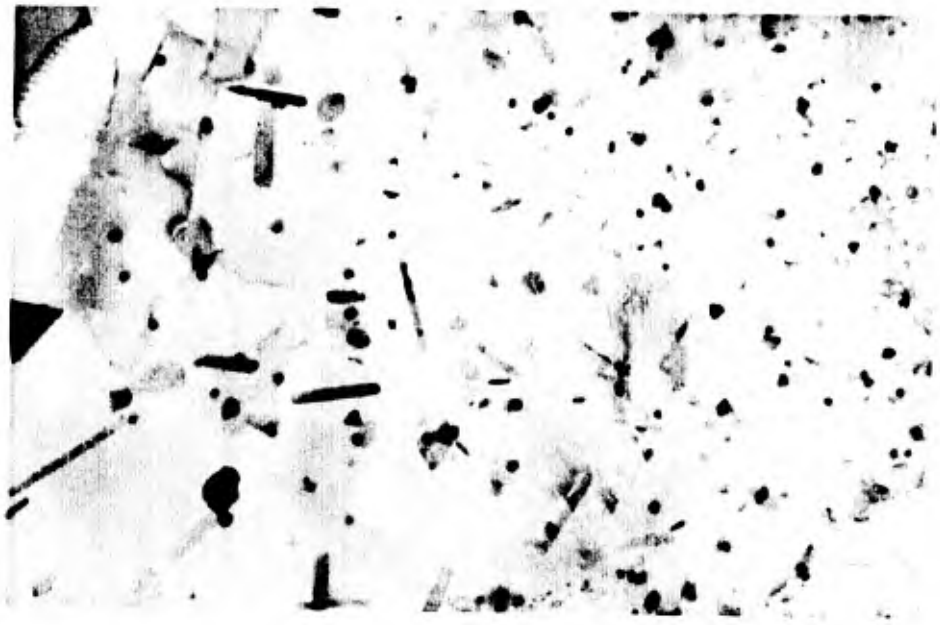

X 20,000

ITMT + conv. cycle (C)

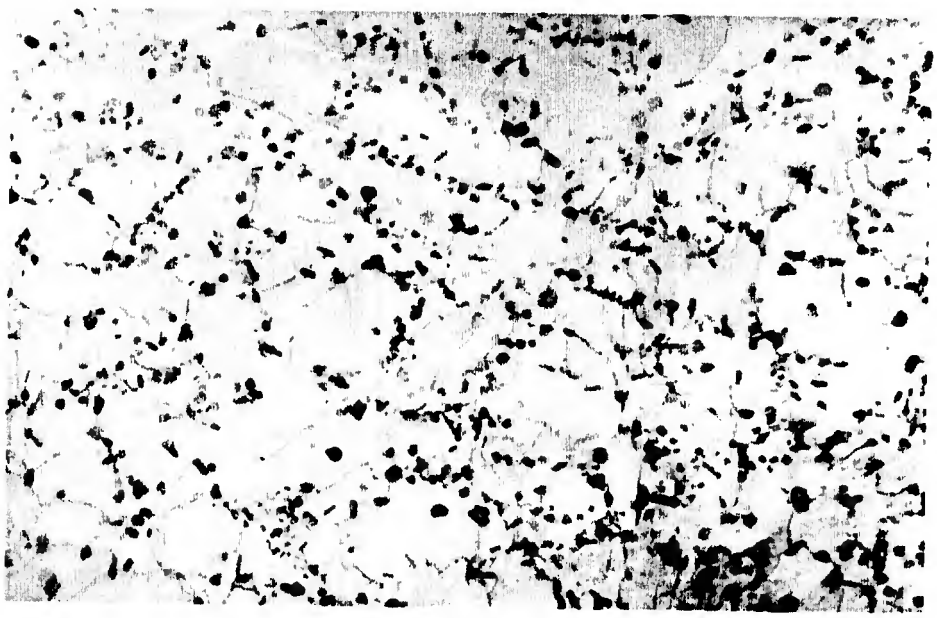

X 20,000

Fig.8 Transmission electron micrographs of rolled plates (t = 10 mm) of h.p. 7075 alloy produced by conventional and ITMT + conventional cycles (processes A and C), after TA temper

c.p. 7075

h.p.7050

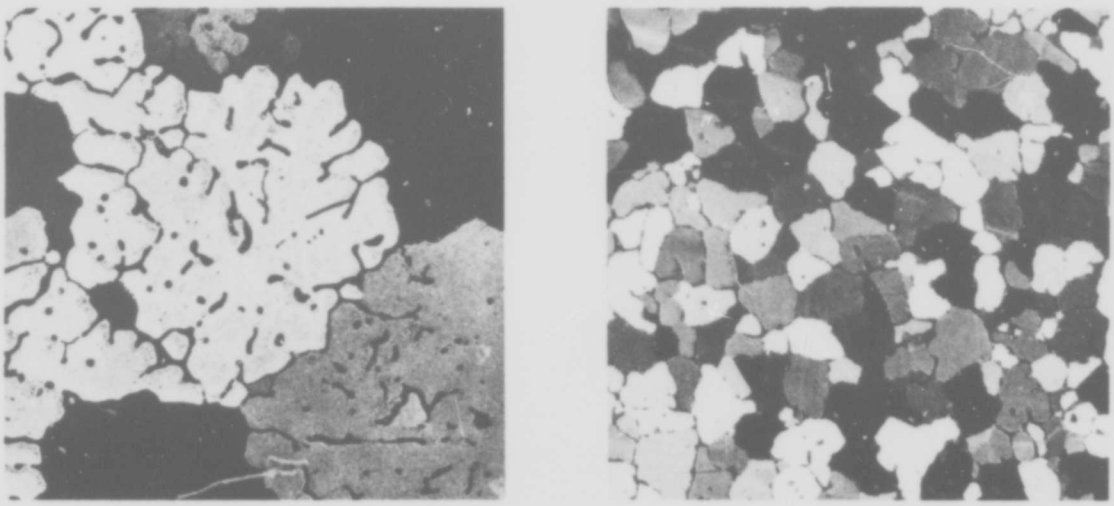

Fig.9 Typical microstructures of the ingots (Ø 180 mm) of c.p. 7075 and h.p. 7050 alloys after pre-homogenization at 400°C x 15 h
Magn. X100 — Anodic etching in HF 2%

Conv. cycle

c.p. 7075

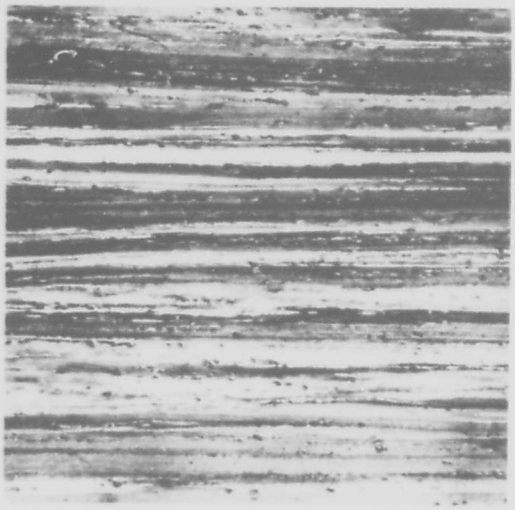

h.p. 7050

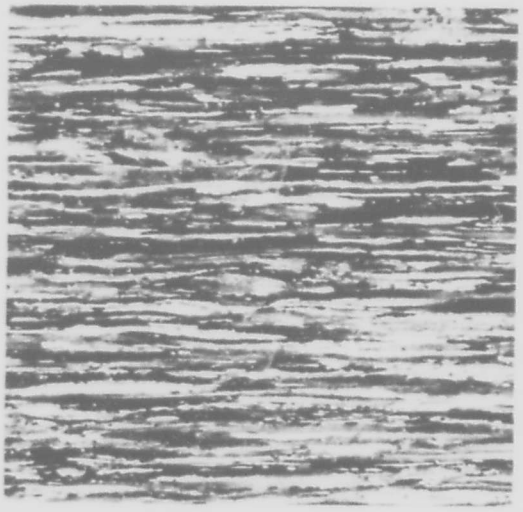

ITMT + conv. cycle

c.p. 7075

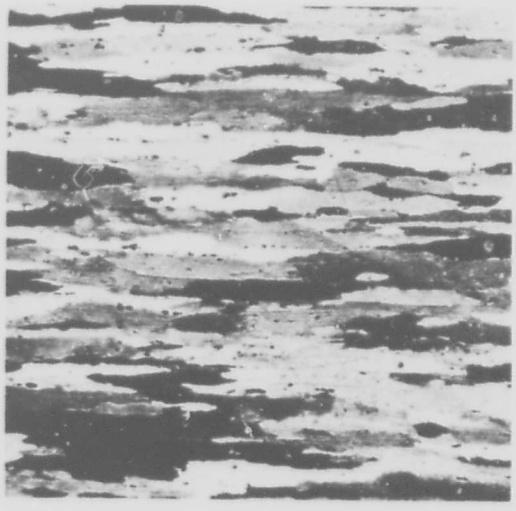

h.p.7050

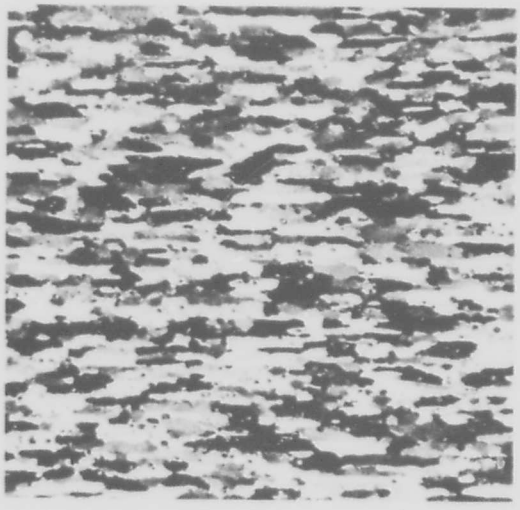

Fig.10 Typical microstructures of the forged-rolled plates (t = 25 mm) of c.p. 7075 and h.p. 7050 alloys, produced by conventional and ITMT + conventional cycles, after TA temper. Longitudinal section (middle plane)
Magn. X 100 — Anodic etching in HF 2%

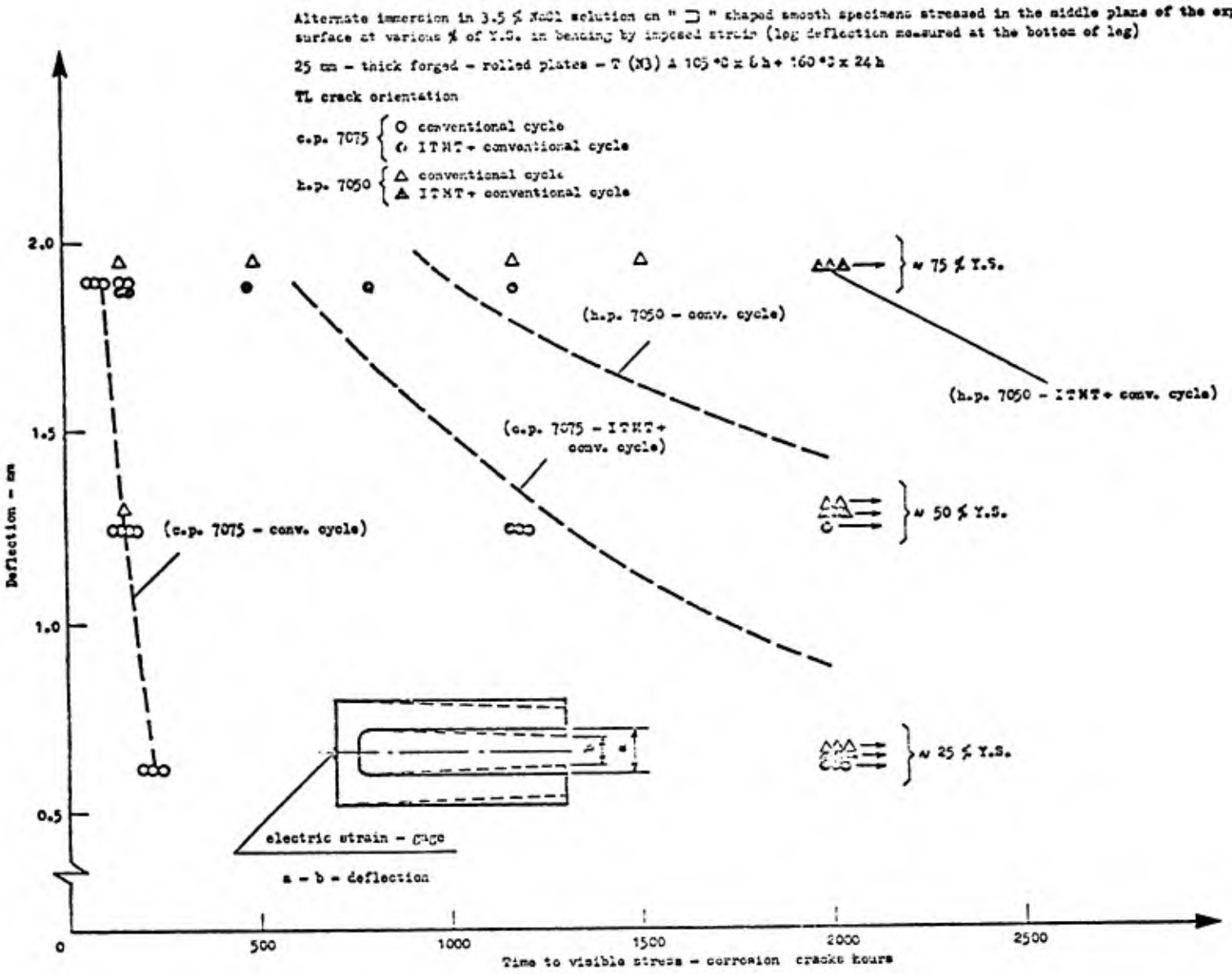

Fig.11 Stress – corrosion behavior (alternate immersion) in the short transverse direction of ~ 25 mm thick forged – rolled plates of c.p. 7075 and h.p. 7050 alloys

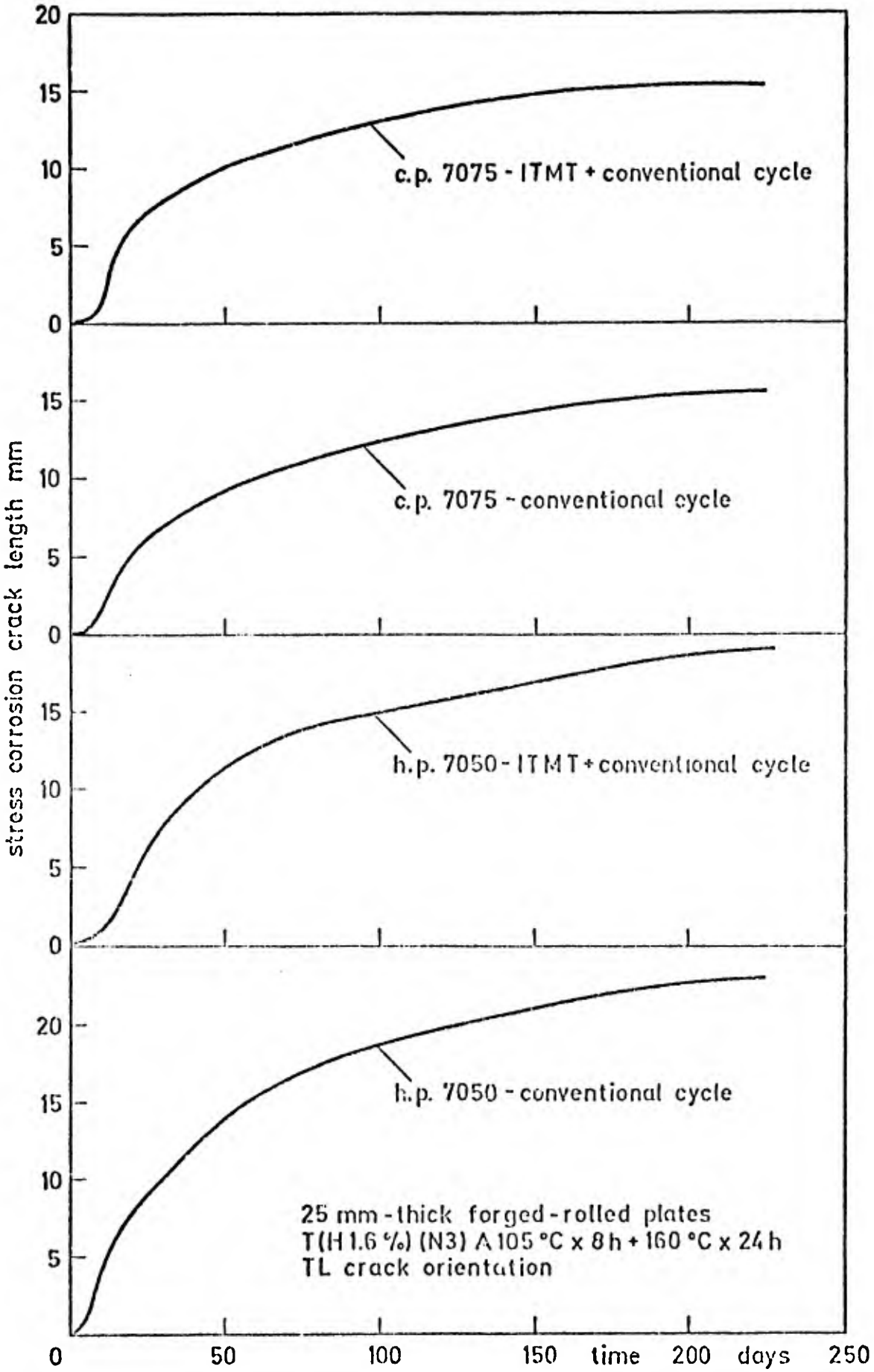

Fig.12 Stress corrosion crack length versus time curves for DCB specimens of c.p. 7075 and h.p. 7050 alloys

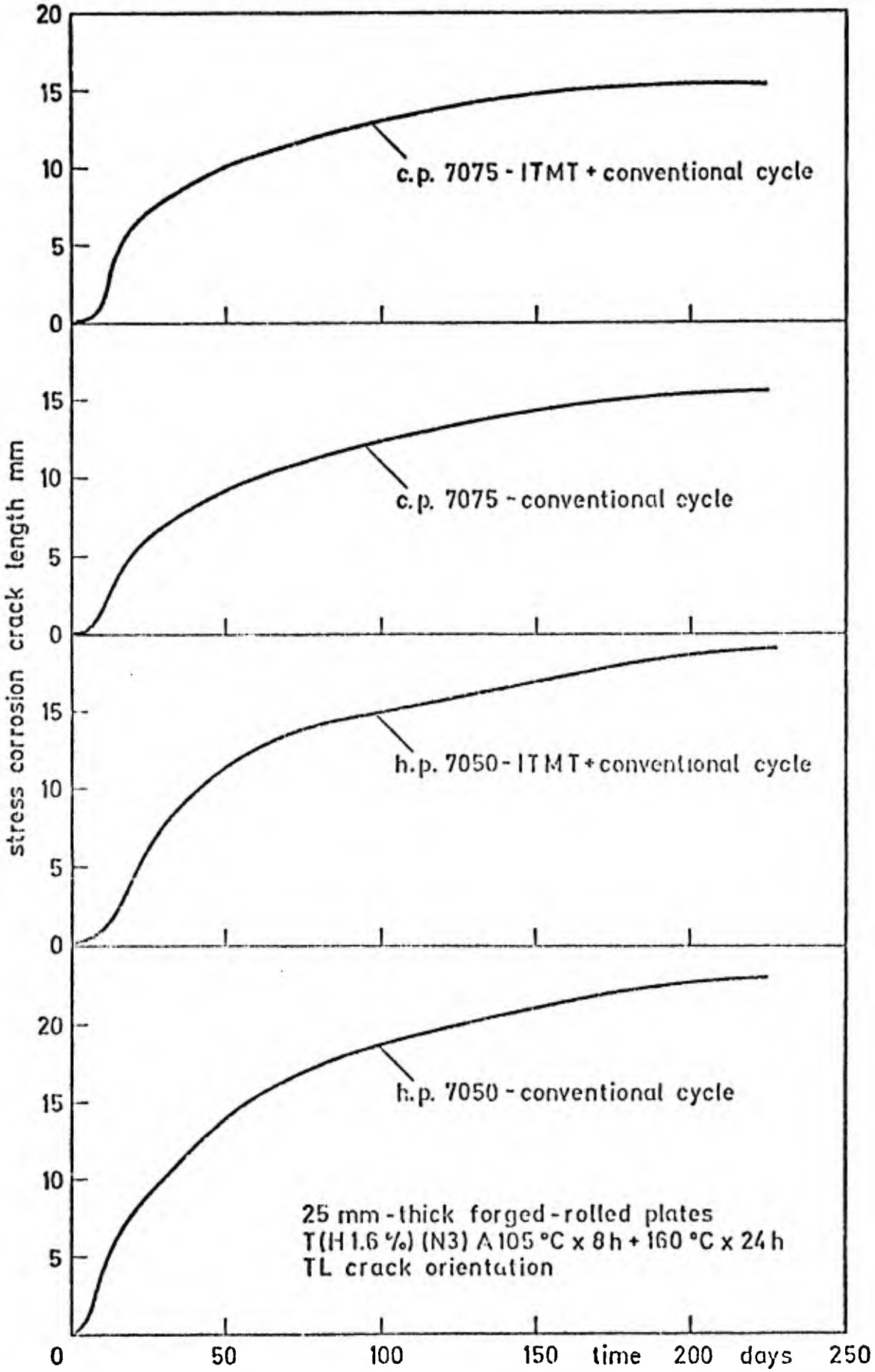

Fig.12 Stress corrosion crack length versus time curves for DCB specimens of c.p. 7075 and h.p. 7050 alloys

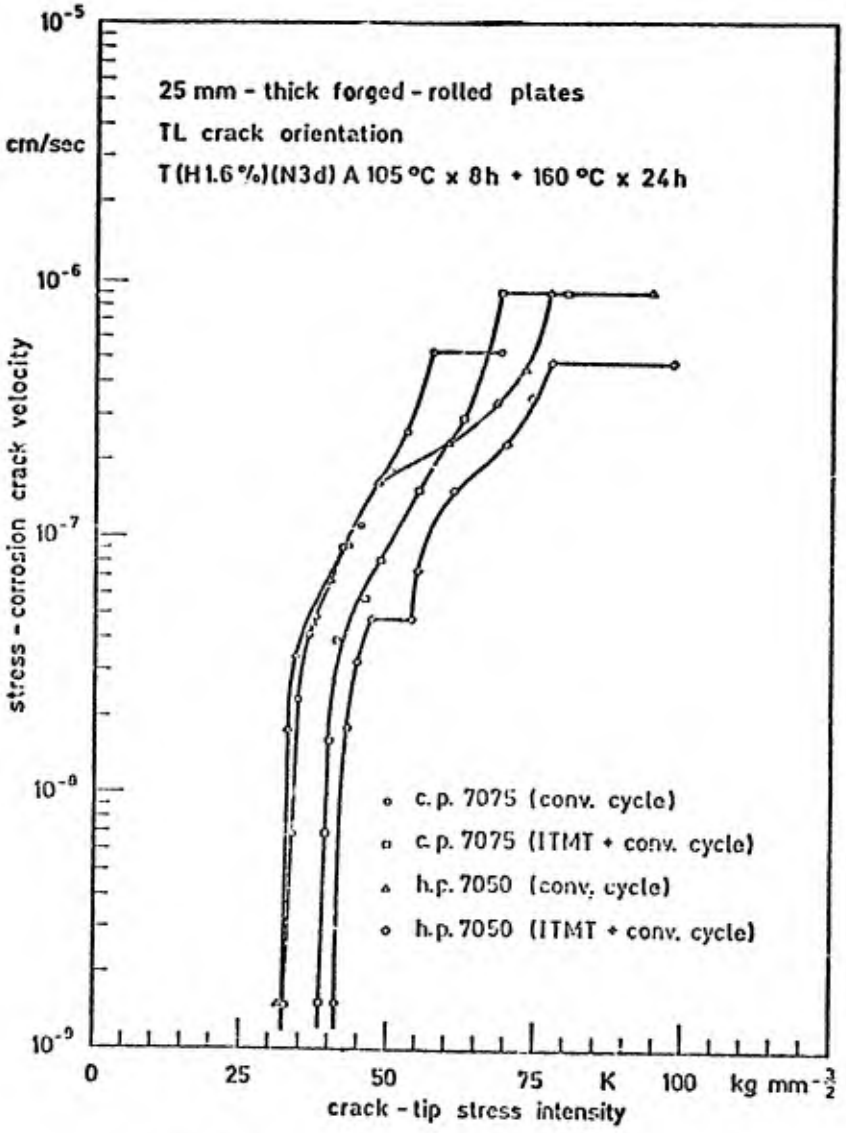

Fig.13 Stress corrosion crack velocity versus crack-tip stress intensity curves for DCB specimens of c.p. 7075 and h.p. 7050 alloys

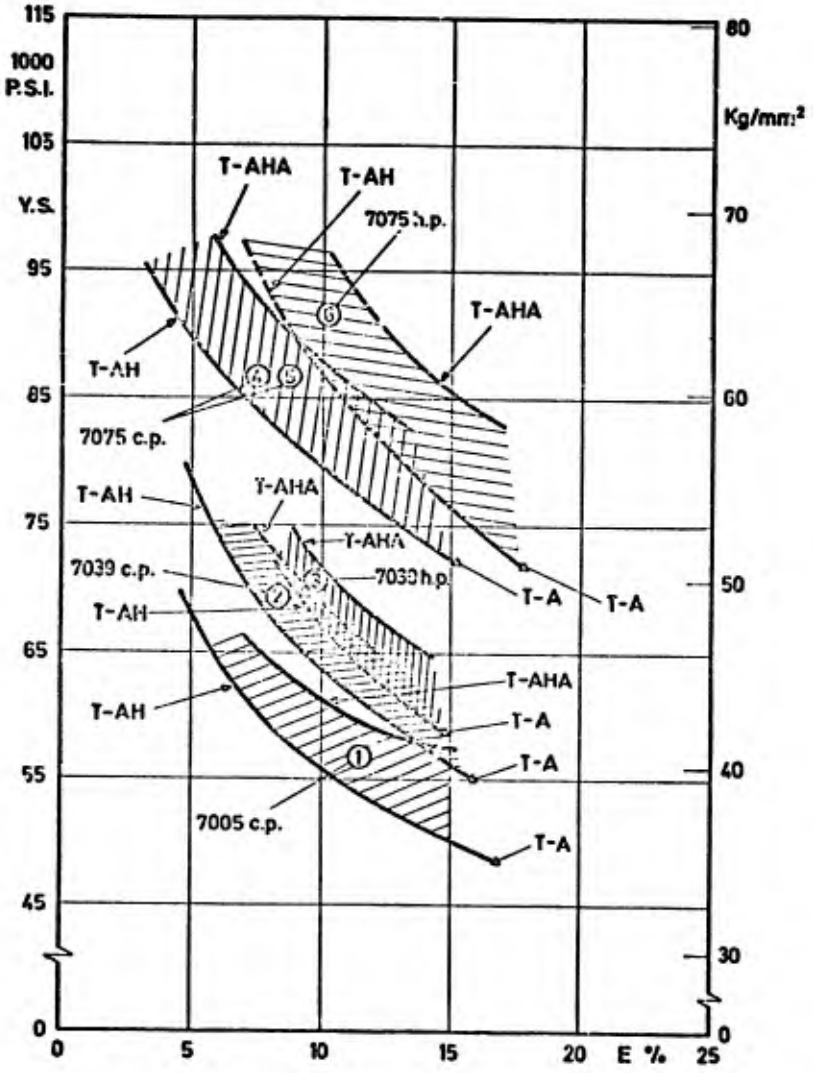

Fig.14 Yield strength values versus elongation of sheets of 7005, 7039 and 7075 alloys in several thermal and thermomechanical tempers

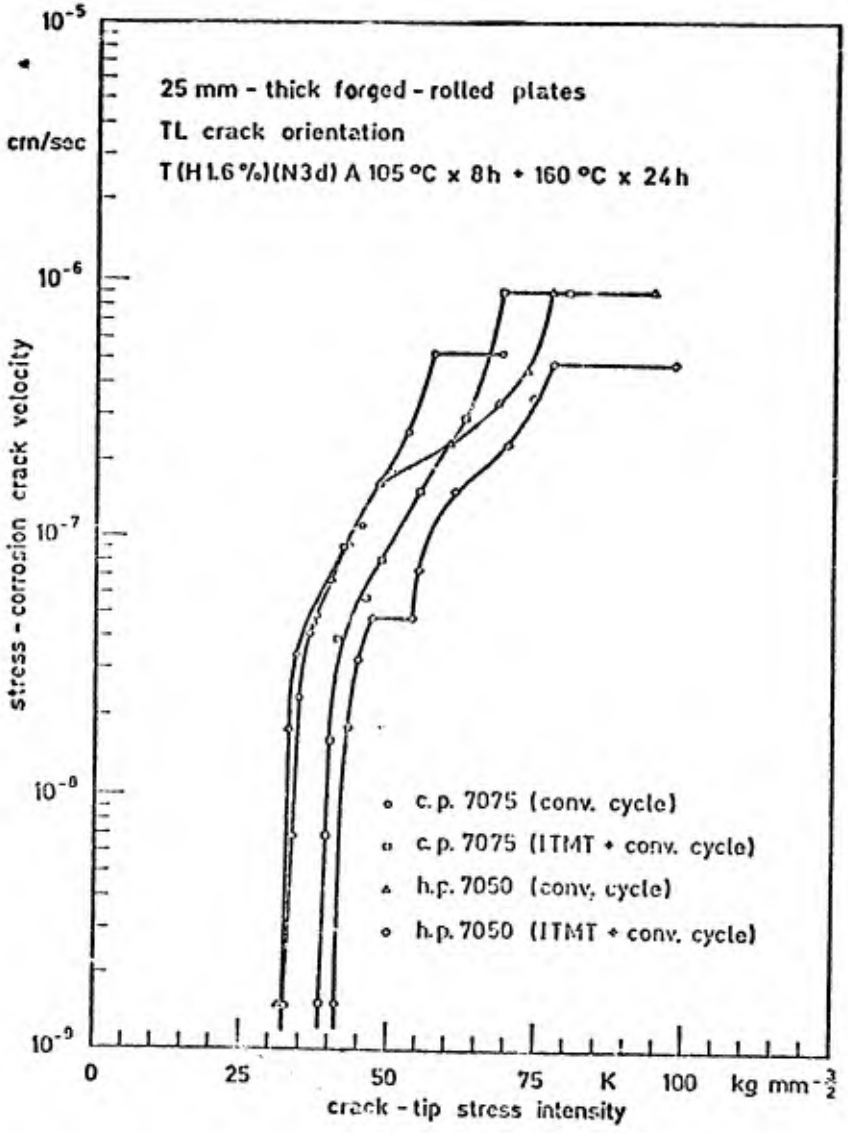

Fig.13 Stress corrosion crack velocity versus crack-tip stress intensity curves for DCB specimens of c.p. 7075 and h.p. 7050 alloys

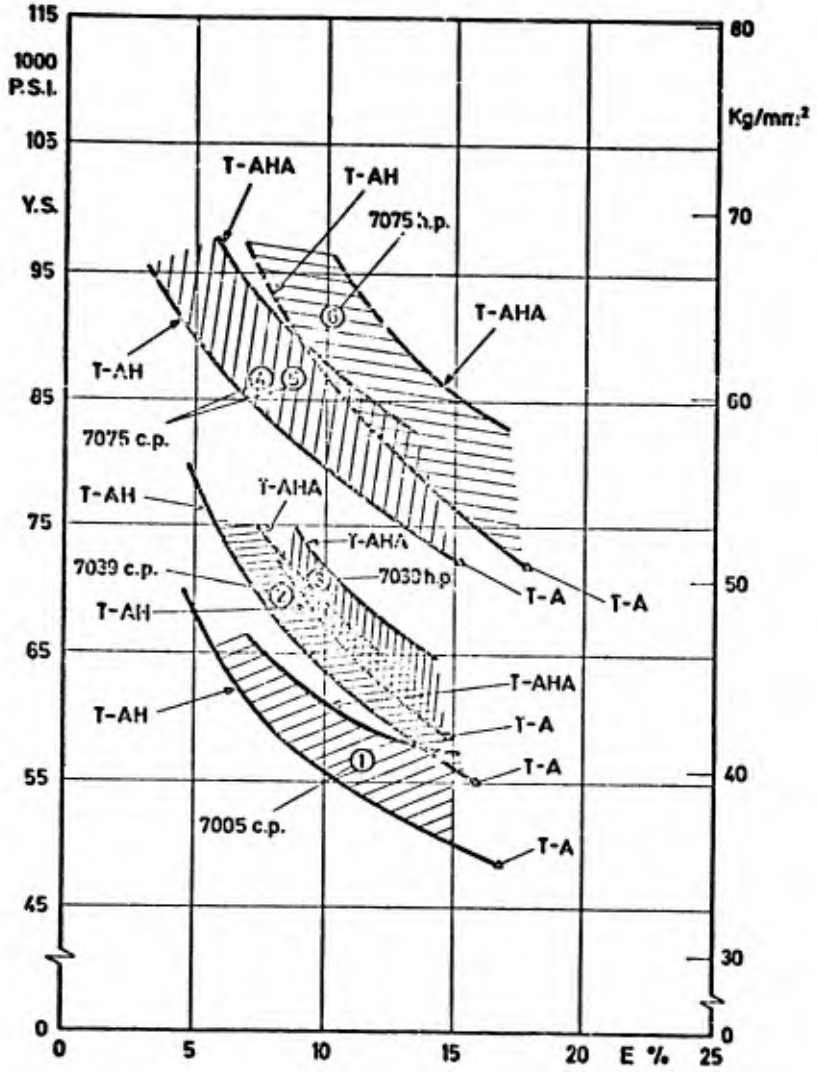

Fig.14 Yield strength values versus elongation of sheets of 7005, 7039 and 7075 alloys in several thermal and thermomechanical tempers

INFLUENCE OF MICROSTRUCTURE ON THE GROWTH OF FATIGUE CRACKS

by

G.Sertour and C.Bathias
Aérospatiale
3, Quai Léon Bluhm
B.P. 376
92153 Suresnes
France

1. INTRODUCTION

The influence of microstructure on fatigue is felt in the initiation as well as in the propagation of cracks. The former aspect, related to the notion of endurance, has probably given rise to the greatest amount of studies; the latter has not assumed its full interest until one has attempted to apply the failure mechanism concepts to the development of fatigue induced cracks.

It is this latter aspect, of interest to the aeronautical industry, which we plan to study.

The influence of microstructure on the propagation of fatigue induced cracks has its roots in a submicroscopic scale. This has led us to survey the metallurgic parameters which play a part at the very level of crack propagation mechanisms. We have endeavoured to break up this phenomenon into several aspects: cyclic hardening or softening at the crack tip, formation of striations and overall results on the macroscopic scale.

From a metallurgic viewpoint, it appears that the most important parameter which governs the development of fatigue induced cracks is the nature of the plastic deformations which occur at the crack tip; such deformations are essentially related to the slip character and to the stacking fault energy. This latter parameter affects essentially the submicroscopic mechanism of crack development, and also, up to a certain extent, the microscopic aspect, that is to say the formation of striations which is the most frequent mode of the local progression of cracks.

Besides ductile striations, which are typical of the fatigue phenomenon, a crack progresses sometimes through the formation of holes or through a brittle mode (brittle striations, quasi-cleavages). These two crack development modes are related to mechanical conditions and to the environment, as well as to the structure and inclusions in the former case, and to precipitations in the latter case.

Therefore, on a microscopic scale, fatigue induced crack development is the result to several possible processes which govern its propagation rate and its progress according to the phases involved.

This paper reviews the influence of structure on fatigue induced crack development, with emphasis on stage II, on the formation of striations and on the environment/structure interaction on crack growth.

2. MECHANISM OF CRACK GROWTH

In laboratory tests on smooth specimens, three stages can usually be differentiated in the fatigue fracture process.

2.1 Initiation and Stage I

The first stage, called initiation stage, develops mainly on the surface of the specimen. In the absence of pre-existing flaws, fatigue induced cracks are initiated in permanent slip bands which appear very early on the specimen surface, that is within the first tenth of the total number of cycles leading to fracture.

In cubic alloys with centered faces, a modification of the slip bands in intrusions and extrusions can be observed[1]. In copper, they appear as early as the first hundredth of the service life. As intrusions are regarded as the first microcracks, their early formation shows that the greatest part of the fatigue process is to be ascribed to crack propagation.

In copper and mild steel, permanent slip bands on the surface are related to the configuration of the fracture cells in underlying layers[2].

In centered cubic metals, it seems that microcracks originate in pores[3]. However, while the presence of intrusions or pores is not systematically observed, there are always slip bands which create humps or dents progressively leading to the formation of microcracks[4].

Finally, it should be noted that the initiation of cracks can be the result of inclusions. In light alloys of the 2024 or 7075 type, inclusions containing iron or silicon are brittle and can be split during machining operations or due to fatigue.

Anyway, when a fatigue crack is initiated in a cleft inclusion, it propagates first according to stage I (Refs 5, 6). However, it has been observed that the initiation of cracks can occur simultaneously in slip bands, around the inclusions. It has not proved possible to determine a critical value for the size of the inclusions: apparently, their size affects service life more than the fatigue limit does. Therefore, when the size of the inclusions is reduced to 2μ, the service life of alloy 2024 is multiplied by a factor of 3, while the fatigue limit remains practically unchanged.

Apart from possible cleavage, inclusions induce stress concentrations which reach a maximum value when they are located under the skin of the specimen[7].

From the surface, the development of the crack usually takes place in two stages. During stage I, the crack propagates, under a flat stress, at an angle of approximately 45° to the surface. It progresses, through a few grains at most, along crystallographic directions.

Stage I depends on the size of the grain in low stacking fault energy alloys. In 70 - 30 brass, for a stress amplitude of 12 daN/mm^2, service life passes on from 3.10^5 to 5.10^6 cycles when the diameter of the grain passes on from 100 to 10μ (Ref.9). This divergence is ascribed to the fact that, in stage I, cracks grow less rapidly in small grains due to the slowing down of the crack development by the grain boundaries. This phenomenon is not observed in copper nor in aluminium because the formation of the dislocation cells conceals the effect of the grain boundaries.

As far as the mechanism of stage I is concerned, it is a known fact that the phenomenon involved is a shearing action along active slip planes; however, the absence of striations on the corresponding fracture is not clearly accounted for. An intense plastic deformation has been revealed around the crack in this stage I (Refs 10--11).

To conclude, it appears that stage I is characterized by a slow propagation velocity ($10^{-3}\mu$/c); the crack propagates from grain to grain along crystallographic directions, at a more or less limited rate according to the stacking fault energy. Besides, the environment seems likely to exert a considerable influence on stage I (Ref.6).

2.2 Stage II

As already mentioned, stage II is characterized by the formation of striations on nearly the whole surface of the fracture. On a macroscopic scale, one can observe one or several incipient cracks, as well as lines or reliefs owing to which, afterwards, the progress of the crack can be determined; however, striations are only visible when magnified by a microscope.

In 1961, Forsyth demonstrated the existence of two types of striations: ductile and brittle striations[12].

At that time, it was observed that a corrosive environment promotes the formation of brittle striations; however, in light alloys fractured in humid air, the two types of striations can be observed simultaneously. The striation development mechanism will be discussed at greater length further on; first, let us study the morphology of the surface of fatigue induced fractures. In brief, the characteristic of this morphology lies in the fact that the striations are more or less laid out perpendicularly to the direction of the crack, at least in low carbon steels and in alloys with a high stacking fault energy; however, there are considerable exceptions to this rule in low fault energy alloys, for instance in some stainless austenitic steels where mixing is involved (Fig.1). One should also mention the case of nodular cast iron, where the lay-out of striations is influenced by the presence of graphite nodules[13]. Actually, the rule mentioned is only confirmed, in general, when the local propagation of the crack is considered.

Besides, the direction of striations is related to the crystallographic orientation of the grains. In alloy 2024, the fracture plane is closed to a plane (100) and the striations are parallel to a direction (110) (Ref.14). The striations in stainless austenitic steel have as well a very pronounced crystallographic characteristic[15]. However, this characteristic seems to be less marked in low carbon steels. As a matter of fact, in mild steels, the orientation of the striations does not vary when they pass through a grain boundary.

It should also be mentioned that the profile of ductile striations is, in principle, more or less serrated; a microcrack is often located at the tip of the striation.

2.3 The Mechanism of Stage II

The plastic deformation at the crack tip plays a twofold part in the crack development process:

- on the one hand. the formation of striations and, consequently, the crack development speed, depends on the nature of the plastic deformations,
- on the other hand, the opening of the crack tip is related to the size of the plastic zone.

In general, the fatigue crack appears to be transgranular, and the related plastic deformation is strictly located in a thin strip. Observations of the plastic zone reveal that the fracture surface microscopic aspect is related to the plastic deformation of the sub-lying layers. In aluminium alloys, striations are associated with dislocation walls oriented along directions 110 (Ref.17).

In low carbon steels, there is also a correlation between striations and dislocation walls[15], while, in stainless austenitic steels, it is the twins, or the martensite platelets which are associated with the striations[19] (Figures 2 to 5).

From this, we conclude that, when the crack opens, for each cycle there is a final re-arrangement of the dislocations to allow the slip at the crack tip; this re-arrangement does not become final until the crack has closed up. According to the nature of the slip, one can observe the formation of a sub-boundary, a twin or a martensite platelet simultaneously with the formation of a striation. The spacing between the striations depends also on the nature of the slip. Likewise, the lay-out of the striations, that is to say their orientation and the growth of the striated areas, is related to the plastic deformation and, firstly, to the stacking fault energy.

Once the crystallographic aspect of the striation formation has been determined, it is interesting to attack the question from the mechanical viewpoint and to review the state-of-the-art on plastic zones.

The first scientist who formulated an expression for the plastic zone was Irwin. Since that time, many authors have proposed other formulae, determined either by calculations or by experiments. In principle, the shape of the plastic zone depends on the hardening coefficient and on the stress mode; however, we assume, as a first approximation, that it consists of two wings inscribed in a circle, and we shall consider two parameters: r_x , which is the size of the plastic zone along the propagation direction; and r_y , which is the size of the plastic zone along the orthogonal direction.

In a flat specimen subjected to tension, the size of the plastic zone at the crack tip such as is currently admitted, in a plane strain is:

$$r_y = \frac{1}{10}\left(\frac{K}{Re}\right)^2$$

K = factor of stress intensity

Re = yield strength

In the presence of cyclic stresses, the formation of the plastic zone at the crack tip is mainly complicated by the local compression which takes place when the crack closes up, even when the nominal stress remains in the traction field[19]. Besides, it is the variation of the stress intensity factor ΔK which has to be taken into consideration, as the maximum value K_{max} is only a secondary parameter[19]. In principle, the conventional yield strength is not suitable in the fatigue field, and Re has to be replaced by Rc , the cyclic yield strength determined on the basis of the cyclic stress-strain curves[20 & 21].

Figures 6 and 7 show, in the form of diagrams, how the plastic zone develops at the tip of a fatigue crack. If we consider a repeated traction loading assuming a triangular form (Fig.6), we assume that, when the crack opens up, plastification takes place when the yield strength is reached locally and that, when it closes up, it is a stress amplitude equal to twice the yield strength which induces a new plastic deformation within the plastic zone during the opening of the crack. Therefore, under fatigue conditions, a twofold plastic zone is to be found. The size of the peripheral plastic zone – also termed "monotonic" – assumes the form $\left(\frac{\Delta K}{Re}\right)^2$, while that of the central zone – also called cyclic – assumes the form $\left(\frac{\Delta K}{Re}\right)^2$.

Therefore, the central plastic zone OR is four times smaller than the peripheral plastic zone OM (Fig.6). The variations of the stress amplitude $\Delta\sigma$ and of the deformation amplitude $\Delta\epsilon$ are represented in Figure 7, considering that the respective positions of the crack end and of the plastic zone are definitely set.

Within the RM zone, the amplitude of the stress is elastic and the cyclic strain is non existent. On the other hand, the monotonic plastic deformation induced by the opening of the crack increases regularly from M to R , according to a function of the $\frac{1}{r}$ form. The plastic deformation reaches a value ϵ_{PR} which can be calculated in mode I of the crack opening, on the analogy of mode III.

If we designate by r'' the size of the peripheral plastic zone, r' that of the central plastic zone and ϵ_y the deformation corresponding to the yield strength, the plastic deformation ϵ_{PR} at a distance r'' from the crack tip is equal to:

$$\epsilon_{PR} = \left(\frac{r''}{r'} - 1\right) y .$$

As mentioned previously:

$$\frac{OM}{OR} = \frac{r''}{r'} = 4 .$$

Therefore:

$$\epsilon_{PR} = 3\epsilon_y .$$

From this, it appears clearly that the monotonic plastic strain at point R is rather slight. In view of what we know of ϵ_y, we assess, on the basis of this calculation, that the plastic strain of the peripheral plastic zone will not exceed a few centimeters. Moreover, it can be assumed that the boundaries of the two plastic zones will be well defined, since they are marked by two different deformation states of the metal.

Theoretical results correlate rather well with experiments. The existence of the two plastic zones is shown by several authors[19 - 22].

Cyclic deformation within the plastic zone does not always lead to a hardening of the metal, but a softening sometimes develops (Figures 8 and 9).

Such softening around the crack has been observed in maraging steels either aged or annealed[19]. Cyclic softening of maraging steels is held responsible for their poor resistance to fatigue cracks.

The example of these high strength steels shows the influence of microstructure on the damage mechanism at the crack tip. The phenomena which takes place in the plastic zone at the tip of a crack are comparable to those observed in the case of low-cycle fatigue (Figures 10 and 11).

From the plastic deformation viewpoint, an increase of the dislocation density and dislocation loops can be observed in the peripheral zone. In the central zone, dislocation cells develop in copper[23], aluminium[17], low carbon steels[24] and even maraging steels[20], and, probably also in the other high stacking fault energy alloys. In stainless austenitic steels[15] with a low fault energy, the central area is occupied by mechanical twins or martensite platelets. When dislocation cells are formed, the diameter of the cells increases with the distance to the crack and, just below the fracture, the cells are laid out in links parallel to the striations.

A similar evolution can be observed in the spacing between the twins or the martensite platelets.

3. INFLUENCE OF STRUCTURE ON CRACK GROWTH

The second stage of fatigue crack growth is not influenced by the size of the grain; only the crystallographic orientation of the grain plays a part which remains to be defined. Neither does the texture seem to be an important factor.

It is a known fact that in 70/30 brass and in stainless austenitic 18–8 steel the crack growth rate hardly depends on the previous strain or on thermomechanical treatments[25]. Stage II is also independent of the rates of residual austenite in martensitic steels[26].

It is not easy to define a rule defining the crack development rate of polyphase alloys; however, it seems that, in many cases, it only depends on a single phase: martensite, for instance, in martensitic steels, and ferrite in steels containing perlite.

For a given alloy, stage II is generally only slightly influenced by the temperature treatments and the associated precipitation. In some high strength steels of the maraging or 35 NCD 16 type, tempering has practically no influence on the crack growth rate[26].

In aluminium alloys, the influence of the ageing temperature is also slight; however, the double ageing treatment of 7075 T73 brings an appreciable improvement over the ageing state T6.

To sum up, this survey of several metallurgic parameters reveals that the latter do not play a leading part in stage II, taking data scattering into account.

An explanation for this phenomenon can be found in the hardening or softening at the crack tip, which tends to restore the metal to a same state for a given type of alloy.

As stressed above, the determining factors of fatigue crack growth are essentially related to the composition of the alloy, the nature of the slips and, sometimes, phase transformations (Fig.1). These factors govern the formation of striations, therefore the local progression of the crack. As far as the other progression modes are concerned, it should be mentioned again that, at high crack development rates, holes may appear. The latter depend on the size and distribution of inclusions, therefore on the percentage of impurities in the alloy.

When the inclusions are not brittle, holes develop and the micrographic aspect of the fracture surface assumes a mixed aspect, composed of striations and holes. In a light 7075 alloy, the influence of the inclusions reaches a critical threshold when their spacing is of the same order of magnitude as the size of the plastic zone[27]. The role of inclusions is mainly recognized in the transition of the fracture mode in thin specimens, and at high propagation speeds. Therefore, a structure containing a large number of inclusions leads to an acceleration of the crack development rate in the field of large ΔK, in the case of plane stress fractures.

In conclusion, it appears that many metallurgic parameters which exert a considerable influence on the initiation stage or on stage I, that is on the fatigue limit and on the propagation threshold ΔK_S, do not affect the set phase of fatigue crack growth.

4. ENVIRONMENT AND STRUCTURE INTERACTION ON CRACK DEVELOPMENT

The environment is undoubtedly the factor which plays the most important part in the fatigue phenomenon, apart from the stress conditions, of course. The environment affects the three stages of fatigue, and endurance as well as the propagation rate. It is essentially the latter point which will be covered here, as the former is better known[28].

Recent work, performed in a controlled atmosphere and in a corrosive medium on steels and light alloys, reveals, from the phenomenological standpoint, the mechanism of stage II in corrosion fatigue, when K_{max} has a value lower than K_{ISCC}, for which stress corrosion takes precedence over fatigue[29 - 30].

In steels, as well as in light alloys, the crack development rate is multiplied by approximately 10, due to corrosion in a saline solution. This effect is related to the time during which the crack tip surface is exposed to the medium. Consequently, at a low frequency (< 10 hertz) or for a cycle form with slow loading, the environmental effect will be better marked. It is assumed that the crack development rate is the sum of two terms:

$$\frac{dl}{dN}(\text{total}) = \frac{dl}{dN}(\text{mechanical}) + \frac{dl}{dN}(\text{corrosion}) .$$

The corrosive effect of an aqueous solution containing 3.5% of sodium chloride on a light 7075 alloy is especially marked for low values of ΔK, where the speed can be multiplied by more than ten.

While the crack development rate in the air does not depend on the state of the alloy, the same does not apply to a corrosive medium.

The corrosion effect is felt differently according to whether the alloy is quenched, aged, or over-aged[29].

Corrosion induced crack development depends on the microstructure, and in particular on precipitation.

Besides, a reduction of the silicon and iron percentage and an increase of copper percentage improves resistance to corrosion fatigue. Silicon and iron combine with copper to form an intermetallic component. Ageing seems to affect the nature of the slips.

2024 alloys are also sensitive to the action of the environment. However, 7075 alloys are still more sensitive, in particular to the humidity of the air[31].

In high strength steels, the same influence of the solution containing 3.5% sodium chloride is felt on the crack development rate. The development of cracks in a maraging steel containing 12% of nickel becomes faster in the corrosive medium defined above when the frequency is lower than 10 hertz[30]. This also applies to American steel HY 80 and to stainless austenitic steel containing molybdenum[32].

In all cases, it appears that the effect of corrosion is mainly felt on coefficient C in the relation:

$$\frac{dl}{dN} = C \qquad \frac{\Delta K^m}{E}$$

which means that the representative curves remain parallel to each other, except in the case of high ΔK for which stress conditions take the lead again.

From the standpoint of microfractography, the effect of corrosion is reflected in surface brittleness. In the 2024 alloy, the conventional surface with ductile striations is perturbed by intergranular micro-cracks[31]. The latter do not appear in alloy 7075, but brittle striations develop[29].

As regards the latter alloy in the T6 state, an anodic current -0.7 volts brings about a ramification of the crack and, therefore, a slight slowing down. In the over-aged state, no ramification is observed. In the T6 state, a cathodic current does not appreciably modify the crack development rate; on the other hand, in the over-aged state, a potential of -1.3 volts slows down the crack and, simultaneously, ductile striations reappear on the fracture surface instead of the brittle striations, typical of the corrosion fatigue cracks of the 7075 in the T6 state (Fig.13).

Still, in the T6 state, an inhibitor such as the nitrate ion brings about a slowing down of the crack development in the same manner as a cathodic potential for the over-aged alloy.

In high strength steels, the effect of corrosion is also marked by the fact that the fracture surface becomes brittle and quasi-cleavage appear[30].

The brittleness mechanism at the tip of the cracks in a corrosive medium is not well understood. The development of brittleness could be due to an ionic adsorption or to the effect of hydrogen. It also depends on precipitation and on the mobility of dislocations.

5. CONCLUSIONS

(a) Out of the three stages of fatigue crack development, it is the second stage, that of the set stage of crack growth, which is the least affected by metallurgic parameters.

(b) From the mechanical standpoint, it is a known fact that stage II is roughly independent of the yield strength and that, in fact, Young's modulus, the hardening coefficient and toughness can be related to the crack development rate.

(c) From the microstructure standpoint, the parameters affecting the nature of the slips seem to prevail. An important part can also be ascribed to inclusions and phase transformations.

(d) Finally, in the presense of an aggressive environment, the aged state and precipitation modify corrosion effects, according to the test conditions.

REFERENCES

1. Forsyth, P.J. — Quelques observations métallographiques sur la fatigue des métaux J. of. Inst. of Metals, 80 (1951) p.181.
2. Lukas, P. et al. — Physica Statuts Solide, 1966, 15, p.71.
3. Wood, W.A. et al. — Systematic Microstructural Changes Peculiar to fatigue deformation – Acta Mat. Vol.11, pp.643-652.
4. Henry, H. Plateau, J. — La Microfractographie, 1967.
5. Erhardt, K. et al. — The role of structure, low-strain rates, high-strain and temperature on the low-cycle fatigue behavior of 2024-T4 aluminum alloy. Techn. AFML-TR-69-85, August 1969.
6. Grosskreutz, J.C. — Fatigue mechanisms in the sub-creep range, 1970 (ASTM STP, to be published).
7. de Leiris, H. Frappier, E. — Sur la relation entre la distance d'une inclusion à la surface et l'influence de cette inclusion sur la fissuration par fatigue. Rev. Metall, 56, No.1, 1959, pp.11-24.
8. Erhardt, K. et al. — Mechanisms of fatigue crack propagation in aluminum alloys. Tech. Report AFML-TR 71-109, May 1971.
9. Thomson, A.W. Backofen, W.A. — The effect of grain size on fatigue, Acta Met. Vol.19, July 1971, pp.597-606.

10. Klesnil, M. Lukas, P. — *Dislocation Structure Associated with Fracture Surface of Fatigued Copper-Single-Crystals*. Phil. Mag. 17, 1968, p.1295.

11. Gell, M Leverant, G.R. — The characteristics of stage I fatigue fracture in a high strength nickel alloy. Acta Mel. 16, 1968, p.1295.

12. Forsyth, P.J. Ryder, D.A. — Some results of the examination of aluminum alloy specimen fracture surfaces-Metallurgia, Vol.63 1961, pp.117-124.

13. Maillard, A. et al. — Etude des caractéristiques microfractographiques des fontes G.S. sollicitées en fatigue. Journées d'Automne 1972.

14. Pelloux, R.M.N. — Mechanisms of formation of ductile fatigue striations Trans. of the ASM, Vol.62, 1969, pp.281-285.

15. Bathias, C. — Thèse d'Etat-Université de Poitiers – Juin 1972.

16. Pomey, G. — Endommagement et modifications de structure par fatigue. Rev. de Métall. Avril 70, pp.327-341.

17. Broek, D. Bowles, A.C. — On the formation of fatigue striations. International J. of Fract. mech. Vol.8, No.1 March 1972, p.75.

18. Rice, J.R. — *Mechanics of Crack Tip Deformation and Extension by Fatigue* – ASTM STP 415, 1966, p.247.

19. Bathias, C. Pelloux, R.M. — Etude de la zone plastifiée à fond de fissure. Application à la propagation des fissures de fatigue dans les aciers maraging et les aciers austénitiques 15ème colloque de métallurgie de Saclay, 1972.

20. Landgraf, R.W. — The Resistance of Metals to Cyclic Deformation ASTM STP 467, 1970, pp.3-36.

21. Defouquet, J. Levasseur, J. — Sur un critère du comportement en fatigue des métaux indépendant du mode de sollicitation – CR AST 262, pp.296-299.

22. Hahn, G.T. et al. — Local Yielding Attending Fatigue Crack Growth. Metallurgical Trans. Vol.3, May 1972, p.1189.

23. Lukas, P. et al. — Plastic zone around the propagating fatigue crack, Phil. Mag. Vol.20, Oct. 1969, p.799.

24. Bathias, C. — Contribution à l'étude des couches sous-jacentes des cassures par fatigue dans les aciers au carbone. Mem. Sc. Rev. Metalbuy Mars 1970, pp.165-171.

25. Weber, J.H. — Effects of crystallography and the mechanical treatment on fatigue-crack propagation – PhD – Lehigh University, 1969.

26. Lieurade, H.P. Rabbe, P. — Etude à l'aide de la mécanique de la rupture de la vitesse de fissuration en fatigue d'une gamme étendue d'aciers IRSID, p.138, Mars 1972.

27. El-Soudani, S.M. Pelloux, R.M. — Influence of inclusion content on fatigue crack propagation in aluminium alloys, Mit, March 1972.

28. Cazaud, R. et al. — La fatigue des métaux, Dunod 1969, p.444.

29. Selines, R.J. et al. — Corrosion – fatigue crack propagation in aluminum alloys, AFML-TR-72-21, Feb. 1972.

30. Barson, J.M. — Effect of cyclic stress form in corrosion fatigue crack propagation below K_{ISSC} – Intern. Conf. on Corrosion Fatigue, Storrs, Connecticut, June 1971.

31. Feeney, J.A. et al. — Environmental Fatigue Crack Propagation of Aluminum Alloys at Low-Stress Intensity Levels – Metallur. Trans. Vol.1, June 1970, p.1741.

32. Gallagner, J.P. Wei, R.P. — Crack propagation behavior in steels – Inter. Conf. on Corrosion Fatigue, June 1971.

33. van Swan, L. — Fatigue behavior of maraging steel 300, PhD Thesis, June 1973, MIT.

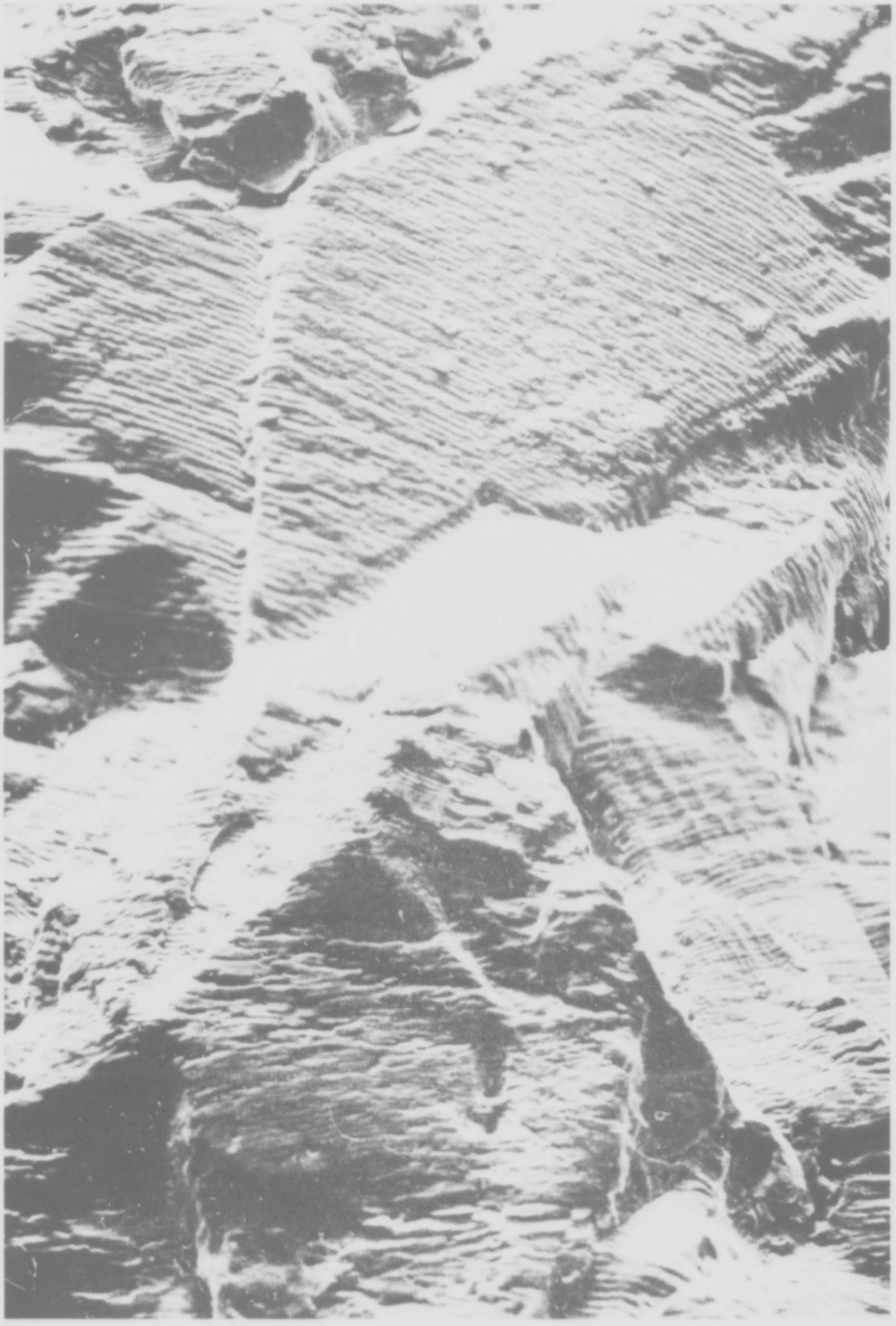

Fig.1 - Micrographic aspect of a fatigue fracture surface on a stainless austenitic steel 25 - 20.
$\Delta K = 45$ MPa$\sqrt{m}$

Fig.2 Fatigue fracture in a mild steel after smoothing and electrolytic attack. Network of dislocation walls perpendicular to the propagation direction indicated by the arrow.

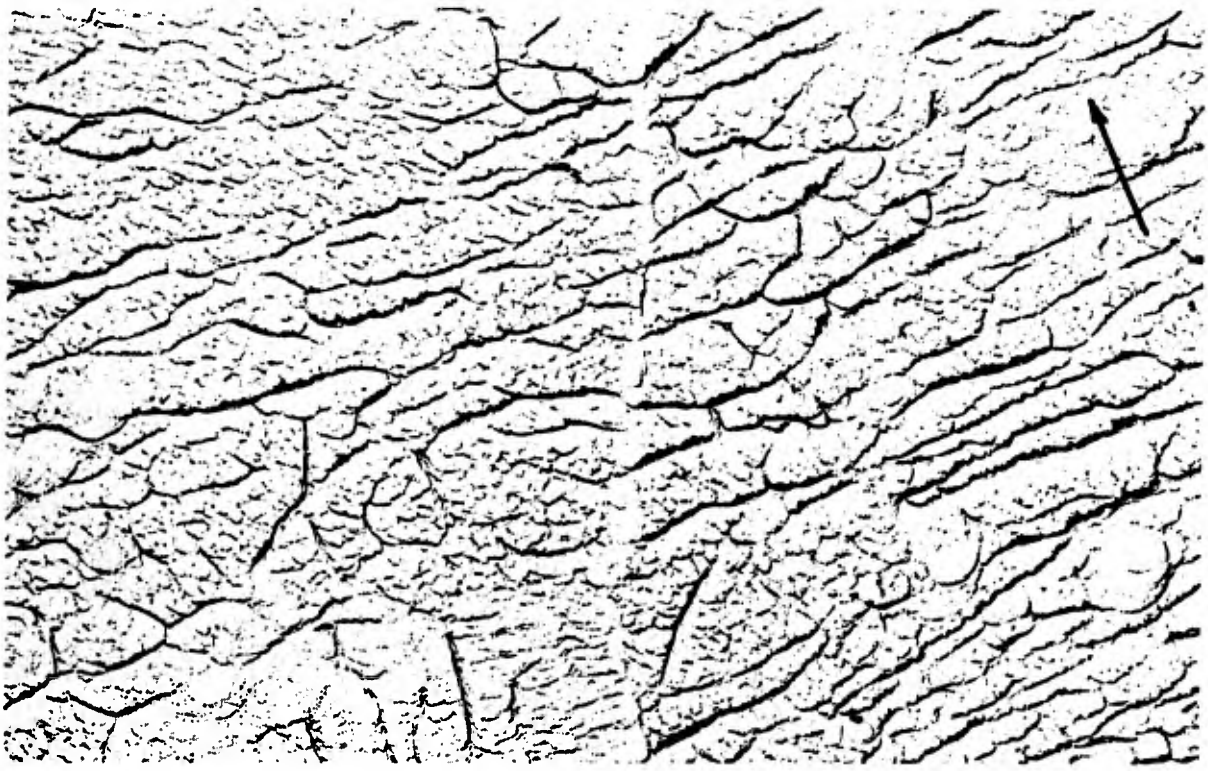

Fig.3 Field close to Figure 2, observed on both sides of a grain boundary a few dislocation cells appear clearly on this picture

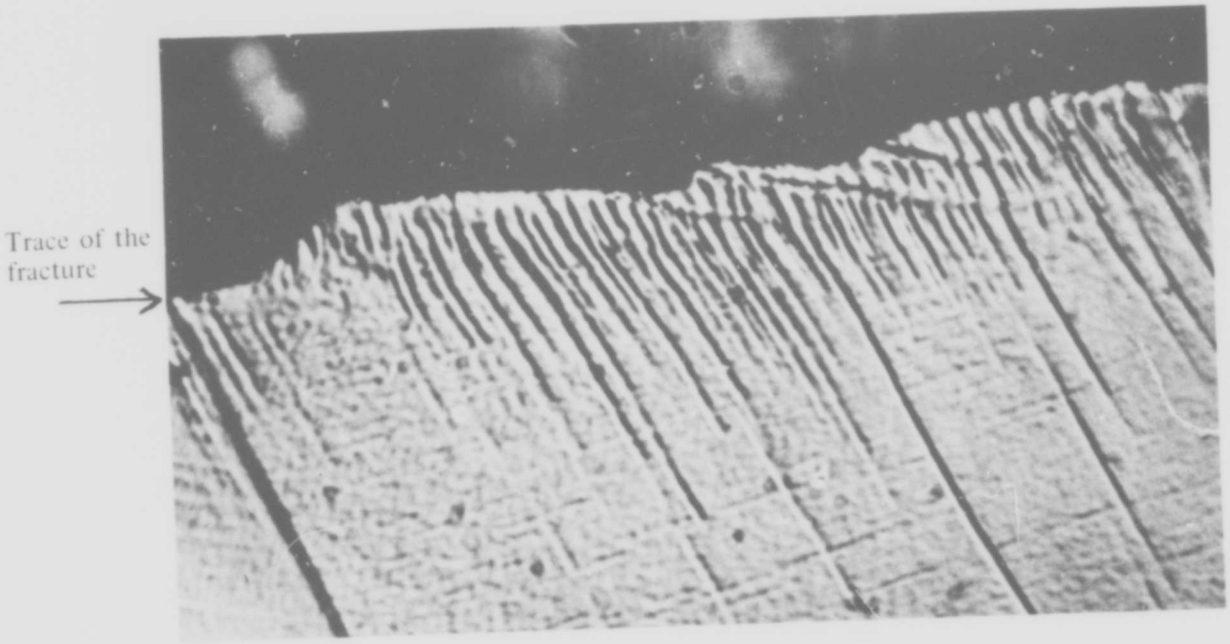

Fig.4 Mechanical twins emerging on the surface of a fatigue fracture in a stainless austenitic steel 25–20

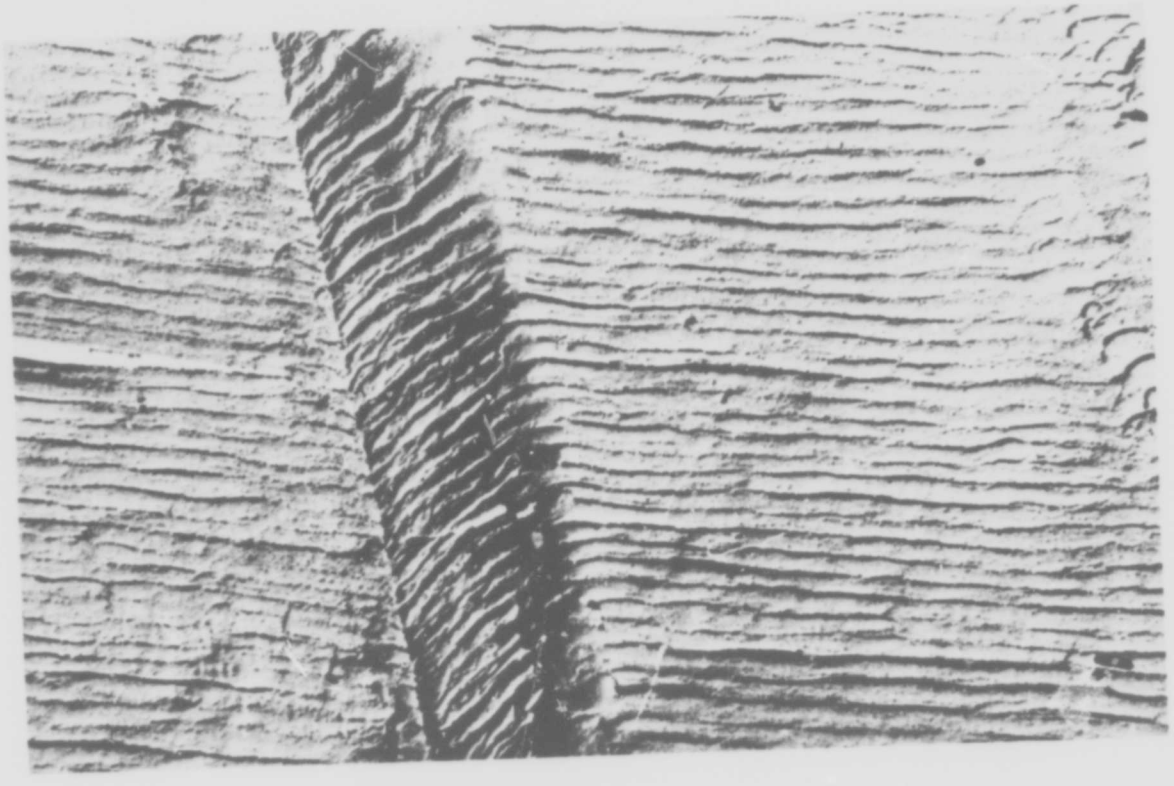

Fig.5 Fracture aspect in stainless steel 25–20

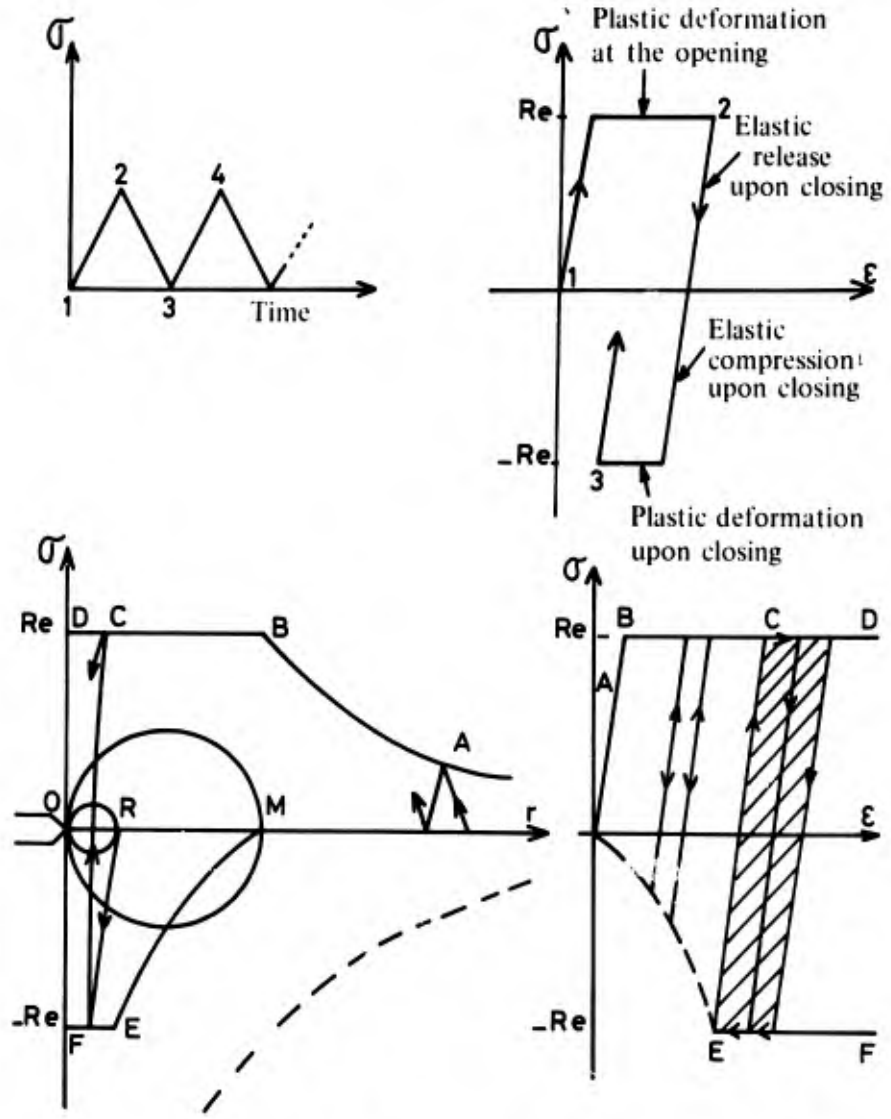

Fig.6 Mechanism of plastic deformation at the tip of a fatigue crack

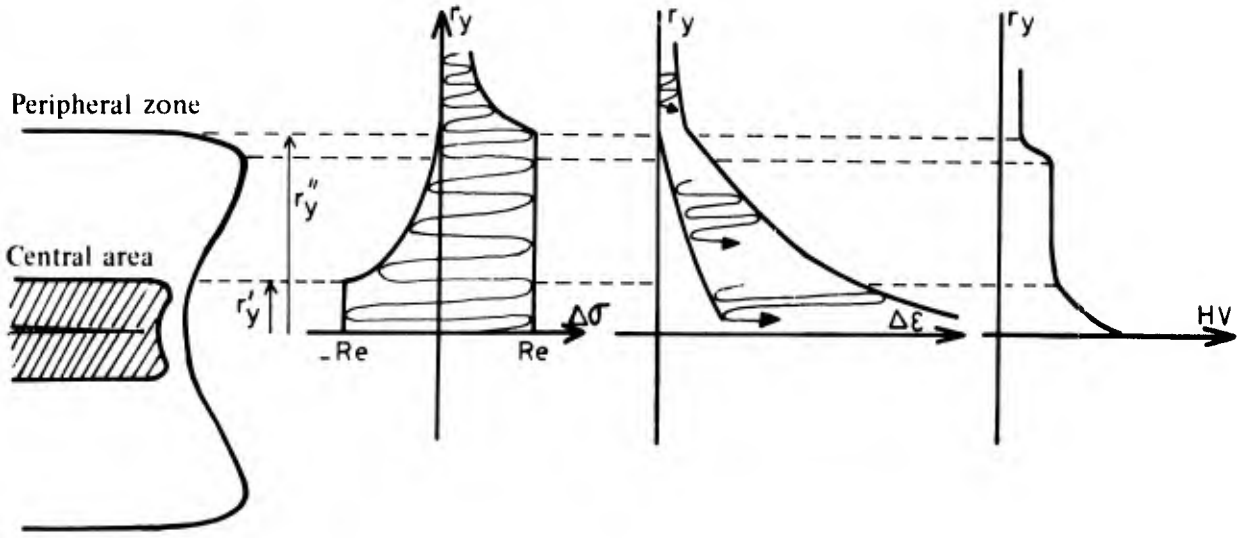

Fig.7 Diagrammatic representation of stresses and strains at the tip of a fatigue crack. Evolution of microhardness

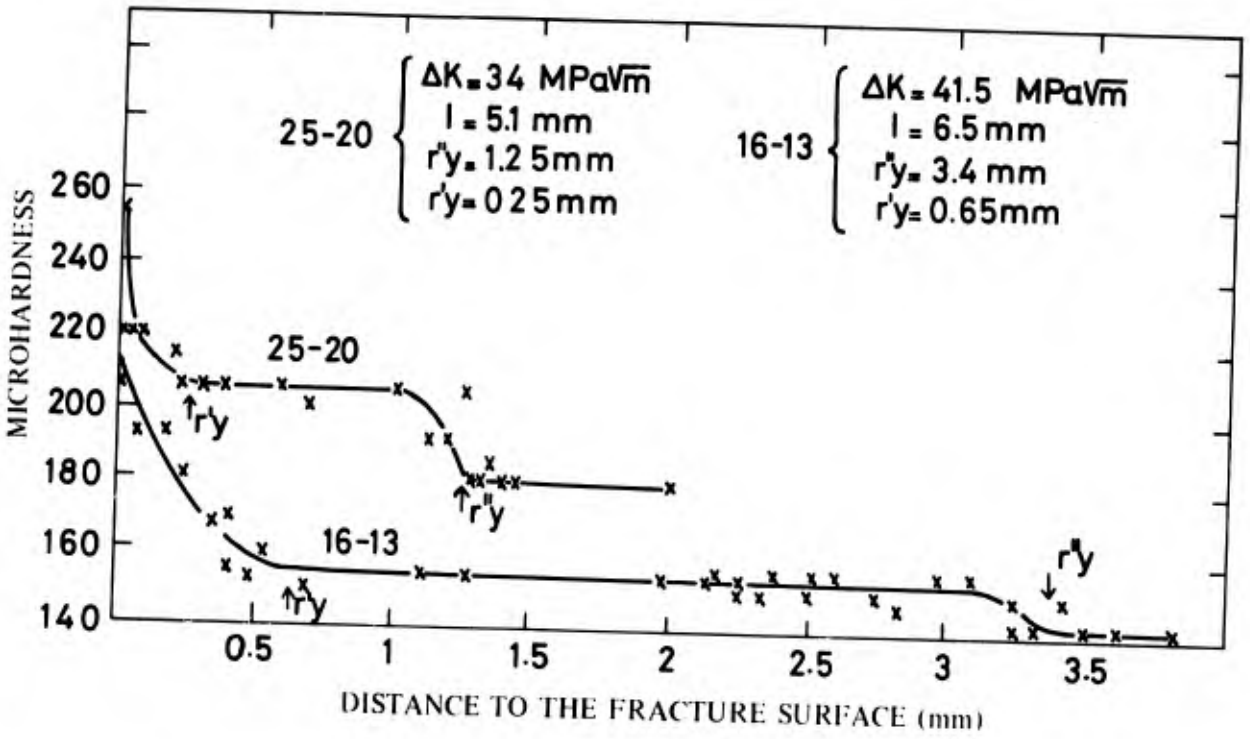

Fig.8 Evolution of microhardness under the fracture of two austenitic steels containing chromium-nickel

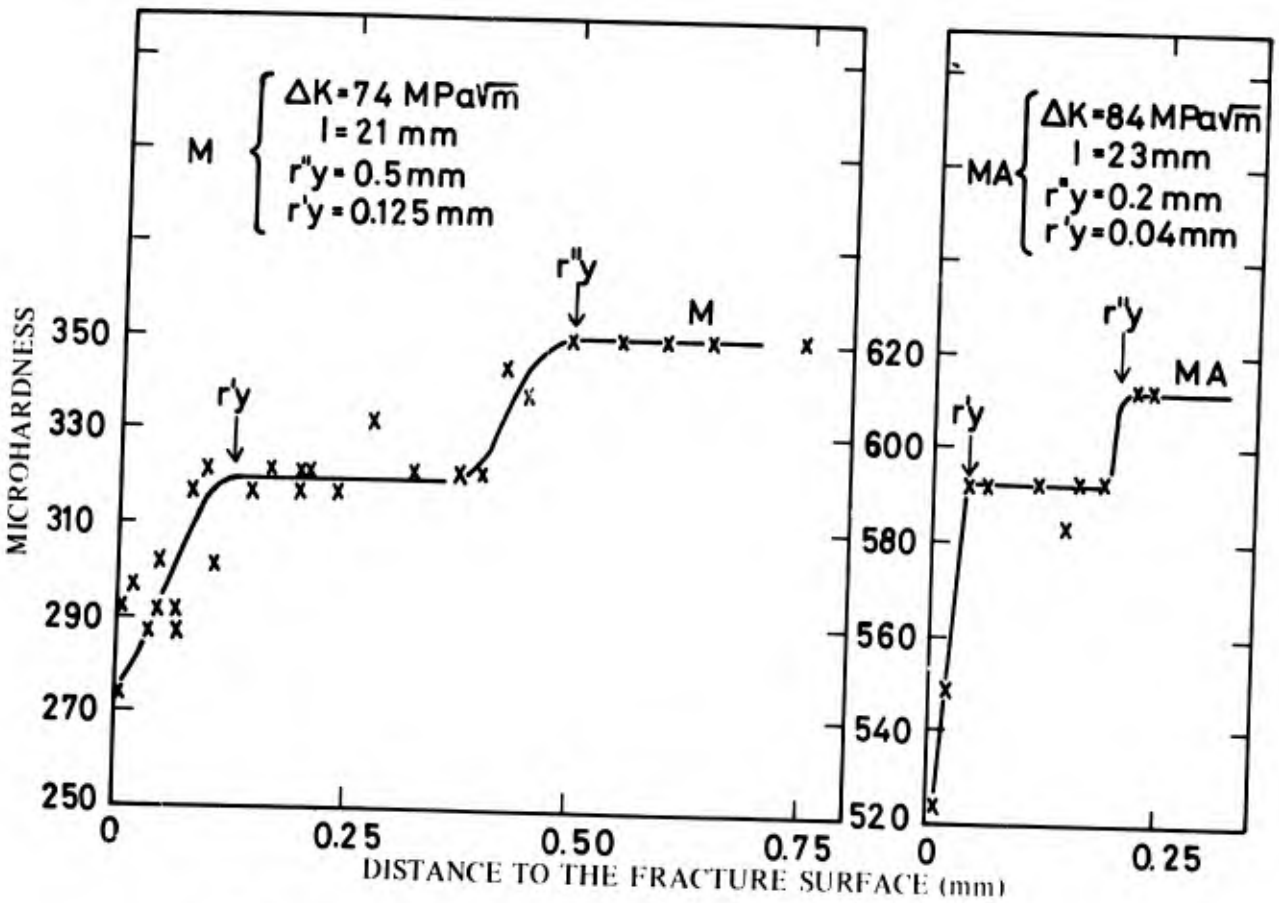

Fig.9 Evolution of microhardness under the fracture of a maraging steel

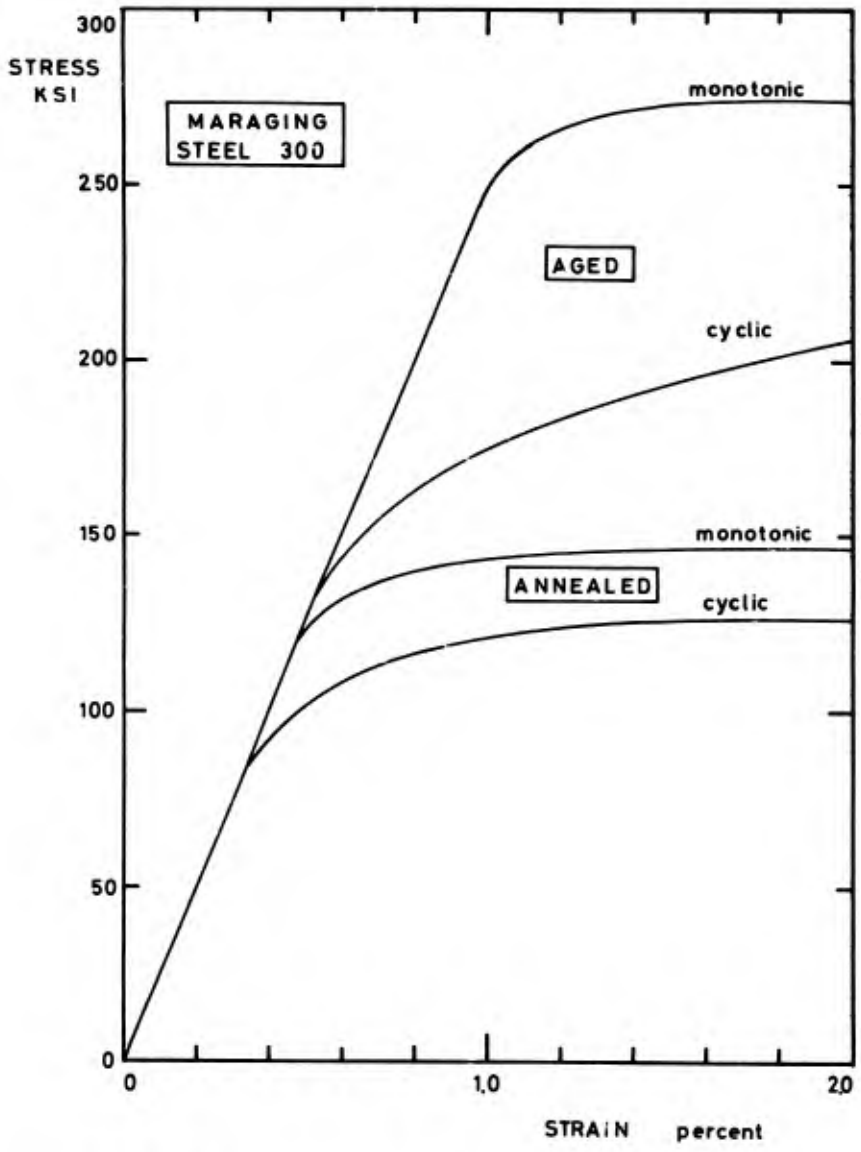

Fig.10 Cyclic stress-strain curves of a maraging steel (from 33)

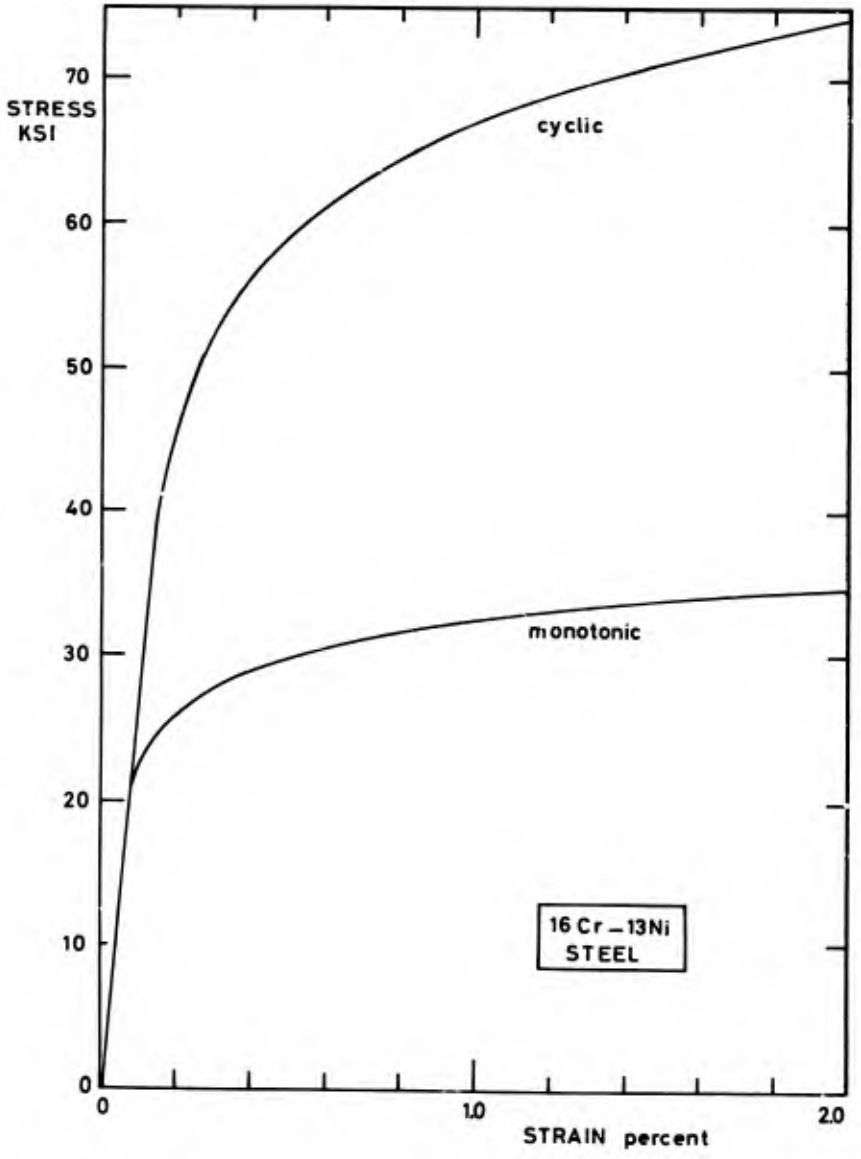

Fig.11 Cyclic stress-strain curve of a stainless austenitic steel (from 33)

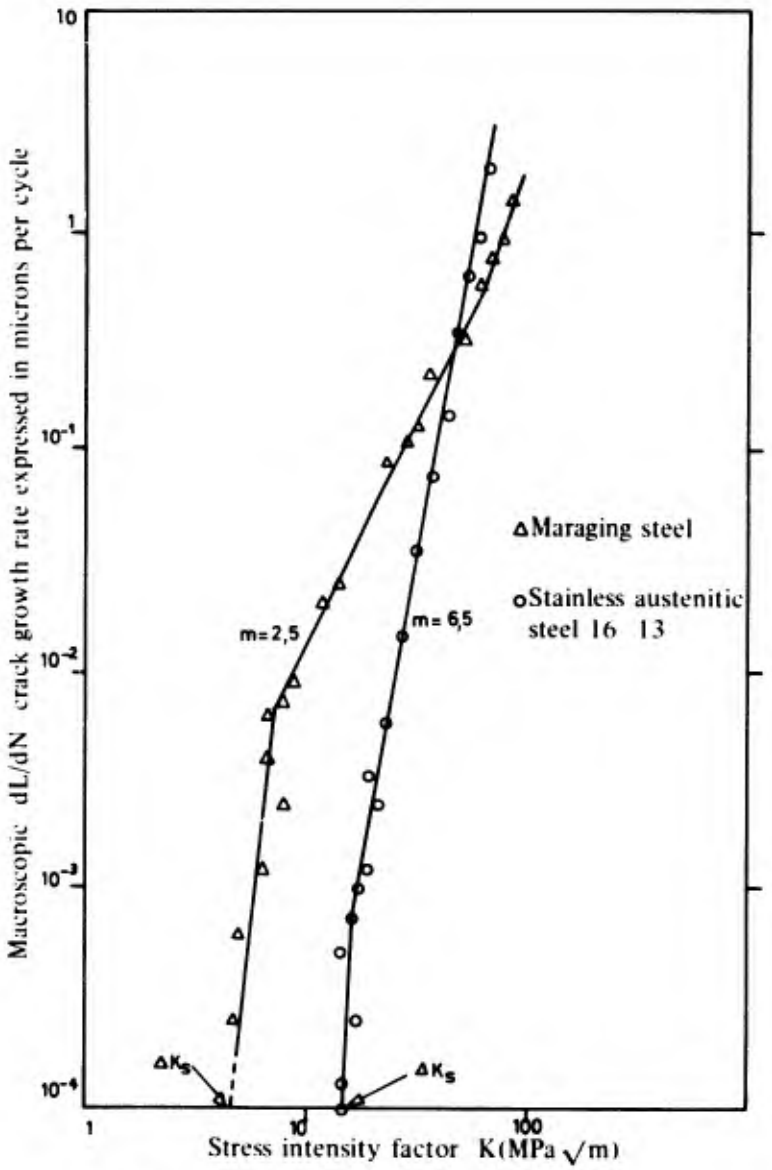

Fig.12 This diagram shows clearly the propagation threshold in a maraging steel and a stainless austenitic steel

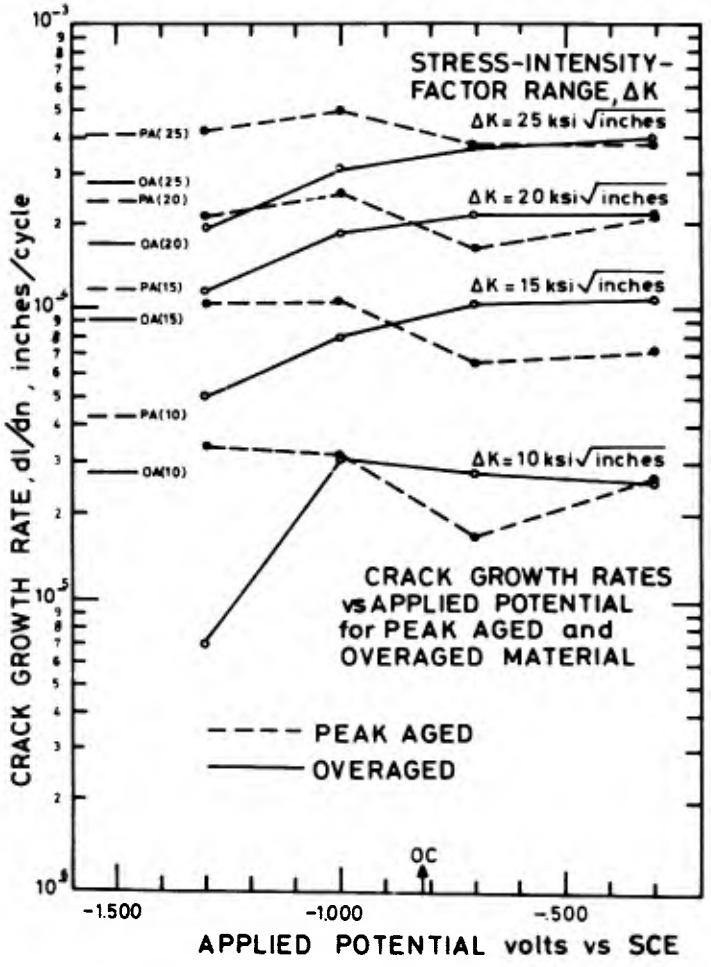

Fig.13 Influence of a potential and of ageing on the crack growth rate of a light alloy 7075 (from 29)

DISTRIBUTION OF UNCLASSIFIED AGARD PUBLICATIONS

NOTE: Initial distributions of AGARD unclassified publications are made to NATO Member Nations through the following National Distribution Centres. Further copies are sometimes available from these Centres, but if not may be purchased in Microfiche or photocopy form from the Purchase Agencies listed below. **THE UNITED STATES NATIONAL DISTRIBUTION CENTRE (NASA) DOES NOT HOLD STOCKS OF AGARD PUBLICATIONS, AND APPLICATIONS FOR FURTHER COPIES SHOULD BE MADE DIRECT TO THE APPROPRIATE PURCHASE AGENCY (NTIS).**

NATIONAL DISTRIBUTION CENTRES

BELGIUM
Coordonnateur AGARD – VSL
Etat-Major de la Force Aérienne
Caserne Prince Baudouin
Place Dailly, 1030 Bruxelles

CANADA
Defence Scientific Information Service
Defence Research Board
Department of National Defence
Ottawa, Ontario K1A OZ3

DENMARK
Danish Defence Research Board
Østerbrogades Kaserne
Copenhagen Ø

FRANCE
O.N.E.R.A. (Direction)
29, Avenue de la Division Leclerc
92, Châtillon sous Bagneux

GERMANY
Bundesministerium der Verteidigung
Registratur Ru Fo 4
53 Bonn 1
Postfach 161

GREECE
Hellenic Armed Forces Command
D Branch, Athens

ICELAND
Director of Aviation
c/o Flugrad
Reykjavik

ITALY
Aeronautica Militare
Ufficio del Delegato Nazionale all'AGARD
3, Piazzale Adenauer
Roma/EUR

LUXEMBOURG
See Belgium

NETHERLANDS
Netherlands Delegation to AGARD
National Aerospace Laboratory, NLR
P.O. Box 126
Delft

NORWAY
Norwegian Defence Research Establishment
Main Library
P.O. Box 25
N-2007 Kjeller

PORTUGAL
Direccao do Servico de Material
da Forca Aerea
Rua de Escola Politecnica 42
Lisboa
Attn: AGARD National Delegate

TURKEY
Turkish General Staff (ARGE)
Ankara

UNITED KINGDOM
Defence Research Information Centre
Station Square House
St. Mary Cray
Orpington, Kent BR5 3RE

UNITED STATES
National Aeronautics and Space Administration (NASA)
Langley Field, Virginia 23365
Attn: Report Distribution and Storage Unit
(See Note above)

PURCHASE AGENCIES

Microfiche or Photocopy

National Technical
Information Service (NTIS)
5285 Port Royal Road
Springfield
Virginia 22151, USA

Microfiche

ESRO/ELDO Space
Documentation Service
European Space
Research Organization
114, Avenue Charles de Gaulle
92200 Neuilly sur Seine, France

Microfiche

Technology Reports
Centre (DTI)
Station Square House
St. Mary Cray
Orpington, Kent BR5 3RE
England

Requests for microfiche or photocopies of AGARD documents should include the AGARD serial number, title, author or editor, and publication date. Requests to NTIS should include the NASA accession report number.

* * *

Full bibliographical references and abstracts of AGARD publications are given in the following bi-monthly abstract journals

Scientific and Technical Aerospace Reports (STAR),
published by NASA,
Scientific and Technical Information Facility
P.O. Box 33, College Park
Maryland 20740, USA

Government Reports Announcements (GRA),
published by the National Technical
Information Services, Springfield
Virginia 22151, USA

Printed by Technical Editing and Reproduction Ltd